DOKUZ EYLÜL UNIVERSITY

GRADUATE SCHOOL OF NATURAL AND APPLIED

SCIENCES

VIBRATION ANALYSIS OF CRACKED FRAME STRUCTURES

by
Ahmad M. İBRAHEM

July, 2010

İZMİR

VIBRATION ANALYSIS OF CRACKED FRAME STRUCTURES

A Thesis Submitted to the
Graduate of Natural and Applied Sciences of Dokuz Eylül University
In Partial Fulfillment of the Requirement for The Degree of Master of Science
in Mechanical Engineering, Machine Theory and Dynamic Program

by
Ahmad M. IBRAHEM

July, 2010
İZMİR

Ms.Sc. THESIS EXAMINATION RESULT FORM

We certify that we have read the thesis, entitled **"VIBRATION ANALYSIS OF CRACKED FRAME STRUCTURES"** completed by **AHMAD M. IBRAHEM** under supervision of **PROF. DR. MUSTAFA SABUNCU** and that in our opinion it is fully adequate, in scope and in quality, as a thesis for the degree of Master of Science**.**

Prof. Dr. Mustafa SABUNCU

Supervisor

(Jury Member)   (Jury Member)

Dire Prof. Dr. Mustafa SABUNCU

Director

Graduate School of Natural and Applied Sciences

ACKNOWLEDGMENTS

I would like to express my gratitude to my supervisor Prof.Dr. Mustafa SABUNCU and Dr. Hasan ÖZTÜRK for their expertise, understanding, and patience.

Very special thanks to my family for supporting me.

Finally,
my respect to Turkish people for the hospitality.

Ahmad M. IBRAHEM

VIBRATION ANALYSIS OF CRACKED
FRAME STRUCTURES

ABSTRACT

In this work, the effects of crack depth and crack location on the in-plane free vibration, buckling and dynamic stability of cracked frame structures have been investigated numerically by using The Finite Element Method. For the rectangular cross-section beam a crack element is developed by using the principles of fracture mechanics. The effects of crack depth and location on the first four natural frequency, first critical buckling load and the first dynamic unstable region of multi-bay and multi-store frame structures are presented in 3D graphs. The comparison between the present work and the results obtained from ANSYS and SolidWorks shows a very good agreement.

Keywords: cracked frame, free vibration, multi-bay, multi-story, finite element method, buckling, dynamic stability.

**VIBRATION ANALYSIS OF CRACKED
FRAME STRUCTURES**

ÖZ

Bu Çalışmada, çatlak derinliğinin ve yerinin, çerçeve yapıların düzlem içi serbest titreşimine, burkulma yüküne ve dinamik kararlılığına olan etkileri Sonlu Elemanlar Metodu kullanılarak incelenmiştir. Kırılma mekaniği prensipleri kullanılarak dikdörtgen kesitli bir kiriş için çatlak elemanı geliştirilmiştir. Çatlak derinliğinin ve yerinin, çok bölümlü ve çok katlı çerçevelerin ilk dört doğal frekansına, burkulma yüküne, birinci dinamik kararsızlık bölgesine etkisi üç boyutlu grafikler halinde verilmiştir. ANSYS ve SolidWorks programlarının analiz sonuçları ile çalışmadan elde edilen sonuçların karşılaştırılmasından oldukça yakın değerler elde edildiği görülmüştür.

Anahtar Kelimeler: çatlaklı çerçeve, serbest titreşim, burkulma, dinamik kararlılık

CONTENT

CHAPTER ONE
INTRODUCTION

1.1 Introduction

In many applications, frame structures are widely used, for example in buildings, bridges and gas or steam turbine blade packets. A frame element is formulated to model a straight bar of an arbitrary cross-section, which can deform not only in the axial direction but also in the directions perpendicular to the axis of the bar. The bar is capable of carrying both axial and transverse forces, as well as moments. Therefore, a frame element is seen to possess the properties of both bar and beam elements. In fact, the frame structure can be found in most of our real environment, there are not many structures that deform and carry loadings purely in neither axial direction nor purely in transverse directions. The bar, beam and frame finite elements are illustrated and discussed in many books (G.R.Liu and S.S.Quek, 2003), (Rao, 1995) .The natural frequencies of a single storey and multi-bay frames have been investigated by using the frame finite element. The frame F.E models have also been used for the vibration analysis of shrouded-blade packets. Moreover, the cracks can be seen in frame structures due to reasons like erosion, corrosion, fatigue or accidents. The presence of a crack could not only cause a local variation in the stiffness, but also affect the mechanical behavior of the entire structure to considerable extent. Therefore the effect of crack on the dynamic behaviors of structures has been studied in many papers by using the fracture mechanics methods analytically or numerically. Frames are subjected to concentrated static or dynamic loads which may cause static (buckling) and dynamic instability. Many investigations about the vibration and buckling (static stability), and dynamic stability characteristics of frames of various types have been carried out.

J. Thomas & H. T. Belek (1977), studied, the free-vibration characteristics of shrouded blade packets using the finite element method. The effects of various weight ratios, flexural rigidity ratios and length ratios between the blade and shrouds on the frequencies of vibration of the blade packed were investigated.

M.Chati, R. Rand & S. Mukherjee (1997), studied the modal analysis of a cantilever beam with a transverse edge crack. The open and close cracks were considered.

M.Krawczuk (1994), developed a new finite element model for the static and dynamic analysis of cracked composite beams .A new beam finite element with a single non-propagating one-edge open crack located in its mid-length is formulated for the static and dynamic analysis of cracked composite beam-like structures.

N.F.Rieger and H.McCallion (1964), studied the natural frequency of portal frame , they used a single storey and multi-bay frames in their analysis.

J.M.Chandra Kishen and Avinash Kumar (2004), studied fracture behavior of cracked beam-columns , by using the finite element method in addition they also used the beam-column element which was developed by Tharp (Int. J. Numer. Methods Eng. 24 1987.

M.Krawczuk & W.M.Ostachwicz (1995), carried out modeling and vibration analysis of a cantilever composite beam with a transverse open crack two different models of the beam were presented. In their first model the crack was represented by a massless substitute spring. The flexibility of the spring was calculated on the basis of fracture mechanics and the Castigliano theorem. The second model was based on the finite element method (FEM). The undamaged parts of the beam were modeled by a beam finite element with three nodes and three degrees of freedom at the nodes. The damaged part of the beam was represented by a cracked beam finite element model having the same degrees of freedom to those of the un-cracked one.

M.-H.H.Shen & C.Pierre (1994), investigated free vibrations of beams with a single-edge crack.

G.Bamnios & A.Trochides (1995), studied the dynamic behavior of a cracked cantilever beam.

M.-H.H.Shen & J.E.Taylor (1991), investigated an identification problem for vibrating cracked beams.

T. G. CHONDROS , A. D. DIMAROGONAS & J. YAO (1997), studied vibration analysis of a continuous cracked beam.

P.N.Saavedra & I.A. Cuitino (2001), presented a theoretical and experimental dynamic behavior of different multi-beams systems containing transverse cracks . In their analysis they used free-free beam and U-frames.

G.Gounaris & Dimarogonas (1987), developed a finite element model for a cracked prismatic beam. Strain energy concentration arguments lead to the development of a compliance matrix for the behavior of the beam in the vicinity of the crack. This matrix was used to develop the stiffness matrix for the cracked beam element and the consistent mass matrix. The developed of this finite element can be used in any appropriate matrix analysis of structural element.

D.Y.Zheng & N.J.Kessissoglou (2004), obtained the natural frequencies and mode shapes of a cracked beam by using the finite element method . An 'overall additional flexibility matrix', instead of the 'local additional flexibility matrix', was added to the flexibility matrix of the corresponding intact beam element to obtain the total flexibility matrix. Consequently the stiffness matrix.

Celalettin Karaagac & Hasan Ozturk & Mustafa Sabuncu (2009), investigated the effects of crack ratios and positions on the fundamental frequencies and buckling loads of slender cantilever Euler beams with a single-edge crack both experimentally and numerically using the finite element method, based on energy approach.

P.Gudmundson (1982), discussed "the dynamic behavior of slender structures with cross-sectional cracks" . Two methods were discussed to find the static flexibility matrix from an integration of the stress intensity factor.

G.-L.Qian , S.-N.Gu & J.-S. Jiang (1989), determined the eigen-frequencies for different crack length and location on cantilever beams by using the finite element method.

T.G.Chondros & A.D.DIMAROGONAS (1989), discussed the change in natural frequencies and modes of vibration for the cracked structure when the crack geometry was known by using Rayleigh principle.

H.P.Lee & T.Y.Ng (1995), determined the natural frequencies and modes for the flexural vibration of a beam due to the presence of transverse cracks by using the Rayleigh-Ritz method. The beams with single-sided crack or a pair of double-sided cracks were modeled separately.

M.-H.H.Shen & C.Pierre (1990), studied natural modes of Euler-Bernoulli beams with symmetric cracks.

S.Christides & A.D.S.Barr (1984), studied one-dimensional theory of cracked Euler-Bernoulli beams.

W.M.Ostachowicz & M.Krawczuk (1990) studied the forced vibration of beams and effects of the crack locations and sizes on the vibrational behavior of the structure. Basis identification was discussed.

Thomas and Sabuncu (1979), presented a finite element model for the analysis of vibration characteristics of asymmetric cross section blade packets in a centrifugal field.

Gurkan Sakar and Mustafa Sabuncu (2007), presented a finite element model for the static and dynamic stability of rotating aerofoil cross-section two-blade packets subjected to uniform radial periodic force.

Boltin (1964), studied the dynamic stability problems of various kinds of structural components.

Sakar and Sabuncu (2003 , 2004), used the finite element method to analyze the static and dynamic stability of straight and pre-twisted aerofoil cross section rotating blades subjected to axial periodic forces.

J.Thomas and B.A.H.Abbas (1976), studied the dynamic stability of Timoshenko Beam subjected to periodic axial loads by the finite element method.

Hasan Ozturk and Mustafa Sabuncu (2005), studied the static and dynamic stability of a laminated composite cantilever beam having a linear translation spring and a torsional spring as elastic supports subjected to periodic axial loading. The Euler beam theory was employed and the finite element method was used in the analysis.

1.2 Objective of the Work

In this work, the first fourth natural frequency, buckling and dynamic stability for the multi-bay frame and multi-story frame structures are studied. As seen in figure 1.1. Blade and shroud having rectangular cross-section are used. For the frame structure the dimension and material properties are given in Table 1.1

Table 1.1 properties of the frame structure

Properties		Quantity	Units
E		2e11	N/m^2
Ro		7900	kg/m^3
Cross-section	h	0.5/100	m
	b	2/100	m
Blade length		0.2	m
Shroud length		0.1	m
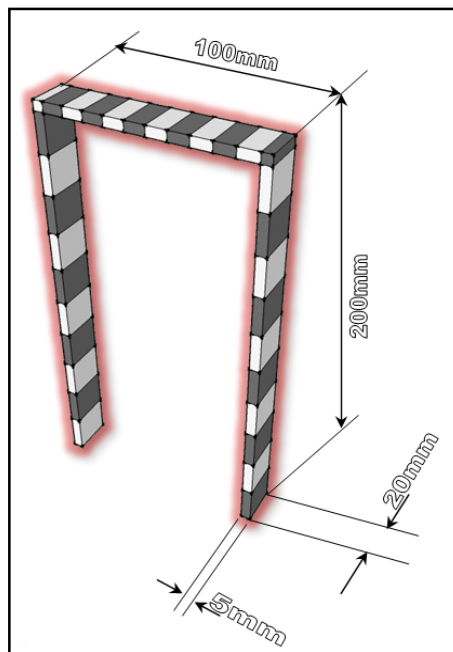
Figure 1.1 Frame structure dimensions

For the multi-bay and multi-story frames, the dimensions are used as shown in Figure 1.2 and Figure 1.3 respectively.
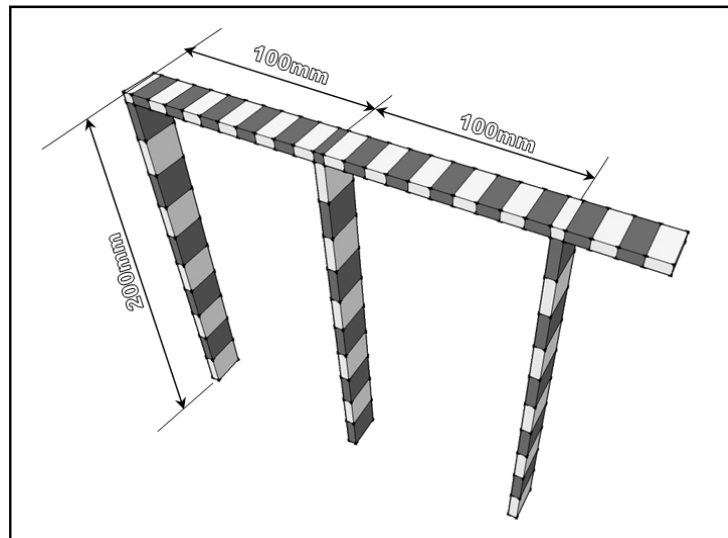
Figure 1.2 multi-bay dimensions
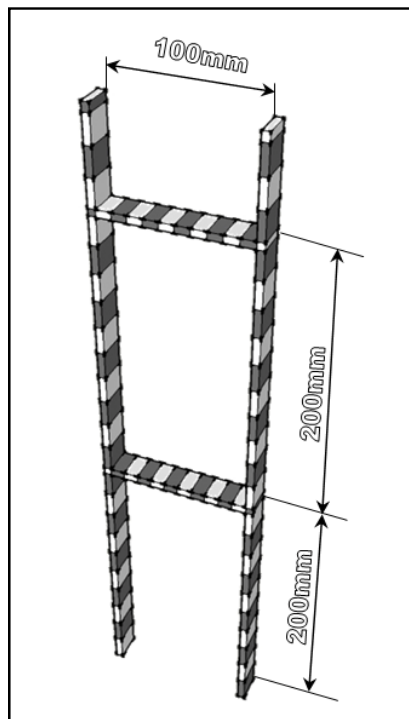
Figure 1.3 multi-story dimension

Chapter two deals with the theory of the finite element method. Bar, beam and Frame Elements are discussed. Mass, Stiffness and Geometric Stiffness matrices of a beam element are obtained. Local and global coordinates are also discussed.

Chapter three presents the cracked beam model, three crack modes, which are opining, sliding and tearing, are considered. A cracked beam element model is developed for the frame structure. And the stiffness, mass and geometrical matrices are obtained for the cracked beam element.

Chapter four deals with the theory of the dynamic stability of elastic systems.

Chapter five deals with the results and charts obtained for different configurations of frame structures (Single, Multi-Bay Frame and Multi- Storey Frame).

CHAPTER TWO
FINITE ELEMENT METHOD

2.1 Finite element method

The finite element method is a numerical method that can be used for the accurate solution of complex mechanical and structural vibration problems. In this method, the actual structure is replaced by several pieces or elements, each of which is assumed to behave as a continuous structural member called a finite element.

The elements are assumed to be interconnected at certain points known as joints or nodes. Since it is very difficult to find the exact solution (such as the displacements) of the original structural under the specified loads, a convenient approximate solution is assumed in each finite element. The idea is that if the solutions of the various elements are selected properly, they can be made to converge to the exact solution of the total structure as the element size is reduced. During the solution process the equation of force at the joints and the compatibility of displacements between the elements are satisfied so the entire structure (assemblage of elements) is made to behave as a single entity. (Rao, 1995)
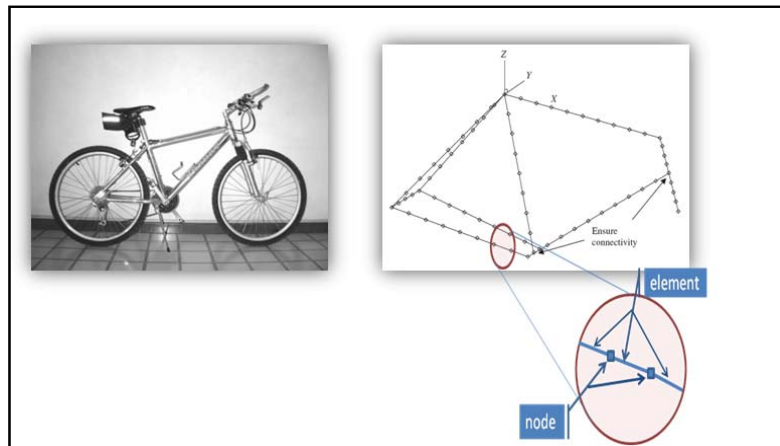
Figure 2.1 Finite Element Nodes and Elements

2.2 Bar

A truss is one of the simplest and most widely used structural members. It is a straight bar that is designed to take only axial forces, therefore it deforms only in its axial direction. A typical example of its usage can be seen in Figure 2.2. The cross-section of the bar can be arbitrary, but the dimensions of the cross-section should be much smaller than that in the axial direction. Finite element equations for such truss members will be developed in this chapter. The element developed is commonly known as the truss element or bar element. Such elements are applicable for analysis of the skeletal type of truss structural systems both in two-dimensional planes and in three-dimensional space. The basic concepts, procedures and formulations can also be found in many existing textbooks (see, e.g. Reddy, 1993; Rao, 1999; Zienkiewicz and Taylor, 2000; etc.).
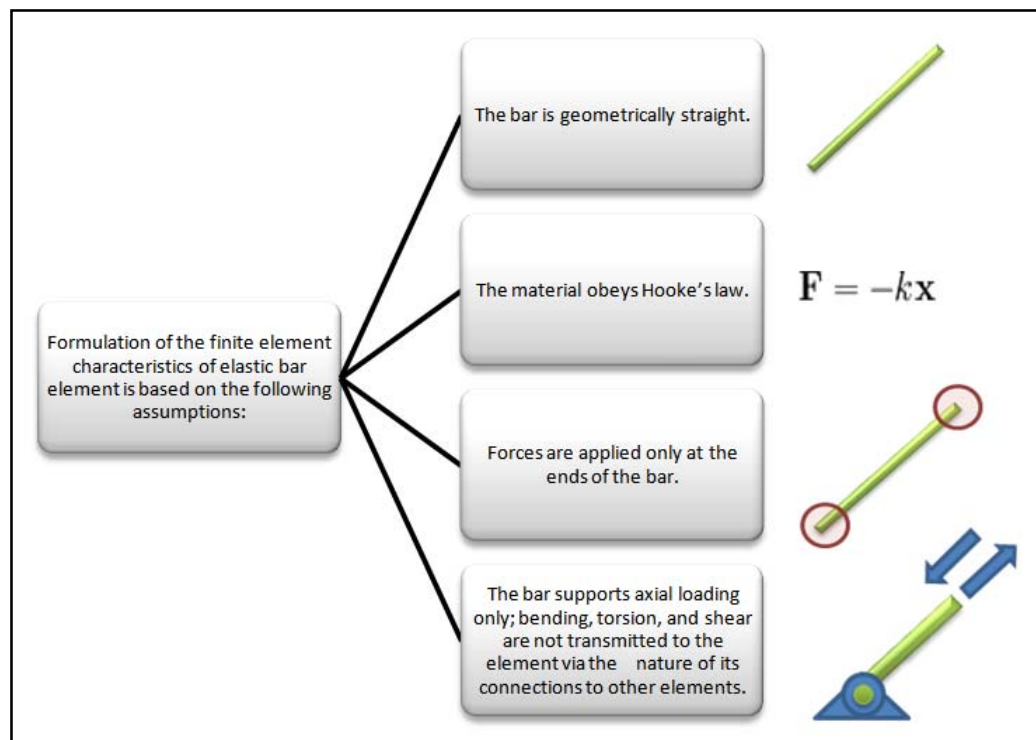
Figure 2.2 Properties of Bar Element

Consider the uniform bar element shown in figure (2-3). For this one-dimensional element, there are two end points called nodes. When the element is subjected to axial loads $f_1(t)$ and $f_2(t)$, the axial displacement within the element is assumed to be linear in x as

$$u(x,t) = a(t) + b(t)x \qquad (2\text{-}1)$$

When the joint displacements $u_1(t)$ and $u_2(t)$ are treated as unknowns, Eq. (2-1) should satisfy the conditions:

$$u(0,t) = u_1(t) \ , \ u(l,t) = u_2(t) \qquad (2\text{-}2)$$

Equations (2-1) and (2-2) lead to

$$a(t) = u_1(t)$$

And

$$a(t) + b(t)l = u_2(t) \ \ or \ \ b(t) = \frac{u_2(t) - u_1(t)}{l} \qquad (2\text{-}3)$$

Substitution for $a(t)$ and $b(t)$ from Eq. (2-3) into Eq. (2-1) gives

$$u(x,t) = \left(1 - \frac{x}{l}\right) u_1(t) + \frac{x}{l} u_2(t) \qquad (2\text{-}4)$$

Or

$$u(x,t) = N_1(x)u_1(t) + N_2(x)u_2(t) \qquad (2\text{-}5)$$
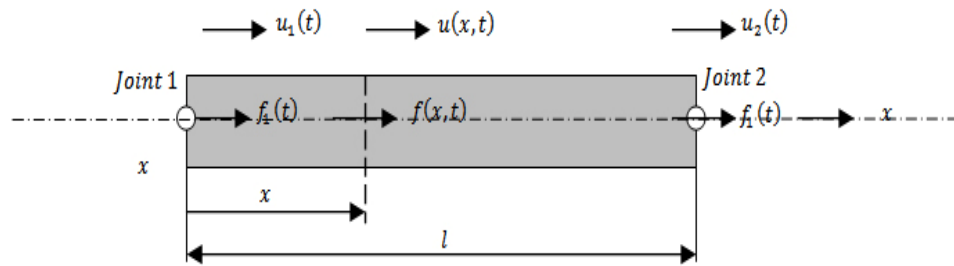
Figure 2.3 Bar Element

Where

$$N_1(x) = \left(1 - \frac{x}{l}\right) , N_2(x) = \frac{x}{l} \tag{2-6}$$

are the shape functions.

The kinetic energy of the bar element can be expressed as

$$T(t) = \frac{1}{2} \int_0^l \rho A \left\{\frac{\partial u(x,t)}{\partial t}\right\}^2 dx$$

$$= \frac{1}{2} \int_0^l \rho A \left\{\left(1 - \frac{x}{l}\right)\frac{du_1(t)}{dt} + \left(\frac{x}{l}\right)\frac{du_2(t)}{dt}\right\}^2 dx$$

$$= \frac{1}{2} \frac{\rho A l}{3} \left(\dot{u}_1^2 + \dot{u}_1\dot{u}_2 + \dot{u}_2^2\right) \tag{2-7}$$

Where

$$\dot{u}_1 = \frac{du_1(t)}{dt} \quad , \quad \dot{u}_2 = \frac{du_2(t)}{dt}$$

ρ is density of the material

A is the cross-section area of the element.

By expressing Eq. (2-7) in matrix form,

$$T(t) = \frac{1}{2} \dot{\vec{u}}(t)^T [m] \, \dot{\vec{u}}(t) \tag{2-8}$$

Where

$$\dot{\vec{u}}(t) = \begin{Bmatrix} \dot{u}_1(t) \\ \dot{u}_2(t) \end{Bmatrix}$$

And the superscript T indicates the transpose, the matrix [m] can be identified as

$$[m] = \frac{\rho A l}{6} \begin{bmatrix} 2 & 1 \\ 1 & 2 \end{bmatrix} \tag{2-9}$$

The strain energy of the element can be written as

$$V(t) = \frac{1}{2} \int_0^l E\,A \left\{ \frac{\partial\, u(x,t)}{\partial x} \right\}^2 dx$$

$$= \frac{1}{2} \int_0^l E\,A \left\{ -\frac{1}{l}\, u_1(t) + \frac{1}{l}\, u_2(t) \right\}^2 dx$$

$$= \frac{1}{2} \frac{E\,A}{l} \left(u_1{}^2 - 2\, u_1 u_2 + u_2{}^2 \right) \tag{2-10}$$

Where $u_1 = u_1(t)$, $u_2 = u_2(t)$, and E is Young's modulus. By expressing Eq. (2-10) in matrix form as

$$V(t) = \frac{1}{2}\, \vec{u}(t)^T\, [k]\, \vec{u}(t) \tag{2-11}$$

Where

$$\vec{u}(t) = \begin{Bmatrix} u_1(t) \\ u_2(t) \end{Bmatrix} \quad and \quad \vec{u}(t)^T = \{ u_1(t)\ u_2(t) \}$$

The stiffness matrix [k] can be identified as

$$[k] = \frac{E\,A}{l} \begin{bmatrix} 1 & -1 \\ -1 & 1 \end{bmatrix} \tag{2-12}$$

2.3 Beam

A beam is another simple but commonly used structural component. It is also geometrically a straight bar of an arbitrary cross-section, but it deforms only in directions perpendicular to its axis. Note that the main difference between the beam and the truss is the type of load they carry. Beams are subjected to transverse loading, including transverse forces and moments that result in transverse deformation. Finite element equations for beams will be developed in this chapter, and the element developed is known as the beam element. The basic concepts, procedures and formulations can also be found in many existing textbooks (see, e.g. Petyt,1990; Reddy, 1993; Rao, 1999; Zienkiewicz and Taylor, 2000; etc.).
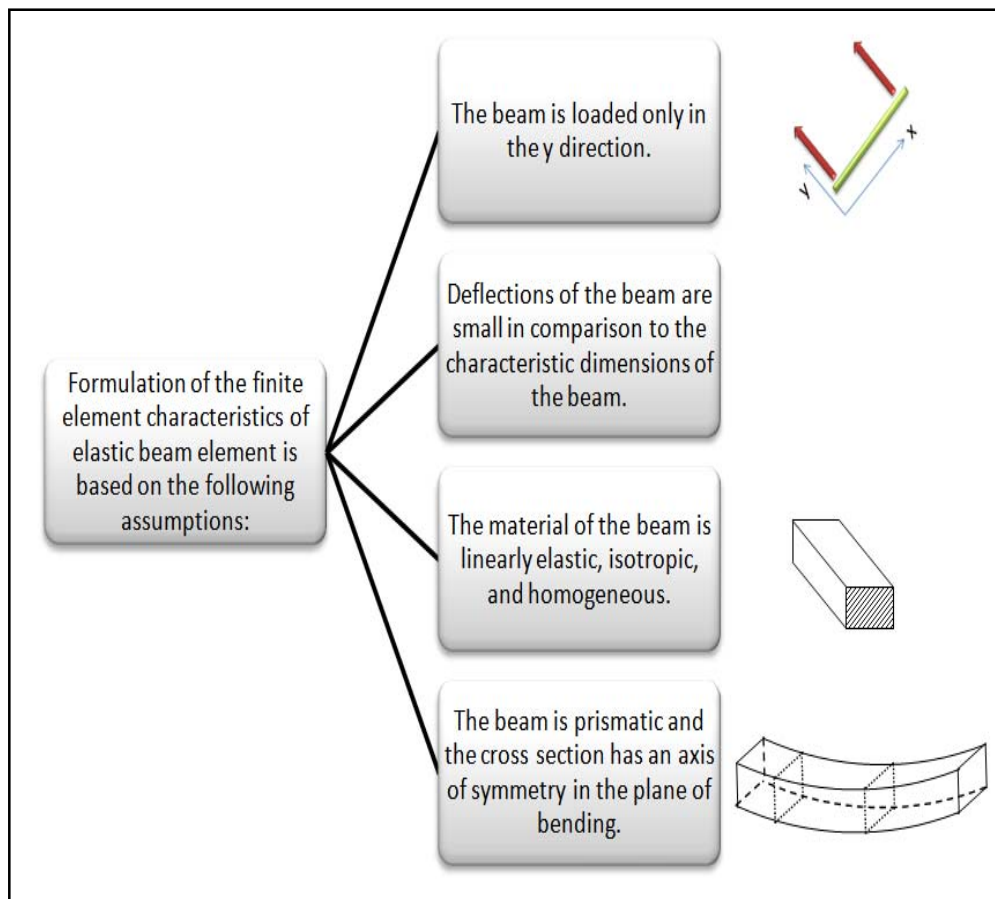
Figure 2.4 Properties of Beam Element

Consider a beam element according to the Euler-Bernoulli theory. Figure (2-5) shows a uniform beam element subjected to the transverse force distribution $f(x, t)$.
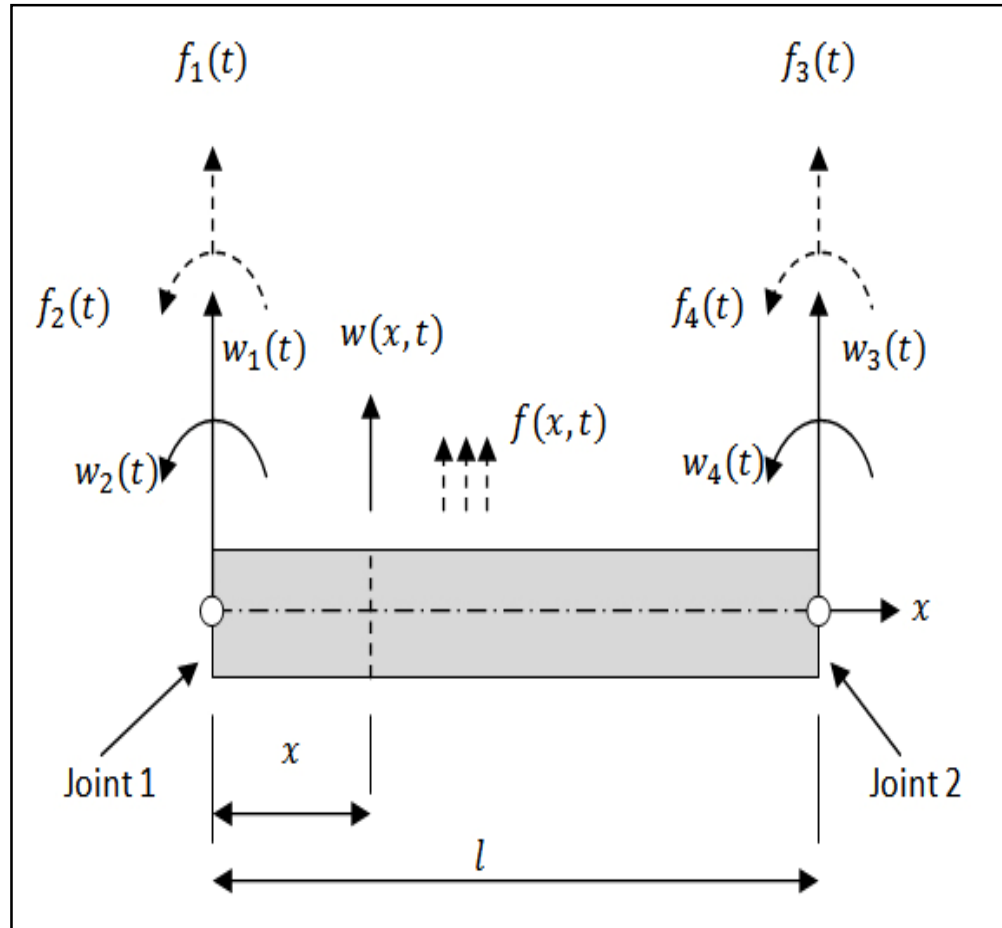
Figure 2.5 Beam Element

In this case , the joint undergoes both translational and rotational displacements, so the unknown joint displacements are labeled as $w_1(t)$, $w_2(t)$, $w_3(t)$ and $w_4(t)$ thus there will be linear joint forces $f_1(t)$ and $f_3(t)$ corresponding to the linear joint displacements $w_1(t)$ and $w_3(t)$ and rotational joint forces (bending moments) $f_2(t)$ and $f_4(t)$ corresponding to the rotational joint displacements $w_2(t)$ and $w_4(t)$, respectively.

The transverse displacement within the element is assumed to be a cubic equation in x (as in the case of static deflection of a beam):

$$w(x,t) = a(t) + b(t)\, x + c(t)\, x^2 + d(t)\, x^3 \qquad (2\text{-}13)$$

The unknown joint displacements must satisfy the conditions

$$\left.\begin{aligned} w(0,t) &= w_1(t) &, \quad \frac{\partial w}{\partial x}(0,t) &= w_2(t)\\ w(l,t) &= w_3(t) &, \quad \frac{\partial w}{\partial x}(l,t) &= w_3(t) \end{aligned}\right\} \qquad (2\text{-}14)$$

Equations (2-13) and (2-14) yield

$$a(t) = w_1(t)$$

$$b(t) = w_2(t)$$

$$c(t) = \frac{1}{l^2}[-3w_1(t) - 2w_2(t)l + 3w_3(t) - w_4(t)l]$$

$$d(t) = \frac{1}{l^3}[2w_1(t) + w_2(t)l - 2w_3(t) + w_4(t)l] \qquad (2\text{-}15)$$

By substituting Eqs. (2-15) into Eq. (2-13), we can express $w(x,t)$ as

$$w(x,t) = \left(1 - 3\frac{x^2}{l^2} + 2\frac{x^3}{l^3}\right) w_1(t) + \left(\frac{x}{l} - 2\frac{x^2}{l^2} + \frac{x^3}{l^3}\right) l w_2(t) + \left(3\frac{x^2}{l^2} - 2x3l3\; w3t + -x2l2 + x3l3\; lw4(t)\right) \qquad (2\text{-}16)$$

This equation can be rewritten as

$$w(x,t) = \sum_{i=1}^{4} N_i(x) w_i(t) \qquad (2\text{-}17)$$

Where $N_i(x)$ are the shape functions given by

$$N_1(x) = 1 - 3\left(\frac{x}{l}\right)^2 + 2\left(\frac{x}{l}\right)^3 \qquad (2\text{-}18)$$

$$N_2(x) = x - 2l\left(\frac{x}{l}\right)^2 + l\left(\frac{x}{l}\right)^3 \qquad (2\text{-}19)$$

$$N_3(x) = 3\left(\frac{x}{l}\right)^2 - 2\left(\frac{x}{l}\right)^3 \qquad (2\text{-}20)$$

$$N_4(x) = -l\left(\frac{x}{l}\right)^2 + l\left(\frac{x}{l}\right)^3 \qquad (2\text{-}21)$$

The kinetic energy, bending strain energy, and virtual work of the element can be expressed as

$$T(t) = \frac{1}{2}\int_0^l \rho A \left\{\frac{\partial w(x,t)}{\partial t}\right\}^2 dx = \frac{1}{2}\dot{\vec{w}}(t)^T [m]\, \dot{\vec{w}}(t) \qquad (2\text{-}22)$$

$$V(t) = \frac{1}{2}\int_0^l E\,I \left\{\frac{\partial^2 w(x,t)}{\partial x^2}\right\}^2 dx = \frac{1}{2}\vec{w}(t)^T [k]\, \vec{w}(t) \qquad (2\text{-}23)$$

$$\delta W(t) = \int_0^l f(x,t)\,\delta w(x,t)\ dx = \delta\vec{w}(t)^T \vec{f}(t) \qquad (2\text{-}24)$$

Where ρ is the density of the beam, E is Young's modulus, I is the moment of inertia of the cross section, A is the area of cross section, and

$$w(t) = \begin{Bmatrix} w_1(t) \\ w_2(t) \\ w_3(t) \\ w_4(t) \end{Bmatrix}, \qquad \dot{\vec{w}}(t) = \begin{Bmatrix} dw_1/dt \\ dw_2/dt \\ dw_3/dt \\ dw_4/dt \end{Bmatrix}$$

$$\delta w(t) = \begin{Bmatrix} \delta w_1(t) \\ \delta w_2(t) \\ \delta w_3(t) \\ \delta w_4(t) \end{Bmatrix}, \qquad \vec{f}(t) = \begin{Bmatrix} f_1(t) \\ f_2(t) \\ f_3(t) \\ f_4(t) \end{Bmatrix}$$

By substituting Eq. (2-16) into Eqs. (2-22) to (2-24) and carrying out the necessary integrations, we obtain

$$[m] = \frac{\rho A l}{420} \begin{bmatrix} 156 & 22l & 54 & -13l \\ 22l & 4l^2 & 13l & -3l^2 \\ 54 & 13l & 156 & -22l \\ -13l & -3l^2 & -22l & 4l^2 \end{bmatrix} \qquad (2\text{-}25)$$

$$[k] = \frac{EI}{l^3} \begin{bmatrix} 12 & 6l & -12 & 6l \\ 6l & 4l^2 & -6l & 2l^2 \\ -12 & -6l & 12 & -6l \\ 6l & 2l^2 & -6l & 4l^2 \end{bmatrix} \qquad (2\text{-}26)$$

2.4 Frame element

A frame element is formulated to model a straight bar of an arbitrary cross-section, which can deform not only in the axial direction but also in the directions perpendicular to the axis of the bar. The bar is capable of carrying both axial and transverse forces, as well as moments. Therefore, a frame element is seen to possess the properties of both truss and beam elements. In fact, the frame structure can be found in most of our real world structural problems see figure (2-6). There are not many structures that deform and carry loadings purely in axial directions nor purely in transverse directions.

The frame element developed is also known in many commercial software packages as the general beam element, or even simply the beam element. Commercial software packages usually offer both pure beam and frame elements, but frame structures are more often used in actual engineering applications. A three-dimensional spatial frame structure can practically take forces and moments of all directions. Hence, it can be considered to be the most general form of element with a one-dimensional geometry.

(a)   (b)
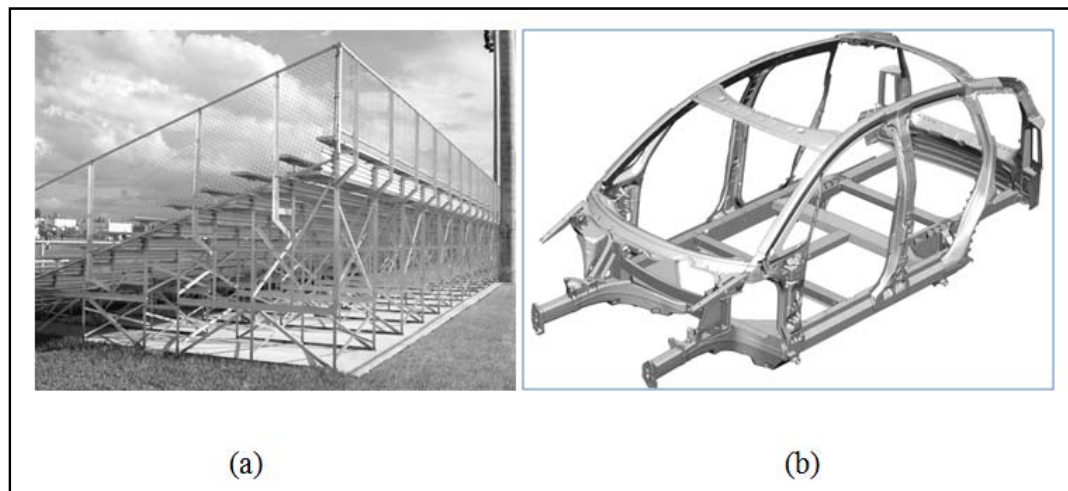
Figure 2.6 Frame Structures

The important note in combination of these two elements is the placement of the use for components in the matrix .i.e. the first three rows refer to the first node components and the second three for the components of second node. As shown in Figure (2-7) .Where the hidden line box refer to 1st node and solid line box refer to 2nd components.
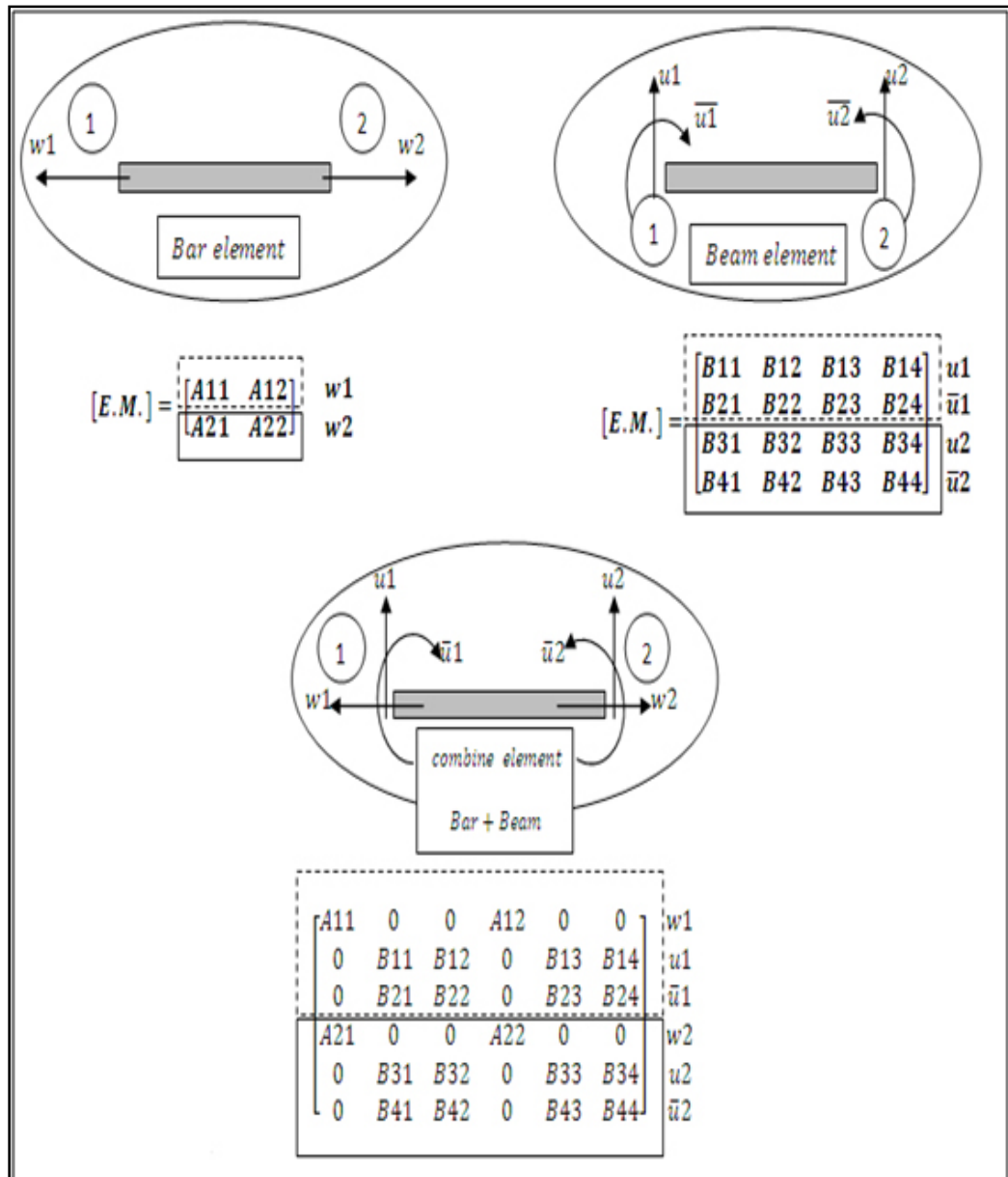
Figure 2.7 Combine Bar and Beam Elements

Where

E.M. = element matrix (mass or stiffness).

A, B just symbols to denote the elements, A for a bar element, B for a beam element.

The frame element matrices can be obtained from Eq.(2-9) , (2-12) ,(2-25) and (2-26)

$$K_{combine} = \begin{bmatrix} \frac{AE}{l} & 0 & 0 & -\frac{AE}{l} & 0 & 0 \\ 0 & \frac{12EI}{l^3} & \frac{6EI}{l^2} & 0 & -\frac{12EI}{l^3} & \frac{6EI}{l^2} \\ 0 & \frac{6EI}{l^2} & \frac{4EI}{l} & 0 & -\frac{6EI}{l^2} & \frac{2EI}{l} \\ -\frac{AE}{l} & 0 & 0 & \frac{AE}{l} & 0 & 0 \\ 0 & -\frac{12EI}{l^3} & -\frac{6EI}{l^2} & 0 & \frac{12EI}{l^3} & -\frac{6EI}{l^2} \\ 0 & \frac{6EI}{l^2} & \frac{2EI}{l} & 0 & -\frac{6EI}{l^2} & \frac{4EI}{l} \end{bmatrix} \tag{2-27}$$

$$M_{combine} = \frac{\rho Al}{420} \begin{bmatrix} 140 & 0 & 0 & 70 & 0 & 0 \\ 0 & 156 & 22l & 0 & 54 & -13l \\ 0 & 22l & 4l^2 & 0 & 13l & -3l^2 \\ 70 & 0 & 0 & 140 & 0 & 0 \\ 0 & 54 & 13l & 0 & 156 & -22l \\ 0 & -13l & -3l^2 & 0 & 22l & 4l^2 \end{bmatrix} \tag{2-28}$$

2.5 Buckling

In engineering, buckling is a failure mode characterized by a sudden failure of a structural member subjected to high compressive stresses, where the actual compressive stress at the point of failure is less than the ultimate compressive stresses that the material is capable of withstanding. This mode of failure is also described as failure due to elastic instability. Mathematical analysis of buckling makes use of an axial load eccentricity that introduces a moment, which does not form part of the primary forces to which the member is subjected.

Study of beam-columns leads to an eigenvalue problem. For example the equation governing onset of buckling of a column subjected to an axial compressive force is N.
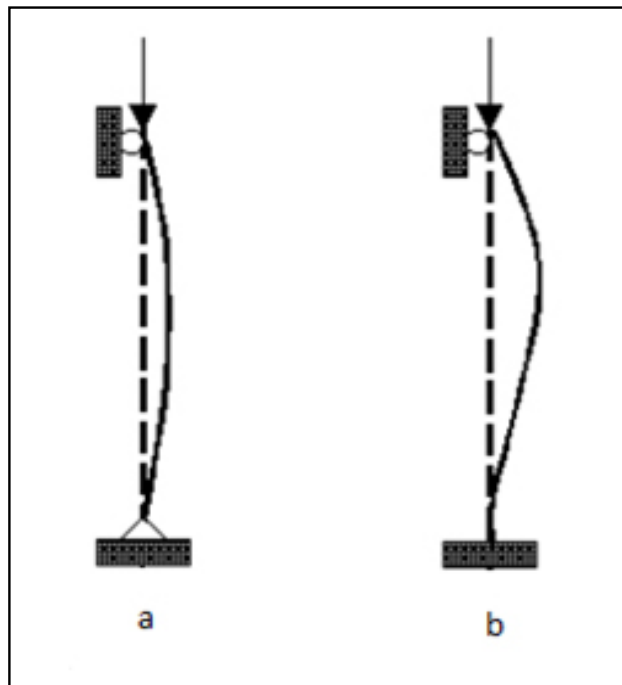
Figure 2.8 (a) pin-pin   (b) fix-pin

$$\frac{d^2}{dx^2}\left(EI\,\frac{d^2w}{dx^2}\right) + N\,\frac{d^2w}{dx^2} = 0 \qquad\qquad (2\text{-}30)$$

Which describes an eigenvalue problem with the smaller value of N is called the *critical buckling load*.

The finite element model of the equation above is

$$[k]\{\Delta\} - N[G]\{\Delta\} = \{Q\} \qquad\qquad (2\text{-}31)$$

Where $\{\Delta\}$ *and* $\{Q\}$ are the columns of generalized displacement and force degree of freedom at the two ends of the Euler-Bernoulli beam element:

$$\{\Delta\} = \begin{Bmatrix} W_1 \\ \left(-\frac{dW}{dx}\right)_1 \\ W_2 \\ \left(-\frac{dW}{dx}\right)_2 \end{Bmatrix} \quad , \quad \{Q\} = \begin{Bmatrix} \left[\frac{d}{dx}\left(EI\,\frac{d^2W}{dx^2}\right) + N^0\,\frac{dW}{dx}\right]_1 \\ \left(EI\,\frac{d^2W}{dx^2}\right)_1 \\ \left[-\frac{d}{dx}\left(EI\,\frac{d^2W}{dx^2}\right) - N^0\,\frac{dW}{dx}\right]_2 \\ \left(-EI\,\frac{d^2W}{dx^2}\right)_2 \end{Bmatrix}$$

Where the subscripts 1 and 2 refer to element nodes 1 and 2 (at $x = x$ *and* $x = x$,*respectively*). The coefficients of stiffness matrix $[k]$ and the stability matrix $[G]$ are:

$$k = \int_{xa}^{xb} EI \frac{d^2\phi}{dx^2} \frac{d^2 \phi}{dx^2} dx \qquad (2\text{-}32)$$

$$GK = \int_{xa}^{xb} EI \frac{d^2\phi}{dx} \frac{d \phi}{dx} dx \qquad (2\text{-}33)$$

Where ϕ are the Hermite cubic interpolations functions . the explicit form of $[GK]$ is

$$[GK] = \begin{bmatrix} 36 & -3h & -36 & -3h \\ -3h & 4h^2 & 3h & -h^2 \\ -36 & 3h & 36 & 3h \\ -3h & -h^2 & 3h & 4h^2 \end{bmatrix} \qquad (2\text{-}34)$$

$$[K_{frame}]\{u\} - P_{cr}[GK_{frame}]\{u\} = \{q\} \qquad (2\text{-}35)$$

Here K_{frame} is the stiffness matrix, GK_{frame} is the geometric stiffness matrix, P_{cr} the critical buckling load and $\{u\}$ $\{q\}$ are the usual nodal displacement and force vectors.

2.6 Transformation from Local Coordinate To Global

The matrices formulated above are for a particular frame element in a specific orientation. A full frame structure usually comprises numerous frame elements of different orientations joined together. As such, their local coordinate system would vary from one orientation to another. To assemble the element matrices together, all the matrices must first be expressed in a common coordinate system, which is called global coordinate system. Figure (2-9).
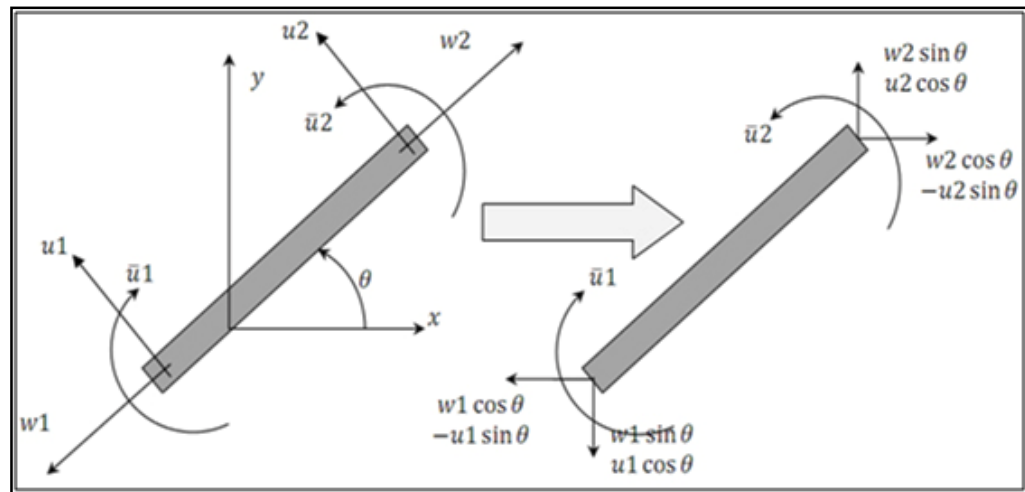
Figure 2.9 Transformations from Local to Global Coordinate

$$[T] = \begin{bmatrix} \cos\theta & \sin\theta & 0 & 0 & 0 & 0 \\ -\sin\theta & \cos\theta & 0 & 0 & 0 & 0 \\ 0 & 0 & 1 & 0 & 0 & 0 \\ 0 & 0 & 0 & \cos\theta & \sin\theta & 0 \\ 0 & 0 & 0 & -\sin\theta & \cos\theta & 0 \\ 0 & 0 & 0 & 0 & 0 & 1 \end{bmatrix} \qquad (2\text{-}36)$$

2.7 Equation of Motion of the Complete System of Finite Elements

Since the complete structure is considered to be an assemblage of several finite element. We shall now extend the equations of motions obtained for single finite elements in the global system to the complete structure. We shall denote the joint displacements of the complete structure in the global coordinate system as $U_1(t), U_2(t), \dots, U_M(t)$ or, equivalently, as a column vector:

$$\vec{U}(t) = \begin{Bmatrix} U_1(t) \\ U_2(t) \\ . \\ . \\ U_M(t) \end{Bmatrix}$$

For convenience, we shall denote the quantities pertaining to an element e in the assemblage by the superscript e .since the joint displacements of any element e can be identified in the vector of joint displacements of the complete structure, the vectors $\vec{U}^{(e)}(t)$ and $\underline{\vec{U}}(t)$ are related:

$$\vec{U}^{(e)}(t) = \left[A^{(e)}\right]\underline{\vec{U}}(t) \tag{2-37}$$

Where $\left[A^{(e)}\right]$ is a rectangular matrix composed of zeros and ones. For example, for element 1 in figure (2-10) , Eq(2-37) becomes

$$\vec{U}^{(1)}(t) \equiv \begin{Bmatrix} U_1(t) \\ U_2(t) \\ U_3(t) \\ U_4(t) \end{Bmatrix} = \begin{bmatrix} 1 & 0 & 0 & 0 & 0 & 0 & 0 \\ 0 & 1 & 0 & 0 & 0 & 0 & 0 \\ 0 & 0 & 1 & 0 & 0 & 0 & 0 \\ 0 & 0 & 0 & 1 & 0 & 0 & 0 \end{bmatrix} \begin{Bmatrix} U_1(t) \\ U_2(t) \\ . \\ . \\ . \\ . \\ . \\ U_8(t) \end{Bmatrix} \tag{2-38}$$

The kinetic energy of the complete structure can be obtained by adding the kinetic energies of individual elements:

$$T = \sum_{e=1}^{E} \frac{1}{2} \, \dot{\vec{U}}^{(e)T} [\overline{m}] \dot{\vec{U}}^{(e)} \tag{2-39}$$

Where E denotes the number of elements in the assemblage. By differentiating Eq(2-37), the relation between the velocity vector can be derived :

$$\dot{\vec{U}}^{(e)}(t) = [A^{(e)}] \dot{\underline{\vec{U}}}^{(e)} \tag{2-40}$$

Substitution of Eq(2-40) into (2-39) leads to

$$T = \sum_{e=1}^{E} \frac{1}{2} \, \dot{\underline{\vec{U}}}^{T} [A^{(e)}]^{T} [\overline{m}^{(e)}] [A^{(e)}] \dot{\underline{\vec{U}}}^{(e)} \tag{2-41}$$

The kinetic energy of the complete structure can also be expressed in terms of joint velocities of the complete structure $\dot{\underline{\vec{U}}}$:

$$T = \frac{1}{2} \, \dot{\underline{\vec{U}}}^{T} [\underline{M}] \, \dot{\underline{\vec{U}}} \tag{2-42}$$

Where $[\underline{M}]$ is called the mass matrix of the complete structure. A comparison of Eqs(2-41) and (2.42) gives the relation

$$[\underline{M}] = \sum_{e=1}^{E} [A^{(e)}]^{T} [\overline{m}^{(e)}] [A^{(e)}] \tag{2-43}$$

Similarly, by considering strain energy, the stiffness matrix of the complete structure, $[\underline{K}]$, can be expressed as

$$[\underline{K}] = \sum_{e=1}^{E} [A^{(e)}]^{T} [\overline{k}^{(e)}] [A^{(e)}] \tag{2-44}$$

Finally the consideration of virtual work yields the vector of joint forces of the complete structure, $\vec{F}$:

$$\vec{F} = \sum_{e=1}^{E} [A^{(e)}]^T \vec{f}^{(e)}$$ (2-45)

Once the mass and stiffness matrices and the force vector are known, Lagrange's equations of motion for the complete structure can be expressed as

$$[\underline{M}]\ddot{\vec{U}} + [\underline{K}]\vec{U} = \vec{F}$$ (2-46)

Note that the joint force vector $\vec{F}$ in Eq (2.46) was generated by considering only the distributing loads acting on the various elements. If there is any concentrated load acting along the joint displacement $U_i(t)$, it must be added to the ith component of $\vec{F}$.
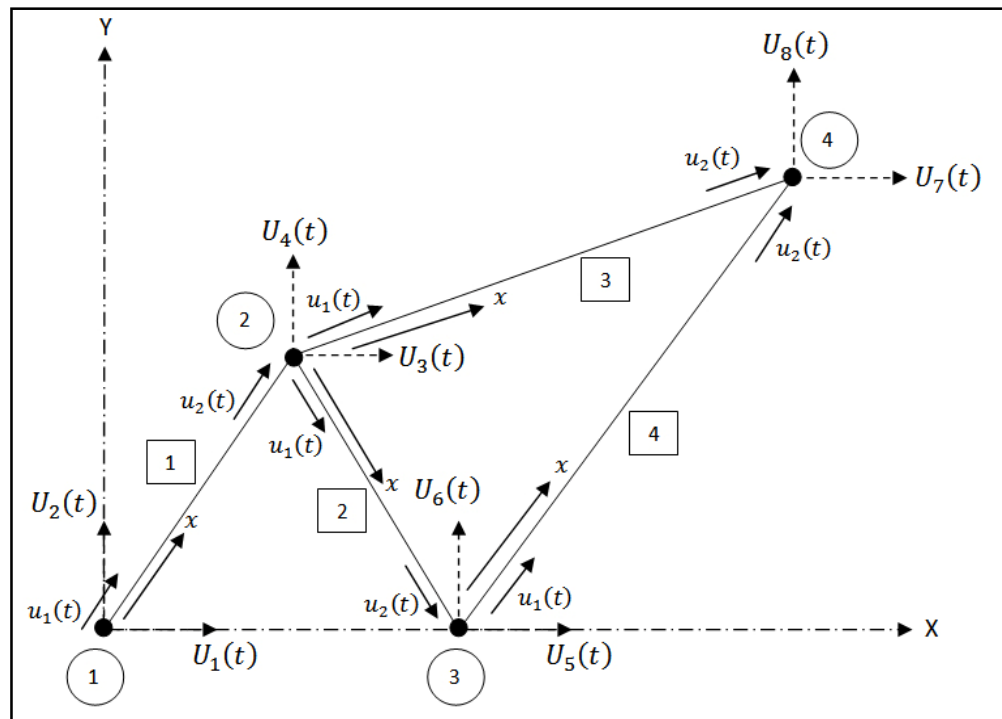
Figure 2.10 a dynamical system (truss) idealized as an assemblage of four bar elements.

CHAPTER THREE
CRACK

3.1 Cracks

Cracks can be caused as a result of the accidental mechanical damage .Other reasons for the appearance of cracks are erosion and corrosion phenomena and the fatigue strength of materials. Cracks on a structure member can change its local flexibility. The stiffness of a structure depends on the localization of the damage and its magnitude, as a result the natural frequency of the structure change.

The crack effect depends on three parameters;

1. Crack depth
2. Crack direction with respect to load direction.
3. Crack location (distance) on a beam from the fixed end.

3.2 Crack modes

There are three ways of applying a force to enable a crack to propagate:

1. Mode I crack – Opening mode (a tensile stress normal to the plane of the crack)
2. Mode II crack – Sliding mode (a shear stress acting parallel to the plane of the crack and perpendicular to the crack front plane)
3. Mode III crack – Tearing mode (a shear stress acting parallel to the plane of the crack and parallel to the crack front plane)
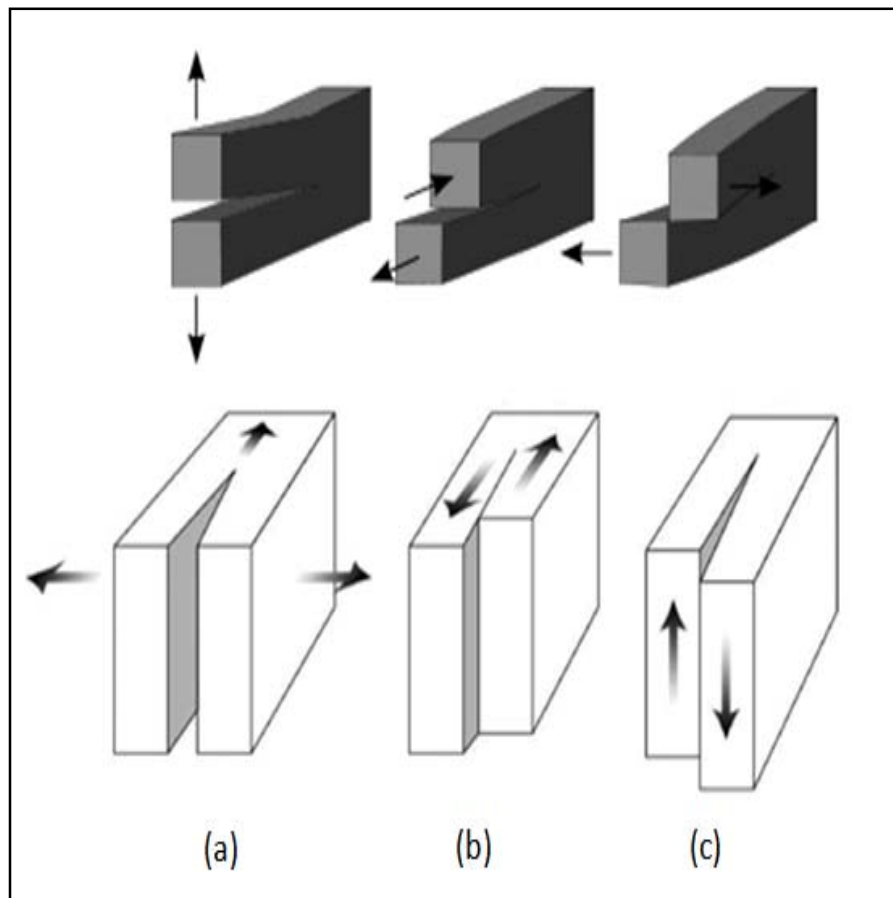
Figure 3.1 (a) Opening mode, (b) Sliding mode, (c) Tearing mode

3.3 The Local Flexibility Due To the Crack

The cracked beam problem has attracted the attention of many researchers in recent years. Various kinds of analytical, semi-analytical and numerical methods have been employed to solve the problem of cracked beams. A common method employed in the analysis is the finite element method (FEM). The key point in using the FEM is how to appropriately obtain the stiffness matrix for the cracked beam element. When the stiffness matrix is obtained, the inverse of this matrix will give the flexibility matrix of the element.

The total flexibility matrix of the cracked beam element includes two parts. The first part is the flexibility matrix of uncracked beam. The second part is the additional flexibility matrix due to the existence of the crack, which leads to energy release and additional deformation of the structure.

In this work, cross section of the beam is assumed to be rectangular. The additional strain energy due to the existence of a crack can be expressed as:

$$\Pi_c = \int_{A_c} G \ dA, \tag{3-1}$$

Where G is the strain energy release rate function and A_c is the effective cracked area. The strain energy release rate function G can be expressed as

$$G = \frac{1}{E'} [(K_{I1} + K_{I2} + K_{I3})^2 + (K_{II2})^2], \tag{3-2}$$

Where $E' = E$ for plane stress problem, $E' = E/(1 - \mu^2)$ for plane strain problem; K_{I1}, K_{I2}, K_{I3} and K_{II2} are the stress intensity factor due to loads $P1, P2$ and $P3$;

$$K_{I1} = \frac{P_1}{bh} \sqrt{\pi\xi} \, F1\left(\frac{\xi}{h}\right) \quad , \quad K_{I2} = \frac{6P_2L_C}{bh^3} \sqrt{\pi\xi} \, F2\left(\frac{\xi}{h}\right) \tag{3-3, 3-4}$$

$$K_{I3} = \frac{6P_3}{bh^2} \sqrt{\pi\xi} \, F2\left(\frac{\xi}{h}\right) \quad , \quad K_{II2} = \frac{P_2}{bh} \sqrt{\pi\xi} \, FII\left(\frac{\xi}{h}\right) \tag{3-5, 3-6}$$

K_{I2} Ignored according to (A.S. Sekhar, 1999) and (A.S. Sekhar, & B.S. Prabhu, 1992)

$$F1(s) = \sqrt{\frac{\tan(\pi s/2)}{(\pi s/2)}} \, \frac{0.752 + 2.02s + 0.37(1 - \sin(\pi s/2))^3}{\cos(\pi s/2)} \tag{3-7}$$

$$F2(s) = \sqrt{\frac{\tan(\pi s/2)}{(\pi s/2)}} \, \frac{0.923 + 0.199(1 - \sin(\pi s/2))^4}{\cos(\pi s/2)} \tag{3-8}$$

$$FII(s) = \frac{1.122 - 0.561s + 0.085s^2 + 0.18s^3}{\sqrt{1-s}} \tag{3-9}$$

In which ξ is the crack depth .F1, F2 and F3 are the correction factors for stress intensity factors. It is worth nothing that a is the final crack depth while ξ is the crack depth during the process of penetration from zero to the final depth.

Using Paris equation, we have

$$\delta_i = \frac{\partial \, \Pi_c}{\partial \, P_i} \quad (i = 1, 2, 3). \tag{3-10}$$

By definition, the elements of the overall additional flexibility matrix c_{ij} can be expressed as

$$c_{ij} = \frac{\partial \delta_i}{\partial P_i} = \frac{\partial^2 \Pi_c}{\partial P_i \partial P_j} \quad (i, j = 1, 2, 3). \tag{3-11}$$

Substituting Eqs. (3-3)- (3-6) into Eq. (3-2), and then into Eqs. (3-1) and (3-11), considering that all K's are independent of η, we obtain.

$$C_{ij} = \frac{b}{E'} \frac{\partial^2}{\partial P_i \partial P_j} \int_0^a \left\{ \left[\frac{P_1}{bh} \sqrt{\pi\xi} \, F_1 \left(\frac{\xi}{h} \right) + \frac{6P_2 L_c}{bh^2} \sqrt{\pi\xi} \, F_2 \left(\frac{\xi}{h} \right) + \frac{6P_3}{bh^2} \sqrt{\pi\xi} F_2 \left(\frac{\xi}{h} \right) \right]^2 + \right.$$

$$\left. \frac{P_2{}^2}{b^2 h^2} \pi\xi \, F_{II}{}^2 \left(\frac{\xi}{h} \right) \right\} \, d\xi \quad (i, j = 1, 2, 3).$$

$$\tag{3-12}$$

$$c_{ij} = \begin{bmatrix} c11 & c12 & c13 \\ c21 & c22 & c23 \\ c31 & c32 & c33 \end{bmatrix} \tag{3-13}$$

3.4 The crack finite element model

A finite element model is developed to represent a cracked beam element of length d and the crack is located at a distance d1 from the left end of the element as shown in figure 3-2.
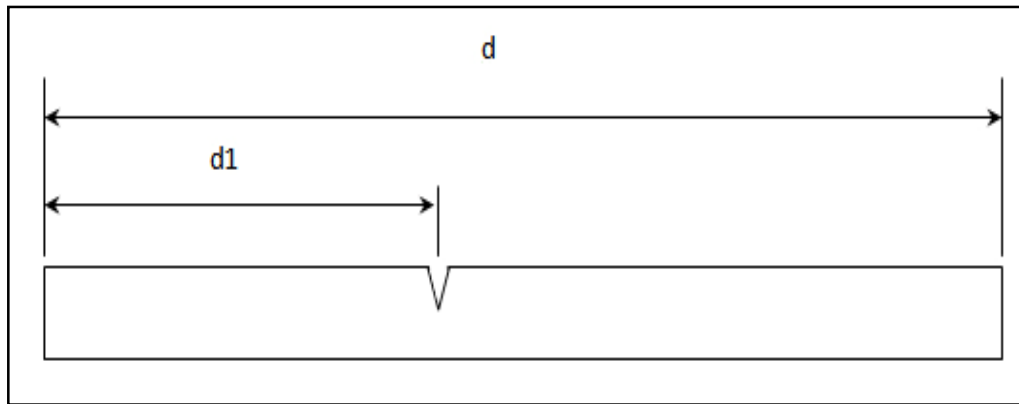
Figure 3.2 Crack Locations in Crack Element

The element is then considered to be split into two segments by the crack. The left and right segments are represented by non-cracked sub elements while the crack is represented by a massless rotational spring of length zero. The reason of the fact that the crack represents net ligament effect created by loadings, this effect can be related to the deformation of the net ligament through the compliance expressions by replacing the net ligament with a fictitious spring connecting both faces of the crack (Yokoyama T, Chen MC.1998).

So, the spring effects are introduced to the system by using the local flexibility matrix given by Eq.(3-13) . The cracked element has 2 nodes with three degrees of freedom in each node. They are denoted as lateral bending displacements ($\mathcal{V}_1, \mathcal{V}_2$), slopes ($\hat{\mathcal{V}}_1, \hat{\mathcal{V}}_2$), and longitudinal displacements ($\mathcal{U}_1, \mathcal{U}_2$).

For $0 \leq x \leq d_1$,

$$\mathcal{V}_1(x) = a_1 + a_2\, x + a_3\, x^2 + a_4\, x^3 \tag{3-14a}$$

$$\mathcal{U}_1 = c_1 + c_2\, x$$

For $d_1 \leq x \leq d$,

$$\mathcal{V}_2(x) = b_1 + b_2\, x + b_3\, x^2 + b_4\, x^3 \tag{3-14b}$$

$$\mathcal{U}_2 = d_1 + d_2\, x$$

Lateral bending

$$\mathcal{V}_1(0) = q_1 \quad , \quad \dot{\mathcal{V}}_1(0) = q_2 \tag{3-15a}$$

$$\mathcal{V}_2(d) = q_3 \quad \dot{\mathcal{V}}(d) = q_4$$

Longitudinal displacement

$$\mathcal{U}_1(0) = q_5 \quad , \quad \mathcal{U}_2(d) = q_6 \tag{3-15b}$$

At the crack location d_1 , the flexibility concept requires:

For lateral bending:

Continuity of the vertical displacement

$$\mathcal{V}_1(d_1) = \mathcal{V}_2(d_1) \tag{3-16a}$$

Discontinuity of the cross-sectional rotation (slope)

$$\grave{\mathcal{V}}_2(d_1) = \grave{\mathcal{V}}_1(d_1) + c_{33}\, M_1\,(d_1) \tag{3-16b}$$

Where $\quad M_1(d_1) = E\,I\,\mathcal{V}_1{}''|_{x=d_1}$

Continuity of bending moment

$$M_1(d_1) = M_2(d_1) \tag{3-16c}$$

Continuity of shear force

$$S_1(d_1) = S_2(d_1) \tag{3-16d}$$

For longitudinal displacement

Discontinuity of longitudinal displacement

$$\mathcal{U}_2(d_1) = \mathcal{U}_1(d_1) + c_{11}\, T_1(d_1) \tag{3-17a}$$

Where $\quad T_1(d_1) = E\,I\,\mathcal{U}_1{}'|_{x=d_1}$

Continuity of force

$$T_1(d_1) = T_2(d_1) \qquad\qquad (3\text{-}17b)$$

By considering Eq.3-10 describing the displacement for the left and right part if the element and rearranging Eqs.(3-15)-(3-17) , the nodal displacement can be expressed in matrix forms as

$$
\begin{Bmatrix} q_1 \\ q_2 \\ 0 \\ 0 \\ 0 \\ 0 \\ q_3 \\ q_4 \end{Bmatrix}
=
\begin{bmatrix}
1 & 0 & 0 & 0 & 0 & 0 & 0 & 0 \\
0 & 1 & 0 & 0 & 0 & 0 & 0 & 0 \\
0 & 0 & 1 & 0 & 0 & 0 & -1 & 0 \\
0 & 0 & 0 & 1 & 0 & 0 & 0 & -1 \\
-1 & 0 & S1 & S2 & 1 & 0 & 0 & 0 \\
0 & -1 & S3 & S4 & 0 & 1 & 0 & 0 \\
0 & 0 & 0 & 0 & 1 & d & d^2 & d^3 \\
0 & 0 & 0 & 0 & 0 & 1 & 2d & 3d^2
\end{bmatrix}
\begin{Bmatrix} a_1 \\ a_2 \\ a_3 \\ a_4 \\ b_1 \\ b_2 \\ b_3 \\ b_4 \end{Bmatrix}
\qquad (3\text{-}18)
$$

$$
\begin{Bmatrix} q_5 \\ 0 \\ 0 \\ q_6 \end{Bmatrix}
=
\begin{bmatrix}
1 & 0 & 0 & 0 \\
0 & 1 & 0 & -1 \\
-1 & S5 & 1 & 0 \\
0 & 0 & 1 & d
\end{bmatrix}
\begin{Bmatrix} c_1 \\ c_2 \\ d_1 \\ d_2 \end{Bmatrix}
\qquad (3\text{-}19)
$$

Where

$$S1 = 2\,c_{11}\,E\,I\,d_1$$
$$S2 = 6\,c_{11}\,E\,I\,d_1{}^2$$
$$S3 = -2\,c_{11}\,E\,I$$
$$S4 = -6\,c_{11}\,E\,I\,d_1$$
$$S5 = -c_{33}\,E\,I$$

CHAPTER FOUR
THEORY OF STABILITY ANALYSIS

4.1 Static stability

The modern use of steel and high-strength alloys in engineering structures, especially in bridges, ships and aircraft, has made elastic instability a problem of great importance. Urgent practical requirements have given rise in recent years to extensive theoretical investigations of the conditions governing the stability of beams, plates and shells.

The first problems of elastic instability, concerning lateral buckling of compressed members, were solved about 400 years ago by L. Euler. At that time the relatively low strength of materials necessitated stout structural members for which the question of elastic stability is not of primary importance. Thus Euler's theoretical solution, developed for slender bars, remained for a long time without a practical application. Only with the beginning of extensive steel constructions did the question of buckling of compression members become of practical importance. The use of steel led naturally to types of structures embodying slender compression members, thin plates and thin shells.

Stability problems can be treated in a general manner using the energy methods. As an introduction to such methods, the basic criteria for determining the stability of equilibrium is derived in this study for, conservative linearly elastic systems.

To establish the stability criteria, a function Π, called the potential of the system must be formulated. This function is expressed as the sum of the internal potential energy U (strain energy) and the potential energy Λ of the external forces that act on a system, i.e.,

$$\Pi = U + \Lambda \qquad\qquad (4.1)$$

Disregarding a possible additive constant, $\Lambda = -W_e$, i.e., the loss of potential energy during the application of forces is equal to the work done on the system by external forces. Hence, equation (4.1) can be rewritten as

$$\Pi = U - W_e \qquad\qquad (4.2)$$

As is known from classical mechanics, for equilibrium the total potential Π must be stationary, therefore its variation $\delta\Pi$ must equal zero,

$$\delta\Pi = \delta U - \delta W_e = 0 \qquad\qquad (4.3)$$

For conservative, elastic systems this relation agrees with $\delta W_e = \delta W_{ei}$ equation (δW_{ei} : the external work on the internal elements of a body, δW_e : the total work), which states the virtual work principle. This condition can be used to determine the position of equilibrium. However, equation (4.3) cannot discern the type of equilibrium and there by establish the condition for the stability of equilibrium. Only by examining the higher order terms in the expression for increment in Π as given by Taylor's expansion must be examined. Such an expression is

$$\Delta\Pi = \delta\Pi + \frac{1}{2!}\delta^2\Pi + \frac{1}{3!}\delta^3\Pi + ... \qquad\qquad (4.4)$$

Since for any type of equilibrium $\delta\Pi = 0$, it is the first nonvanishing term of this expansion that determines the types of equilibrium. For linear elastic systems the second term suffices. Thus, from equation (4.4), the stability criteria are

$\delta^4\Pi > 0$ for stable equilibrium

$\delta^4\Pi < 0$ for unstable equilibrium

$\delta^4\Pi = 0$ for neutral equilibrium associated with the critical load

The meaning of these expressions may be clarified by examining the simple example shown in Figure 4.1, where the shaded surfaces represent three different

types of Π functions. It can be concluded at once that the ball on the concave spherical surface (a) is in stable equilibrium, while the ball on the convex spherical surface (b) is in unstable equilibrium. The ball on the horizontal plane (c) is said to be in different or neutral equilibrium. The type of equilibrium can be ascertained by considering the energy of the system. In the first case (Figure 4.1(a)) any displacement of the ball from its position of equilibrium will raise the center of gravity. A certain amount of work is required to produce such a displacement; thus the potential energy of the system increases for any small displacement from the position of equilibrium. In the second case (Figure 4.1 (b)), any displacement from the position of equilibrium will decrease the potential energy of the system. Thus in the case of stable equilibrium the energy of the system is a minimum and in the case of unstable equilibrium it is a maximum. If the equilibrium is indifferent (Figure 4.1 (c)), there is no change in energy during a displacement.

| (a) | (b) | (c) |
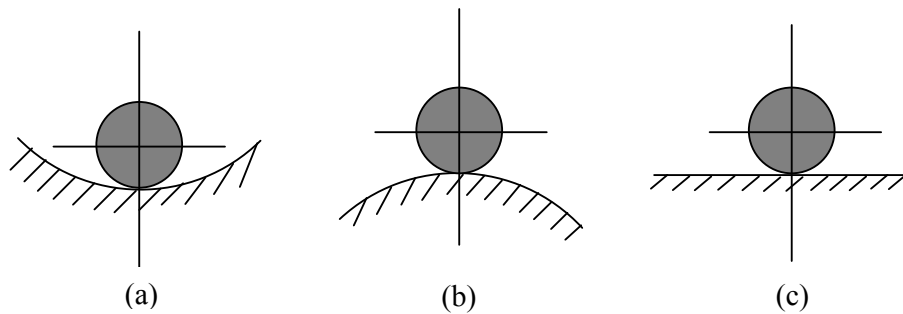
Figure 4.1 Three cases of equilibrium

For each of the systems shown in figure 4.1 stability depends only on the shape of the supporting surface and does not depend on the weight of the ball. In the case of a compressed column or plate it is found that the column or plate may be stable or unstable, depending on the magnitude of the axial load.

4.1.1   The formulation of static stability

If the displacements are large, then the deformed geometry will obviously differ significantly from the undeformed geometry. This results in a nonlinear strain-displacement relationship. Large displacement problems of this type are said to be "geometrically nonlinear" which is a feature of elastic instability problems. From the design point of view calculation of the critical loads of structures is of considerable importance. In general case the strain energy of a system,

$$U = \frac{1}{2}\{q\}^{T}[K_{e}]\{q\} \tag{4.5}$$

The additional strain energy which is function of applied external load

$$U_{g} = \frac{1}{2}\{q\}^{T}[K_{g}]\{q\} \tag{4.6}$$

In which $[K_{e}]$ and $[K_{g}]$ are elastic stiffness and geometric stiffness matrices.

The total potential energy of a system in equilibrium is constant when small displacements are given to the system. So

$$\delta(U + U_{g}) = 0 \tag{4.7}$$

$(U + U_{g})$ and δ define the total potential energy and the change of the virtual displacements. Applying the above formulation to equations (4.5) and (4.6)

$$\left[[K_{e}] - P[K_{g}]\right]\{q\} = 0 \tag{4.8}$$

The roots of the eigenvalue equation (4.8) gives the buckling loads and the eigenvectors of this equation are the buckling mode shapes.

4.2 Dynamic stability

If the loading is nonconservative the loss of stability may not show up by the system going into another equilibrium state but by going into unbounded motion. To encompass this possibility we must consider the dynamic behavior of the system because stability is essentially a dynamic concept.

Whenever static loading of a particular kind causes a loss of static stability, vibrational loading of the same kind will cause a loss of dynamic stability. Such a loading is characterized by the fact that it is contained as a parameter on the left hand side of the equations of perturbed equilibrium (or motion). We will call such loading parametric; this term is more appropriate because it indicates the relation to the phenomenon of parametric resonance.

In the mechanical systems, parametric excitation occurs due to the following reasons;

   a) periodic change in rigidity

   b) periodic change in inertia

   c) periodic change in the loading of the system.

In this section firstly the differential equation related with dynamic stability is introduced and then, the determination of boundaries of the regions of instability and the amplitudes of parametrically excited vibrations for multi-degrees of freedom systems is presented.

An important special case of linear variational equations with variable coefficients occurs when the coefficient functions are periodic. Owing to their great practical importance in the theory of vibrations, a special theory has even been developed for the systems of differential equations with periodic coefficients are known as Mathieu-Hill differential equation. The Hill differential equation is in the following form,

$$\overset{''}{y}+\left[a-bf(t)\right]y=0 \qquad\qquad (4.9)$$

in which a and b are constant parameters, and f(t) is a function having the period T. The prime denotes differentiation with respect to time. If $f(t)=2\cos 2t$ substituted into the Hill differential equation, the Mathieu differential equation which may be described a system that is subjected to parametric excitation is obtained in the standard form as

$$\overset{''}{y}+\left[a-2b\cos 2t\right]y=0 \qquad\qquad (4.10)$$

The results of solving Mathieu's equation (4.10) for two different combinations of a and b are shown in figure 4.2. Although the parameter b of the system is the same in both cases (b=0,1), the vibrations are greatly different because of the difference between the values of the parameter a (a=1; a=1,2). In the first case, they increase, i.e., the system is dynamically unstable, while in the second case they remain bounded, i.e., the system is dynamically stable.
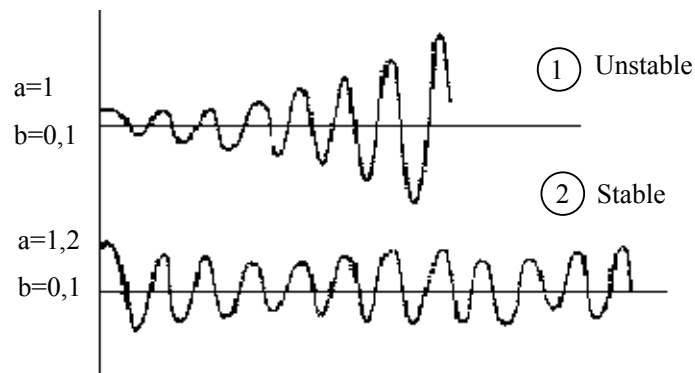
Figure 4.2 Two solutions of Mathieu's equation

The greatest importance, for practical purpose, is attached to the boundaries between the regions of stable and unstable solutions. This problem has been well studied, and the final results have been presented in the form of a diagram plotted in the plane of the parameters a and b. It is called the Haines-Strett diagram. Figure 4.3 shows part of a Haines-Strett diagram for small values of the parameter b. Any given system having the parameters a and b corresponds to the point with the co-ordinates

a and b on the Haines-Strett diagram. If the representative point is in the shaded parts of the diagram, the system is dynamically unstable, while stable systems correspond to representative points in the unshaded parts. The shaded regions are called the regions of dynamic instability.
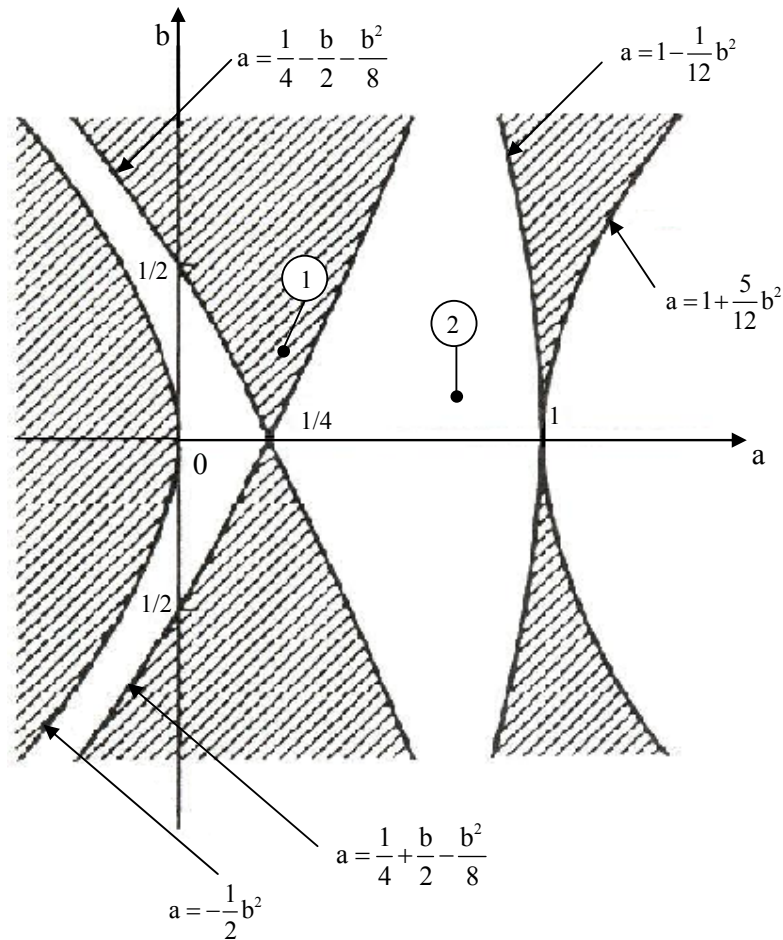
Figure 4.3 Part of Haines-Strett diagram the points ◯ and ② correspond to the solutions 1 and 2 in figure 4.2

As an example, the diagram in figure 4.3 shows the points 1 and 2 corresponding to the parameter $a_1=1$ and $b_1=0,1$, and $a_2=1,2$ and $b_2=0,1$. The point 1 is in the region of dynamic instability and the vibration occurs with increasing amplitude as shown in figure 4.2. The point 2 is in the stable region and it corresponds to motion with a limited amplitude.

4.2.1 The formulation of dynamic stability

The matrix equation for the free vibration of an axially loaded system can be written as:

$$[M]\{\ddot{q}\} + [K_e]\{q\} - [K_g]\{q\} = 0 \qquad (4.11)$$

where

$\{q\}$ is the generalized coordinates

$[M]$ is the inertia matrix

$[K_e]$ is the elastic stiffness matrix

$[K_g]$ is the geometric stiffness matrix, which is a function of the compressive axial load P(t).

For a system subjected to a periodic force

$$P(t) = P_o + P_t \, f(t) \qquad (4.12)$$

The static and time dependent components of the load can be represented as a fraction of the fundamental static buckling load P*, in which $P_o = \alpha P*$, $P_t = \beta P*$. By writing $P = \alpha P * + \beta P * f(t)$ then the matrix equation K_g becomes

$$K_g = \alpha P * [K_{gs}] + \beta P * [K_{gt}] \qquad (4.13)$$

where the matrices $[K_{gs}]$ and $[K_{gt}]$ reflect the influence of P_o and P_t respectively. Substituting Equation (4.13) into Equation (4.11), the following system of n second order differential equations with a periodic coefficient of the known Mathieu-Hill type is obtained;

$$[M]\{\ddot{q}\}+\Big[[K_e]-\alpha P*[K_{gs}]-\beta P*f(t)[K_{gt}]\Big]\{q\}=0 \qquad (4.14)$$

f(t) is a periodic function with period T. Therefore

$$f(t+T)=f(t) \qquad (4.15)$$

Equation (4.14) is a system of n second order differential equations which may be written as

$$\{\ddot{q}(t)\}+[Z]\{q(t)\}=0 \qquad (4.16)$$

where

$$[Z]=[M]^{-1}\Big[[K_e]-\alpha P*[K_{gs}]-\beta P*[K_{gt}]\Big] \qquad (4.17)$$

It is convenient to replace the n second order equations with 4n first order equations by introducing

$$\{h\}=\begin{Bmatrix} q \\ \dot{q} \end{Bmatrix} \qquad (4.18)$$

and

$$[\phi]=\begin{bmatrix} 0 & -[I] \\ [Z] & 0 \end{bmatrix} \qquad (4.19)$$

then, equation (4.16) becomes

$$\{\dot{h}(t)\}+[\phi(t)]\{h(t)\}=\begin{Bmatrix} \dot{q} \\ \ddot{q} \end{Bmatrix}+\begin{bmatrix} 0 & -[I] \\ [Z] & 0 \end{bmatrix}\begin{Bmatrix} q \\ \dot{q} \end{Bmatrix}=0 \qquad (4.20)$$

Equation (4.19) needs not be solved completely in order to determine the stability of the system. It is merely necessary to determine whether the solution is bounded or unbounded.

It is assumed that the 4n linearly independent solutions of equation (4.20) are known over the interval t = 0 to t = T. Then they may be represented in matrix form as

$$[H(t)] = \begin{bmatrix} h_{1,1} & . & . & . & h_{1,2n} \\ . & . & . & . & . \\ . & . & . & . & . \\ . & . & . & . & . \\ h_{2n,1} & . & . & . & h_{2n,2n} \end{bmatrix} \qquad (4.21)$$

Since f(t), and therefore $[\phi(t)]$ is periodic with period T, then the substitution t = t + T will not alter the form of the equations, and the matrix solutions, at time t + T, $[H(t+T)]$ may be obtained from $[H(t)]$ by a linear transformation

$$[H(t+T)] = [R][H(t)] \qquad (4.22)$$

where $[R]$ is the transformation matrix and is composed only of constant coefficients.

It is desirable to find a set of solutions for which the matrix $[R]$ can be diagonalized. Hence the ith solution vector after period T, $\{\bar{h}(t+T)\}_i$ may be determined from $\{\bar{h}(t)\}_i$ using the simple expression

$$\{\bar{h}(t+T)\}_i = \rho_i \{\bar{h}(t)\}_i \qquad (4.23)$$

The behavior of the solution is determined by ρ_i.

If $\rho_i > 1$, then the amplitude of vibration will increase with time. If $\rho_i < 1$, then the amplitude will decrease. For $\rho_i = 1$, the amplitude will remain unchanged, and this represents the stable boundary.

In order to diagonalize the matrix $\left[R\right]$, the characteristic equation

$$\left|\left[R\right] - \rho\left[I\right]\right| = 0 \qquad (4.24)$$

must be solved for its 2n roots, where $\left[I\right]$ is the identity matrix. The roots of the equations, ρ_i, are eigenvalues, each having a corresponding eigenvector.

The 2n resulting eigenvectors are chosen as the 2n solutions to equation (4.20). They can be placed in a matrix, $\left[\overline{H}(t)\right]$, which will then satisfy the expression

$$\left[\overline{H}(t)\right] = \left[\overline{R}\right]\left[\overline{H}(t+T)\right] \qquad (4.25)$$

where

$$\left[\overline{R}\right] = \begin{bmatrix} \rho_1 & 0 & . & . & 0 \\ 0 & \rho_2 & . & . & 0 \\ . & . & . & . & . \\ . & . & . & . & . \\ 0 & . & . & 0 & \rho_{2n} \end{bmatrix} \qquad (4.26)$$

$\left[\overline{R}\right]$ is the diagonalized matrix of $\left[R\right]$ composed of the 4n eigenvalues of equation (4.24).

The periodic vector, $\{Z(t)\}_i$, with period T is introduced so that

$$\{\overline{h}(t)\}_i = \{Z(t)\}_i\, e^{(t/T)\ln\rho_i} \qquad (4.27)$$

For an even function of time like $\left[\phi(t)\right]$, it is true that

$$\left[\phi(t) \right] = \left[\phi(-t) \right] \tag{4.28}$$

Hence equation (4.27) can be written as

$$\left\{ \overline{h}(-t) \right\}_i = \left\{ Z(-t) \right\}_i e^{-(t/T)\ln \rho_i} \tag{4.29}$$

then

$$\left\{ \overline{h}(-t) \right\}_i = \left\{ Z(-t) \right\}_i e^{(t/T)\ln(1/\rho_i)} \tag{4.30}$$

It is clear from (4.30) that $1/\rho_i$ is also an eigenvalue. This property is not restricted to even functions, but is also preserved in the case of arbitrary periodic functions as shown by Bolotin, (1964).

In general, the eigenvalues ρ_i are complex numbers of the form

$$\rho_i = a_i + j b_i \tag{4.31}$$

and the natural logarithm of a complex number is given by

$$\ln \rho_i = \ln \left| \rho_i \right| + j \ (\text{argument } \rho) \tag{4.32}$$

or in this case

$$\ln \rho_i = \ln \sqrt{a_i^2 + b_i^2} + j \tan^{-1}(b_i / a_i) \tag{4.33}$$

where $j = \sqrt{-1}$

From equation (4.27), it is clear that if the real part of $\log \rho_i$ is positive for any of the solutions, then that solution will be unbounded with time. A negative real part means that the corresponding solution will damp out with time. It therefore follows that the boundary case for a given solution is that for which the characteristic exponent has a zero real part. This is identical to saying that absolute value of ρ_i is unity. For the system to remain stable, every one of the solutions must remain

bounded. If even one of the solutions has a characteristic exponent which is positive, then the corresponding solution is unbounded and therefore the system is unstable. It has been shown that if ρ_i is a solution, then $1/\rho_i$ is also a solution. These two solutions can be written as

$$\rho_i = a_i + jb_i \qquad (4.34)$$

$$\rho_{i+n} = (a_i - jb_i)/(a_i^2 + b_i^2) \qquad (4.35)$$

Another restriction on the solutions of the characteristic equation is that the complex eigenvalues must occur in complex conjugate pairs. Hence it follows that ρ_{i+1} and ρ_{i+n+1} are also solutions where

$$\rho_{i+1} = a_i - jb_i \qquad (4.36)$$

$$\rho_{i+n+1} = (a_i + jb_i)/(a_i^2 + b_i^2) \qquad (4.37)$$

These solutions are presented in figure 4.4 which shows a unit circle in the complex plane. The area inside the unit circle represents stable or bounded solutions, while the area outside the unit circle represents unstable or unbounded solutions. For each stable solution which lies inside the circle, there corresponds an unstable solution outside the circle due to the reciprocity constraint. Therefore the only possible stable solutions must lie on the unit circle.

Points on this unit circle may be represented in polar co-ordinates by $r = 1$ and $\theta = \tan^{-1} b/a$ where $-\pi \leq \theta \leq \pi$. For each root on the upper semicircle, there is a corresponding root on the lower semicircle due to the fact that the roots occur in complex conjugate pairs. The logarithm of ρ_i, when ρ_i lies on the unit circle will be

$$\ln \rho_i = j\theta \qquad (4.38)$$

and equation (4.27) becomes

$$\{\overline{h}(t)\}_i = \{Z(t)\}_i \, e^{j\left(\frac{\theta t}{T}\right)} \qquad (4.39)$$
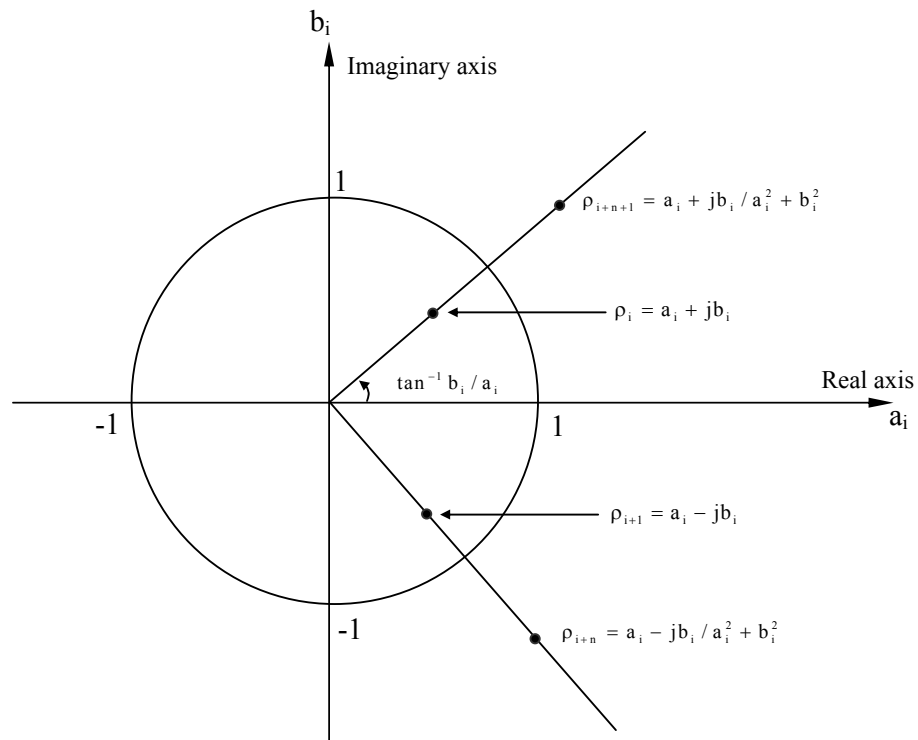
Figure 4.4 Unit circle in the complex plane

Since the eigenvalues occur in complex conjugate pairs, the limiting values of θ are zero and π.

When $\theta = 0$, equation (4.39) becomes

$$\{\overline{h}(t)\}_i = \{Z(t)\}_i \tag{4.40}$$

and, therefore, the solution $\{\overline{h}(t)\}$ is periodic with period T when $\theta = \pi$, equation (4.39) becomes

$$\{\overline{h}(t)\}_i = \{Z(t)\}_i \, e^{j\left(\frac{\pi t}{T}\right)} \tag{4.41}$$

$$\left\{\overline{h}(t+2T)\right\}_i = \left\{Z(t+2T)\right\}_i e^{j\left(\frac{\pi(t+2T)}{T}\right)} = \left\{\overline{h}(t)\right\}_i \quad (4.42)$$

It is clear from equation (4.42) that the solution $\left\{\overline{h}(t)\right\}$ is also periodic with a period 2T.

It can be concluded that equation (4.11) has periodic solutions of period T and 2T. Also the boundaries between stable and unstable regions are formed by periodic solutions of period T and 2T.

For a system subjected to the periodic force

$$P = P_0 + P_t \cos \omega t \quad (4.43)$$

Where ω is the disturbing frequency, equation (4.11) becomes

$$[M]\{\ddot{q}\} + \left[\left[K_e\right] - \alpha \, P * \left[K_{gs}\right] - \beta \, P * \cos \omega t \left[K_{gt}\right]\right]\{q\} = 0 \quad (4.44)$$

Now we seek periodic solutions of period T and 2T of equation (4.44) where $T = 2\pi/\omega$.

When a solution of period 2T exists, it may be represented by the Fourier series

$$\{q\} = \sum_{k=1,3,5}^{\infty} \left[\{a\}_k \sin \frac{k\omega t}{2} + \{b\}_k \cos \frac{k\omega t}{2}\right] \quad (4.45)$$

Where $\{a\}_k$ and $\{b\}_k$ are time-independent vectors. Differentiating equation (4.45) twice with respect to time yields

$$\{\ddot{q}\} = \sum_{k=1,3,5}^{\infty} -\left(\frac{k\omega}{2}\right)^2 \left[\{a\}_k \sin \frac{k\omega t}{2} + \{b\}_k \cos \frac{k\omega t}{2}\right] \quad (4.46)$$

Substituting equations (4.45) and (4.46) into equation (4.44) and using the trigonometric relations

$$\sin A + \sin B = 2\,\sin\frac{A+B}{2}\,\cos\frac{A-B}{2}$$

$$\sin A - \sin B = 2\,\cos\frac{A+B}{2}\,\sin\frac{A-B}{2}$$

$$\cos A + \cos B = 2\,\cos\frac{A+B}{2}\,\cos\frac{A-B}{2} \qquad (4.47)$$

$$\cos A - \cos B = 2\,\sin\frac{A+B}{2}\,\sin\frac{A-B}{2}$$

and comparing the coefficients of $\sin\dfrac{k\omega t}{2}$ and $\cos\dfrac{k\omega t}{2}$ lead to the following matrix

equations relating the vectors $\{a\}_k$ and $\{b\}_k$.

$$\begin{bmatrix} [K_e]-\alpha P^*[K_{gs}]+\dfrac{1}{2}\beta P^*[K_{gt}]-\dfrac{\omega^2}{4}[M] & -\dfrac{1}{2}\beta P^*[K_{gt}] & 0 & . \\[2mm] -\dfrac{1}{2}\beta P^*[K_{gt}] & [K_e]-\alpha P^*[K_{gs}]-\dfrac{9\omega^2}{4}[M] & -\dfrac{1}{2}\beta P^*[K_{gt}] & . \\[2mm] 0 & -\dfrac{1}{2}\beta P^*[K_{gt}] & [K_e]-\alpha P^*[K_{gs}]-\dfrac{25\omega^2}{4}[M] & . \\[2mm] . & . & . & . \end{bmatrix} \begin{Bmatrix} \{a\}_1 \\ \{a\}_3 \\ \{a\}_5 \\ . \end{Bmatrix} = 0$$

$$(4.48)$$

and

$$\begin{bmatrix} [K_e]-\alpha P^*[K_{gs}]-\dfrac{1}{2}\beta P^*[K_{gt}]-\dfrac{\omega^2}{4}[M] & -\dfrac{1}{2}\beta P^*[K_{gt}] & 0 & . \\[2mm] -\dfrac{1}{2}\beta P^*[K_{gt}] & [K_e]-\alpha P^*[K_{gs}]-\dfrac{9\omega^2}{4}[M] & -\dfrac{1}{2}\beta P^*[K_{gt}] & . \\[2mm] 0 & -\dfrac{1}{2}\beta P^*[K_{gt}] & [K_e]-\alpha P^*[K_{gs}]-\dfrac{25\omega^2}{4}[M] & . \\[2mm] . & . & . & . \end{bmatrix} \begin{Bmatrix} \{b\}_1 \\ \{b\}_3 \\ \{b\}_5 \\ . \end{Bmatrix} = 0$$

$$(4.49)$$

The orders of matrices in equations (4.48) and (4.49) are infinite. If solutions of period 2T exist, then the determinants of these matrices must zero. Combining these two determinants, the condition may be written as

$$\left| \begin{array}{cccc} \left[K_e\right]-\alpha P^*\left[K_{gs}\right]\pm\dfrac{1}{2}\beta P^*\left[K_{gt}\right]-\dfrac{\omega^2}{4}[M] & -\dfrac{1}{2}\beta P^*\left[K_{gt}\right] & 0 & . \\[3mm] -\dfrac{1}{2}\beta P^*\left[K_{gt}\right] & \left[K_e\right]-\alpha P^*\left[K_{gs}\right]-\dfrac{9\omega^2}{4}[M] & -\dfrac{1}{2}\beta P^*\left[K_{gt}\right] & . \\[3mm] 0 & -\dfrac{1}{2}\beta P^*\left[K_{gt}\right] & \left[K_e\right]-\alpha P^*\left[K_{gs}\right]-\dfrac{25\omega^2}{4}[M] & . \\[3mm] & . & . & . \end{array} \right| = 0$$

(4.50)

If a solution to equation (4.44) exists with a period $T=2\pi/\omega$ then it may be expressed as Fourier series

$$\{q\}=\frac{1}{2}b_0 + \sum_{k=2,4,6}^{\infty}\left[\{a\}_k \sin\frac{k\omega t}{2}+\{b\}_k \sin\frac{k\omega t}{2}\right]$$

(4.51)

Differentiating equation (4.51) twice with respect to time yields

$$\{\ddot{q}\}=\sum_{k=2,4,6}^{\infty}-\left(\frac{k\omega}{2}\right)^2\left[\{a\}_k \sin\frac{k\omega t}{2}+\{b\}_k \cos\frac{k\omega t}{2}\right]$$

(4.52)

Substituting equations (4.51) and (4.52) into equation (4.44), the following condition for the existence of solution with period T is obtained;

$$\left[\begin{array}{cccc} \left[K_e\right]-\alpha P^*\left[K_{gs}\right]-\omega^2[M] & -\dfrac{1}{2}\beta P^*\left[K_{gt}\right] & 0 & . \\[3mm] -\dfrac{1}{2}\beta P^*\left[K_{gt}\right] & \left[K_e\right]-\alpha P^*\left[K_{gs}\right]-4\omega^2[M] & -\dfrac{1}{2}\beta P^*\left[K_{gt}\right] & . \\[3mm] 0 & -\dfrac{1}{2}\beta P^*\left[K_{gt}\right] & \left[K_e\right]-\alpha P^*\left[K_{gs}\right]-9\omega^2[M] & . \\[3mm] & . & . & . \end{array} \right] \left\{ \begin{array}{c} \{a\}_2 \\ \{a\}_4 \\ \{a\}_6 \\ . \end{array} \right\}=0$$

(4.53)

and

$$\begin{bmatrix} \frac{1}{2}\{[K_e]-\alpha P*[K_{gs}]\} & -\frac{1}{2}\beta P*[K_{gt}] & 0 & 0 & \cdot \\ -\frac{1}{2}\beta P*[K_{gt}] & [K_e]-\alpha P*[K_{gs}]-\omega^2[M] & -\frac{1}{2}\beta P*[K_{gt}] & 0 & \cdot \\ 0 & -\frac{1}{2}\beta P*[K_{gt}] & [K_e]-\alpha P*[K_{gs}]-4\omega^2[M] & -\frac{1}{2}\beta P*[K_{gt}] & \cdot \\ 0 & & -\frac{1}{2}\beta P*[K_{gt}] & [K_e]-\alpha P*[K_{gs}]-9\omega^2[M] & \cdot \\ 0 & \cdot & \cdot & \cdot & \end{bmatrix} \begin{Bmatrix} \{b\}_0 \\ \{b\}_2 \\ \{b\}_4 \\ \{b\}_6 \\ \cdot \end{Bmatrix} = 0$$

$$(4.54)$$

It has been shown by Bolotin (1964), that solutions with period 2T are the ones of the greatest practical importance and that as a first approximation the boundaries of the principal regions of dynamic instability can be determined from the equation

$$\left[[K_e]-\alpha P*[K_{gs}]\pm\frac{1}{2}\beta P*[K_{gt}]-\frac{\omega^2}{4}[M]\right]\{q\}=0 \qquad (4.55)$$

The two matrices $[K_{gs}]$ and $[K_{gt}]$ will be identical if the static and time dependent components of the loads are applied in the same manner. If $[K_{gs}]\equiv[K_{gt}]\equiv[K_g]$, then equation (4.56) becomes

$$\left[[K_e]-(\alpha\pm\frac{1}{2}\beta)P*[K_g]-\frac{\omega^2}{4}[M]\right]\{q\}=0 \qquad (4.56)$$

Equation (4.56) represents solutions to three related problems

(i) Free vibration with $\alpha = 0$, $\beta = 0$ and $p = \omega/2$ the natural frequency

$$\left[[K_e]-p^2[M]\right]\{q\}=0 \qquad (4.57)$$

(ii) Static stability with $\alpha = 1$, $\beta = 0$ and $\omega = 0$

$$\left[[K_e]-P*[K_g]\right]\{q\}=0 \qquad (4.58)$$

(iii) Dynamic stability when all terms are present

$$\left[[K_e]-(\alpha\pm\frac{1}{2}\beta)P*[K_g]-\frac{\omega^2}{4}[M]\right]\{q\}=0 \qquad (4.59)$$

CHAPTER FIVE
RESULTS AND DISCUSSION

5.1 Program Steps

The finite elemet models of frame and crack developed are discussed and the results obtained from the finite element method are illustrated in this chapter.
Process Steps can be seen in figure 5.1.

1. Usage of geometrical and material properties as input.

2. Formation local stiffness, local geometrical stiffness and local mass matrices for each beam element.

3. Transforming the local coordinate into global coordinates.

4. By assembling the element matrices, main global matrices are formed.

5. Application of the boundary conditions.

6. Eigenvalue solution is carried out to calculate the natural frequencies and the mode shapes, critical buckling load and dynamic stability of system.

geometrical and meteral
properties are used as input.

formilation of Local matrices for
each beam element

transformation elemental
matrices from Local coordinates
into global coordinates

Assembling the global matrix for
the structure

Application of the boundary
conditions

solving eigenvalue problem
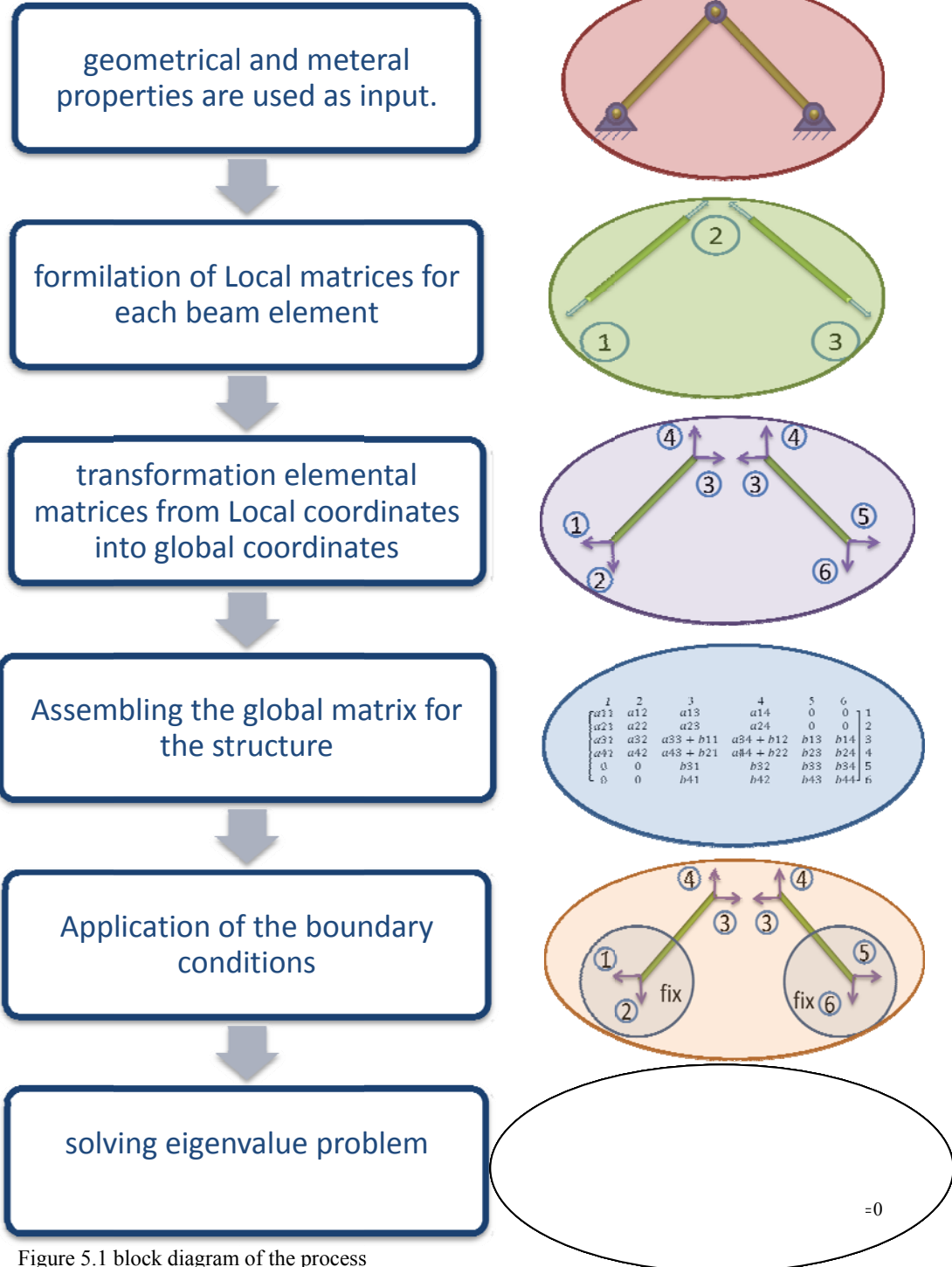
Figure 5.1 block diagram of the process

5.2 Results comparison

In this thesis, comparison made between the natural frequencies of cracked frames obtained using the present model with the results obtained from the ANSYS software. As seen from Table 5.1. Maximum error is 2.3804%. The comparison shows that very good agreement between the results is obtained.

Table 5.1 comparison between present work and ANSYS results.

Crack (a/h)	ANSYS (Hz)	Present work (Hz)	ERROR%
0	118.555	117.2552	1.108522
0.1	118.356	117.2532	0.940545
0.2	117.726	117.2223	0.429685
0.3	116.648	117.0806	0.369526
0.4	115.006	116.6234	1.386837
0.5	112.594	115.3395	2.3804

The modeling of Crack in ANSYS is built by using the method of concentrate meshing around the crack location. which is explained step by step in "ANSYS TUTORIAL -2D Fracture Analysis" by Dr. A.-V. Phan , from University of South Alabama.

By using KSCON a concentration key-point is defined about which mesh area will be skewed. This is useful for modeling stress concentrations and crack tips. During meshing, elements are initially generated circumferentially about, and radially away, from the key-point. Lines attached to the key-point are given appropriate divisions and spacing ratios.

If the normal meshing procedure is applied, the results become very different. Figure 5.2 and Figure 5.3 show the normal and special crack meshing (KSCON command in ANSYS) respectively.
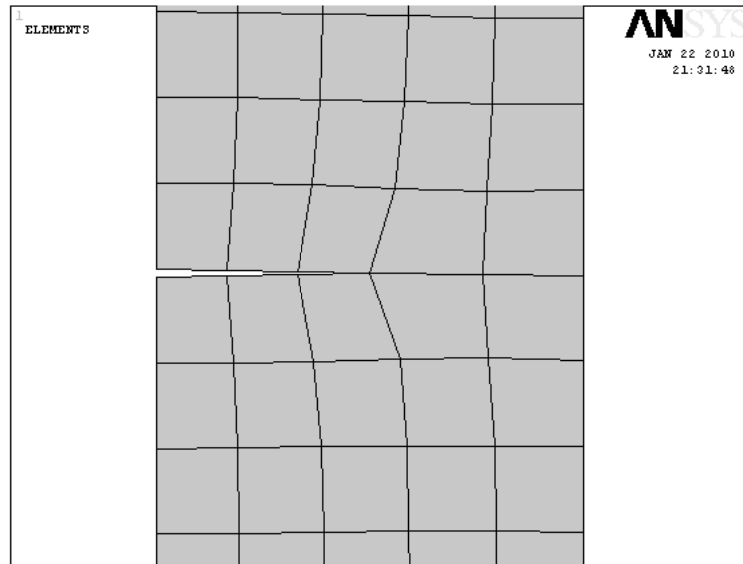
Figure 5.2 Normal meshing of crack
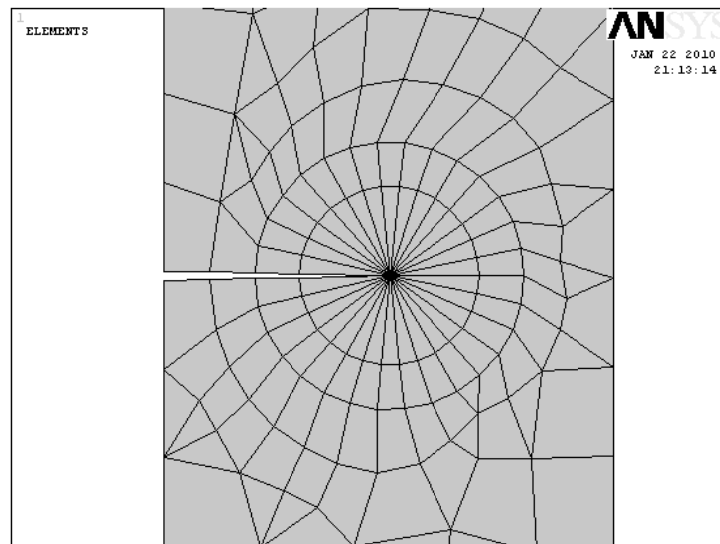
Figure 5.3 Special meshing of crack (KSCON)

The comparison of the results in   Table 5.1 shows that when the crack ratio is equal to zero that means there is no crack in the frame structure , the error percentage equal to 1.108 % the difference between the two result shows the effect of meshing methods in ANSYS solid meshing and in present work beam meshing are used.

When the crack is created the beam meshing for intact section and the special element developed for the cracked section are used. When the crack is considered in ANSYS solid meshing for entire body and the concentration meshing on crack tip point are used.

As seen from Table 5.1 the maximum percentage of error is equal to (2.3804) at the crack ratio (0.5), which is the maximum of crack ratio considered. In addition, numerical comparison for the frequency of a single frame without crack is carried out between the results of SolidWorks software using the beam mesh as shown in Figure 5.4 and solid mesh in Figure 5.5.
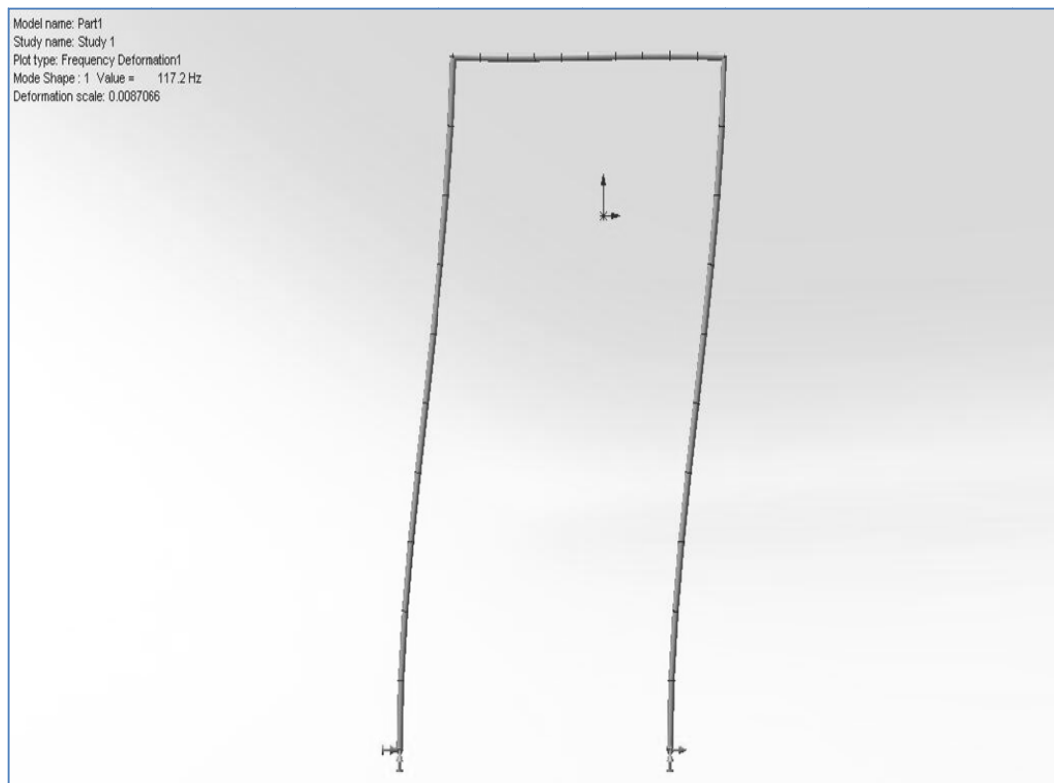
Figure 5.4 beam meshing SolidWorks

```
Model name: Part2
Study name: Study 1
Plot type: Frequency Deformation1
Mode Shape : 1  Value =    119.21 Hz
Deformation scale: 0.00872072
```
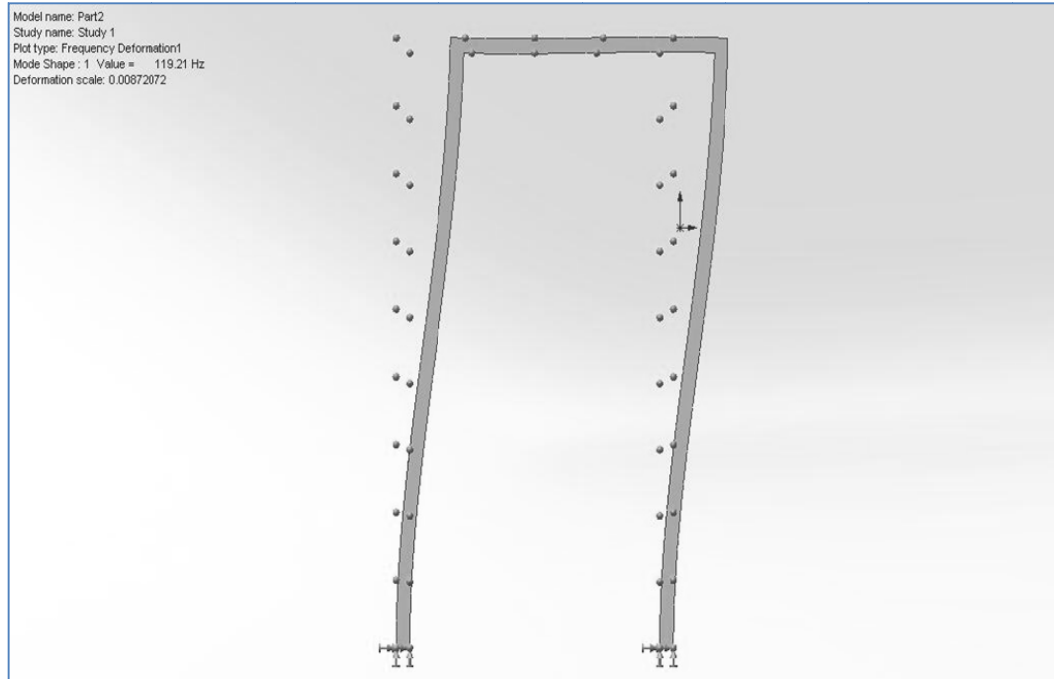
Figure 5.5 solid meshing SolidWorks

In Table 5.2, the numeric results obtained by using three different models for the first natural frequency are shown. It can be noticed that there is a very close agreement between the results of present model and that of beam meshing model.

Table 5.2 Beam & Solid mesh result modeling in SolidWorks

	Present work	SolidWorks (beam meshing)	SolidWorks (solid meshing)
freq. (Hz)	117.255	117.201	119.208
error %		0.0462	1.638

5.3 Natural frequency

5.3.1 Single frame structure

Figure 5.6 shows the effect of crack location and crack depth on the first natural frequency of a single frame structure and its mode shape. As the crack depth increases, the variations of the first natural frequency become significant. When the crack location changes, the variation in the first natural frequency is centered symmetrically around the 15th node of the FE as seen in Figure 5.6©. The maximum decrease in the first natural frequency occurs when the crack is at the fixed points (roots of the frame). The decrease in the frequency when it is at the corners is about 49.06% of those of the fixed points. Moreover, the crack does not affect the first natural frequency of the single frame structure when it is located at the mid-points of the blades and the shroud lengths because the stresses in these points are so small.

Figure 5.7 shows the effect of crack location and crack depth on the second natural frequency of the single frame structure and its mode shape. As seen in Figure 5.7©, similar to the effect of the crack on the first natural frequency, the left and the right hand side of the results obtained from maximum crack depth condition around the 15th node is symmetric and the maximum decrease in the second natural frequency occurs when the crack is at the fixed points of the single frame. There is no effect of the crack on the second frequency when the crack is located at approximately near the 3rd, 10th, 20th and 27th nodes, because the stress in these points are small. When the crack is located in the mid-points of the blades and shroud, the decrease in the second natural frequency is significant. The reason for this is that the stress is large at these areas.

Figure 5.8 shows the effect of crack location and crack depth on the third natural frequency of the single frame structure and its mode shape. Similar to Figure 5.6© and 5.7©, Figure 5.8© shows the effect of location of maximum crack depth, and has

a symmetric appearance around the 15th node and the maximum decrease in the third natural frequency occurs when the crack is at the fixed points of the frame i.e. the roots. Also, there is a decrease in the third natural frequency when the crack is at the mid-point of the blades and the corners. However, there is no effect of the crack on the third natural frequency, when the crack is located by 3rd, 7th, 15th, 23rd and 27th nodes considered in the finite element method.

Figure 5.9 shows the effect of crack location and crack depth on the fourth natural frequency of the single frame structure and its mode shape. Figure 5.9© has similarities to Figures 5.6©, 5.7© and 5.8©. When the crack is located at the mid-point of shroud, contrarily to the results of the first three natural frequencies the maximum decrease occurs in the fourth natural frequency. In addition, the crack does not effect when it is located at approximately near the 2nd, 6th, 10th, 20th, 25th and 29th nodes.

5.3.2 Two-bay frame structure

Figure 5.10 shows the effect of crack location and crack depth on the first natural frequency of the two-bay frame structure and its mode shape. As the crack depth increases, the variation of the first natural frequency becomes significant. When the crack location changes, the variation in the first natural frequency is centered symmetrically around the 25th node of FE except for the region between 20th and 30th nodes as seen in Figure 5.10©. The maximum decrease in the first natural frequency occurs when the crack is at 30th node (root of the middle blade). The decreases in the frequency when the crack is at the roots of the first and third blades (1st and 50th nodes), in the corner of the middle blade (20th node), at 10th and 40th nodes are approximately 81.34%, 66.17%, 38.33% respectively. The percentages of the decrease in the first natural frequency are calculated with respective to maximum decrease in the frequency when the crack is at 30th node.

Figure 5.11 shows the effect of crack location and crack depth on the second natural frequency of the two-bay frame structure and its mode shape. As seen in Figure 5.11© , similar to the effect of the crack on the first natural frequency , the left and the right hand side of the results obtained from the maximum crack depth condition around 20th node are symmetric except for the area between 20th and 30th nodes. The maximum decrease in the second natural frequency occurs when the crack is at the root of the middle blade 30th node. Moreover, the decreases in the second natural frequency also exist when the crack is at the roots of the first and third blade (1st and 50th nodes) and approximately at the mid-point of the blades (5th, 25th and 45th nodes).

Figure 5.12 shows the effect of crack location and crack depth on the third natural frequency of the two-bay frame structure and its mode shape. Similar to Figure 5.10© and 5.11©, Figure 5.12© shows the effect of location of the maximum crack depth, and has a symmetric appearance around the 25th node. The maximum decrease in the third natural frequency occurs if the crack is at the roots of the first and the third blades (1st and 50th nodes). There is no effect of the crack if it is at the middle blade (from the 20th node to the 30th node), because the middle blade does not vibrate as seen from its mode shape. The decreases in the third natural frequency occur approximately if the crack is at the mid-point (5th and 45th nodes) and in the corners (10th and 40th nodes) of the first and third blades.

Figure 5.13 shows the effect of crack location and crack depth on the fourth natural frequency of the two-bay frame structure and its mode shape. Figure 5.13© shows similarity with Figures 5.10© and 5.11©. When the crack is located at the root of the middle blade 30th node, the maximum decrease in the fourth natural frequency occurs. In addition, the decreases in the natural frequency are observed if the crack is at around 1st, 5th, 10th, 20th, 25th, 40th, 45th and 50th nodes.

5.3.3 Three-bay frame structure

Figure 5.14 shows the effect of crack location and crack depth on the first natural frequency of the three-bay frame structure and its mode shape. As the crack depth increases, the variation of the first natural frequency becomes significant. When the crack location changes, the variation in the first natural frequency is centered symmetrically around the 35th node of FE as seen in figure 5.14©. The maximum decrease in the first natural frequency occurs if the crack is at the 30th and 50th nodes (roots of the internal blades). The decrease in the frequency if the crack is at the roots of the first and fourth blades (1st and 70th nodes), in the corner of the middle blades (20th and 40th nodes), at 10th and 60th nodes are approximately 85.28%, 63.59%, 41.67% respectively. The percentages of the decrease in the first natural frequency are calculated with respective to maximum decrease in the frequency when the crack is at 30th and 50th nodes.

Figure 5.15 shows the effect of crack location and crack depth on the second natural frequency of the three-bay frame structure and its mode shape. As seen in figure 5.15©, similar to the effect of the crack on the first natural frequency, the left and the right hand side of the results obtained from the maximum crack depth condition when the crack is around 35th node is symmetric. The maximum decrease in the second natural frequency occurs if the crack at the root of the external blades (1st and 70th nodes). Moreover, the decreases in the second natural frequency also exist if the crack is at the roots of the second and third blade (30th and 50th nodes) and approximately at the mid-point of the blades and corners (5th, 13th, 25th, 45th, 57th and 65th nodes).

Figure 5.16 shows the effect of crack location and crack depth on the third natural frequency of the three-bay frame structure and its mode shape. Similar to Figure 5.14© and 5.15©, Figure 5.16© shows the effect of location of the maximum crack depth, and has a symmetric appearance around the 35th node. The maximum decrease

in the third natural frequency occur when the crack is at the roots of the first and the fourth blades (1st and 70th nodes). The decreases in the third natural frequency occurs approximately when the crack is at the $5^{th,}$ 13th, 20th, 25th 30th, 40th, 45th, 50th 60th and 65th nodes.

Figure 5.17 shows the effect of crack location and crack depth on the fourth natural frequency of the three-bay frame structure and its mode shape. Figure 5.17© shows similarity to Figures 5.14©, 5.15© and 5.16©. When the crack located at the root of the internal blades nodes 30th and 50th the maximum decrease in the fourth natural frequency occurs. In addition, the decreases in the natural frequency are observed when the crack is at around 1st , 5th , 10th ,20th ,25th ,40th ,45th ,60th ,65th and 70th nodes.

5.3.4 Four-bay frame structure

Figure 5.18 shows the effect of crack location and crack depth on the first natural frequency of four-bay frame structure and its mode shape. As the crack depth increases, variation of the first natural frequency becomes significant. When the crack location changes, variation in the first natural frequency is centered symmetrically around the 45th node of FE except for the area between 40th and 50th nodes as seen in Figure 5.18©. The maximum decrease in the first natural frequency occurs when the crack is at the 30th and 70th nodes (root of the second and fourth blades). The decreases in frequency when it is at the root of the third blade 50th node, in the roots of the first and fifth blades, in the corners of the second and third blades 20th and 60th nodes, in the corner of the middle blade 40th nodes, in the corners of the first and fifth blades 10th and 80th nodes are approximately 95.96%, 84.44%, 64.81%, 58.27%, 41.02% respectively. The percentage decrease in the first natural frequency is calculated with respective to maximum decrease in the frequency at 30th and 70th nodes.

Figure 5.19 shows the effect of crack location and crack depth on the second natural frequency of four-bay frame structure and its mode shape. As seen in Figure 5.19©, similar to the effect of crack on the first natural frequency , the left and the right hand side of the results obtained from the maximum crack depth condition around 45th node is symmetric except for the area between 40th and 50th nodes. The maximum decrease in the second natural frequency occurs when the crack is at the root of the first and fifth blades 1st and 90th nodes. Moreover, decreases in the second natural frequency also exist when it is at the mid-point of the first and fifth blades (5th and 85th nodes) and approximately at (13th, 25th, 30th, 50th 65th, 70th and 77th nodes).

Figure 5.20 shows the effect of crack location and crack depth on the third natural frequency of the Four-bay frame structure and its mode shape. Similar to Figure 5.18© and 5.19.c, Figure 5.20© shows the effect of location of the maximum crack depth, and has a symmetric appearance around 45th node. The maximum decrease in the third natural frequency occurs when the crack is at the roots of the first and the fifth blades (1st and 90th nodes). There is no effect of the crack when it is at the middle blade (from the 40th node to the 50th node), because the middle blade does not vibrate as seen from its mode shape. The decreases in the third natural frequency occur approximately when the crack is at 5th ,12th ,25th ,30th ,40th ,50th ,60th ,65th ,78th and 85th nodes .

Figure 5.21 shows the effect of crack location and crack depth on the fourth natural frequency of the Four-bay frame structure and its mode shape. Figure 5.21© shows similarity to Figures 5.18©, 5.19© and 5.20©. When the crack located at the root of the middle blade 50th node, the maximum decrease in the fourth natural frequency occurs.

5.3.5 Five-bay frame structure

Figure 5.22 shows the effect of crack location and crack depth on the first natural frequency of five-bay frame structure and its mode shape. As the crack depth increase, the variation of the first natural frequency becomes significant. When the crack location changes, the variation in the first natural frequency is centered symmetrically around the 55th node of FE as seen in Figure 5.22©. The maximum decrease in the first natural frequency occurs if the crack is at the 30th or 90th node (roots of the second and fifth blades). The decrease in the frequency if crack is at the roots of the third and fourth blade 50th and 70th nodes, at the roots of the first and sixth blade 1st and 110th nodes, at the corner of the second and fifth blade 20th and 80th nodes, in the corner of the third and fourth blade 40th and 60th nodes, in the corner of the first and sixth blade 10th and 100th nodes are approximately 96.77%, 84.57%, 64.97%, 59.71% and 41.95% respectively. The percentages of the decrease in the first natural frequency are calculated with respective to maximum decrease in the frequency when the crack is at 30th and 90th nodes.

Figure 5.23 shows the effect of crack location and crack depth on the second natural frequency of five-bay frame structure and its mode shape. As seen in figure 5.23©, similar to the effect of the crack on the first natural frequency, the left and the right hand side of the results obtained from the maximum crack depth condition when the crack is around 55th node is symmetric and The maximum decrease in the second natural frequency occurs when the crack is at the root of the external blades (1st and 110th nodes). Moreover, the decreases in the second natural frequency also exist when the crack is at the mid-pint of the first and sixth blade 5th and 105th nodes, approximately at $11^{th,}$ 25th, 30th, 50th, 70th, 85th, 90th and 100th nodes.

Figure 5.24 shows the effect of crack location and crack depth on the third natural frequency of five-bay frame structure and its mode shape. Similar to Figure 5.22© and 5.23©, Figure 5.24© shows the effect of location of the maximum crack depth,

and has a symmetric appearance around the 55th node. The maximum decrease in the third natural frequency occurs when the crack is at the roots of the first and the sixth blades (1st and 110th nodes). The decrease in the third natural frequency occurs approximately when the crack is at the 30th and 90th nodes.

Figure 5.25 shows the effect of crack location and crack depth on the fourth natural frequency of five-bay frame structure and its mode shape. Figure 5.25© shows similarity to Figures 5.22©, 5.23© and 5.24©. When the crack is located at the root of the internal blades (the third and fourth) 50th and 70th nodes the maximum decrease in the fourth natural frequency occurs. In addition, the decreases in the natural frequency are observed when the crack is at around 1st , 6th , 11th ,20th ,30th ,41th ,45th ,61th ,65th , 91st,100th ,105th and 110th nodes.

5.3.6 Six-bay frame structure

Figure 5.26 shows the effect of crack location and crack depth on the first natural frequency of six-bay frame structure and its mode shape. As the crack depth increases, the variation of the first natural frequency becomes significant. When the crack location changes, the variation in the first natural frequency is centered symmetrically around the 65th node of FE except for the area between 60th and 70th nodes as seen in Figure 5.26©. The maximum decrease in the first natural frequency occurs when the crack is at the 30th and 110th nodes (root of the second and sixth blades). The decrease in the frequency when the crack is at the root of the fourth blade 70th node, at the roots of the third and fifth blades 50th and 90th nodes, at the roots of the first and seventh blade 1st and 130th nodes, in the corners of the second and sixth blades 20th and 100th nodes, in the corner of the middle blade 60th nodes, in the corner of the third and fifth blade 40th and 80th nudes, in the corners of the first and seventh blade 10th and 120th nodes are approximately 97.42%, 96.60%, 84.52% ,

65.21%, 60.99%, 59.67% and 42.10% respectively. The percentages of decrease in the first natural frequency are calculated with respective to maximum decrease in the frequency when the crack is at 30th and 110th nodes.

Figure 5.27 shows the effect of crack location and crack depth on the second natural frequency of six-bay frame structure and its mode shape. As seen in Figure 5.27©, similar to the effect of crack on the first natural frequency, the left and the right hand side of the results obtained from the maximum crack depth condition when the crack is around 65th node is symmetric except for the area between 60th and 70th nodes. The maximum decrease in the second natural frequency occurs when the crack is at the root of the first and seventh blades 1st and 130th nodes. Moreover, the decreases in the second natural frequency also exist if the crack is at the mid-point of the first and seventh blades (6th and 124th nodes) and approximately at (11th, 25th, 30th, 50th 70th, 90th, 100th 105th 110th and 120th nodes).

Figure 5.28 shows the effect of crack location and crack depth on the third natural frequency of six-bay frame structure and its mode shape. Similar to Figure 5.26© and 5.27©, Figure 5.28© shows the effect of location of the maximum crack depth, and has a symmetric appearance around 65th node. The maximum decrease in the third natural frequency occurs when the crack is at the mid-point of the fourth blade (65th node). The decreases in the third natural frequency also occur approximately when the crack is at 1st ,6th ,18th ,21th ,25th,30th ,35th ,41st ,45th ,50th ,57th ,61th ,70th ,74th 85th ,90th ,101st ,105th ,110th ,113th ,125th and 130th nodes .

Figure 5.29 shows the effect of crack location and crack depth on the fourth natural frequency of six-bay frame structure and its mode shape. Figure 5.29© shows similarity to Figures 5.26©, 5.27© and 5.28©. When the crack is located at the root

of the middle blade 70th node, the maximum decrease in the fourth natural frequency occurs.

5.3.7 Two-story frame structure

Figure 5.30 shows the effect of crack location and crack depth on the first natural frequency of two-story frame structure and its mode shape. As the crack depth increases, variation of the first natural frequency becomes significant. When the crack location changes, variation in the first natural frequency between 1st and 30th node is centered symmetrically around the 15th node, on the other hand, the changes of frequency when the crack is between 30th and 60th node is centered symmetrically around the 45th node of the FE as seen in Figure 5.30©. The maximum decrease in the first natural frequency occurs when the crack is at 10th and 20th nodes (the joint point between the lower and the upper frame when the stresses due to the moment become maximum). The decreases in the frequency occur when the crack is at the 1st and 30th nodes (the roots of the frame).

Figure 5.31 shows the effect of crack location and crack depth on the second natural frequency of two-story frame structure and its mode shape. As seen in Figure 5.31©, similar to the effect of crack on the first natural frequency , the left and the right hand side of the results obtained from the maximum crack depth is symmetric when the crack is between 1st and 30th nodes. There is also similar symmetry between 30th and 60th nodes. The maximum decrease in the second natural frequency occurs when the crack is at the joint point between the lower and the upper frame 30th and 60th nodes. Moreover, the decreases in the second natural frequency also exist when the crack is at 1st, 10th, 40th and 50th nodes.

Figure 5.32 shows the effect of crack location and crack depth on the third natural frequency of two-story frame structure and its mode shape. Similar to Figure 5.30©

and 5.31©, Figure 5.32© shows the effect of location of the maximum crack depth, and has a symmetric appearance around the 15th node for the range between 1st and 30th nodes, there is similar symmetry around 45th node between 30th and 60th nodes. The maximum decrease in the third natural frequency also occurs when the crack is at the 35th and 55th nodes.

Figure 5.33 shows the effect of crack location and crack depth on the fourth natural frequency of two-story frame structure and its mode shape. Figure 5.33© shows similarity to Figures 5.30© and 5.31©. The maximum decrease in the fourth natural frequency occurs when the crack is in the 10th and 20th nodes. In addition, the decreases in the natural frequency are observed when the crack is at around 1st, 5th, 25th, 30th, 35th, 40th, 50th, 55th and 60th nodes.

5.3.8 Three-story frame structure

Figure 5.34 shows the effect of crack location and crack depth on the first natural frequency of three-story frame structure and its mode shape. As the crack depth increases, variation of the first natural frequency becomes significant. When the crack location changes, the variation in the first natural frequency when the crack is between 1st and 30th node is centered symmetrically around the 15th node, there is the similar symmetric in the area between 30th and 60th nodes, and the area between 60th and 90th nodes of the FE as seen in Figure 5.34©. The maximum decrease in the first natural frequency occurs when the crack is at the 10th and 20th nodes (the joint point between the lower and the middle frame where the stresses due to the moment become maximum). The decreases in the frequency also occur when crack is at the 1st and 30th nodes (the roots of the frame) and when the crack is at 40th, 50th, 60th, 70th, 80th and 90th nodes.

Figure 5.35 shows the effect of crack location and crack depth on the second natural frequency of three-story frame structure and its mode shape. As seen in Figure 5.35©, similar to the effect of the crack on the first natural frequency, the variation in the second natural frequency when the crack is between 1st and 30th nodes is centered symmetrically around the 15th node, there is a similar symmetry centered around 45th and 75th crack nodes for the area between 30th and 60th, 60th and 90th nodes of the FE respectively. The maximum decrease in the second natural frequency occurs when the crack is at the joint point between the middle and upper frame at the 40th and 50th nodes. Moreover, the decreases in the second natural frequency also exist when the crack is at 1st, 10th, 20th, 30th, 60th, 70th, 80th and 90th nodes.

Figure 5.36 shows the effect of crack location and crack depth on the third natural frequency of three-story frame structure and its mode shape. Similar to Figure 5.34© and 5.35©, Figure 5.36© shows the effect of location of the maximum crack depth, and has a symmetric appearance when the crack is between 1st and 30th nodes is centered symmetrically around the 15th node, there are similar symmetric centers around crack locations of 45th and 75th nodes for the area between 30th and 60th, 60th and 90th nodes of the FE respectively. The maximum decrease in the third natural frequency occurs when the crack is at the 60th and 90th nodes.

Figure 5.37 shows the effect of crack location and crack depth on the fourth natural frequency of the three-story frame structure and its mode shape. Figure 5.37© shows similarity to Figures 5.34© and 5.35©. The maximum decrease in the fourth natural frequency occurs when the crack is at 65th and 85th nodes.

5.3.9 Vibration analysis for the multi-bay frame structure

When the results obtained from the free vibration analysis of multi-bay frames, shown in Figures 5.5(c), 5.10(c), 5.14(c), 5.18(c), 5.22(c) and 5.26(c), are examined, generally the first natural frequencies decrease when the crack located either at the roots or at the corner of the frames for all multi-bay frames.

Crack location, first natural frequencies of cracked structure, percentage of decreases and the first natural frequencies without crack are given in Tables 5.3-5.8.

Percentage decrease in the natural frequencies is calculated with respect to the maximum decrease.

Table 5.3 decreases in first natural frequency of the single frame structure with respect to crack location when the crack ratio is 0.5.

Crack location (nodes)	10th , 20th	1st , 30th	Without crack
Natural frequency	116.30	115.33	117.23
Percentage of decreases in the frequency	49.06%	Max. decrease	

Table 5.4 decreases in first natural frequency of the two-bay frame structure with respect to crack location when the crack ratio is 0.5.

Crack location (nodes)	10th , 40th	20th	1st , 50th	30th	Without crack
Natural frequency	110.09	109.72	109.51	109.26	110.61
Percentage of decreases in the frequency	38.33%	66.17%	81.34%	Max. decrease	

Table 5.5 decreases in first natural frequency of the three-bay frame structure with respect to crack location when the crack ratio is 0.5.

Crack location (nodes)	10th , 60th	20th , 40th	1st , 70th	50th , 30th	Without crack
Natural frequency	107.93	107.73	107.53	107.39	108.32
Percentage of decreases in the frequency	41.67%	63.59%	85.28%	Max. decrease	

Table 5.6 decreases in first natural frequency of the four-bay frame structure with respect to crack location when the crack ratio is 0.5.

Crack location (nodes)	10th , 80th	40th	20th , 60th	1st , 90th	50th	30th , 70th	Without crack
Natural frequency	106.66	106.53	106.49	106.34	106.26	106.23	106.96
Percentage of decreases in the frequency	41.02%	58.27%	64.81%	84.44%	95.96%	Max. decrease	

Table 5.7 decreases in first natural frequency of the five-bay frame structure with respect to crack location when the crack ratio is 0.5.

Crack location (nodes)	10th, 100th	40th, 60th	20th, 80th	1st, 110th	50th, 70th	30th, 90th	Without crack
Natural frequency	105.86	105.72	105.72	105.61	105.53	105.51	106.11
Percentage of decreases in the frequency	41.95%	59.71%	64.97%	84.57%	96.77%	Max. decrease	

Table 5.8 decreases in first natural frequency of the six-bay frame structure with respect to crack location when the crack ratio is0.5.

Crack location (nodes)	10th, 120th	40th, 80th	60th	20th, 100th	1st, 130th	50th, 90th	70th	30th, 110th	Without crack
Natural frequency	105.31	105.22	105.21	105.19	105.09	105.03	105.03	105.02	105.52
Percentage of decreases in the frequency	42.1%	59.67%	60.99%	65.21%	84.52%	96.60%	97.42%	Max. decrease	

As seen in Tables 5.3-5.8, the maximum decreases in the first natural frequency of the multi-bay framed occur, if the crack is located at the roots of the 2nd blade or n-1 number of blade (n: number of blades). The similar result can be obtained when crack is at the corners.

The results are given schematically in figure 5.46.

5.4 Buckling

5.4.1 Single frame structure

Figure 5.38 shows the effect of crack location and crack depth on the first buckling critical load of single frame structure and its mode shape. As the crack depth increases, the variation of first buckling critical load becomes significant. When the crack location changes variation in the buckling critical load is centered symmetrically around the 15th node of FE as seen in Figure 5.38©. The maximum decrease in the buckling load occurs when the crack is either at the 1st and 30th nodes (root of the blades) .The decrease in the critical load also occurs when the crack is either at 10th and 20th nodes.

5.4.2 Two-bay frame structure

Figure 5.39 shows the effect of crack location and crack depth on the first buckling critical load of two-bay frame structure and its mode shape. As seen in Figure 5.39©, similar to the effect of the crack shown in Figure 5.38©, the left and the right hand side of the results obtained from the maximum crack depth condition when the crack location is around 25th node is symmetric except the area between 20th and 30th crack location nodes. The maximum decrease in the first buckling critical load occurs when the crack is at the root of the second blade 30th node. The decreases in the critical buckling load also located when the crack is either at the roots of the first and third blades 1st and 50th nodes, or in the corner of the blades 10th, 20th and 40th nodes.

5.4.3 Three-bay frame structure

Figure 5.40 shows the effect of crack location and crack depth on the first buckling critical load of three-bay frame structure and its mode shape. Similar to

Figure 5.38© and 5.39©, Figure 5.40© shows the effect of location of the maximum crack depth, and has a symmetric appearance around 35th node. The maximum decrease in the first buckling critical load is seen to be when the crack is either at the roots of the second and third blades 30th and 50th nodes. The decrease in the buckling load also occurs when the crack is at 1st, 10th, 20th, 40th, 60th or 70th nodes.

5.4.4 Four-bay frame structure

Figure 5.41 shows the effect of crack location and crack depth on the first buckling critical load of four-bay frame structure and its mode shape. As the crack depth increases, the variation of the first buckling critical load becomes significant. When the crack location changes the variation in the buckling load is centered symmetrically around the 45th node of FE except the area between nodes 40th and 50th as seen in figure 5.41©. The maximum decrease in the first buckling critical load occurs when the crack is at the 30th and 70th nodes (roots of the second and fourth blade) .The decrease in the load also occurs when the crack is at 1st , 10th , 20th , 40th , 50th , 60th , 80th and 90th nodes.

5.4.5 Five-bay frame structure

Figure 5.42 shows the effect of crack location and crack depth on the first buckling critical load of five-bay frame structures and its mode shape. As seen in Figure 5.42©, similar to the effect of crack seen in Figures 5.38©, 5.39© and 5.40©, the left and the right hand side of the results obtained from the maximum crack depth condition around 55th node crack position is symmetric and the maximum decrease in the buckling load occurs when the crack is at the root of the second and fifth blades 30th and 90th nodes. The decreases in the buckling load are also seen to be when the crack is at the root of blades and at the corners, approximately at 1st, 10th, 20th, 40th, 50th, 60th, 70th, 80th, 100th and 110th nodes.

5.4.6 Six-bay frame structure

Figure 5.43 shows the effect of crack location and crack depth on the first buckling critical load of six-bay frame structure and its mode shape. As seen in Figure 5.43©, the left and the right hand side of the results obtained from the maximum crack depth condition around 65th node is symmetric except the area between 60th and 70th nodes. The maximum decrease in the buckling load occurs when the crack is either at the root of the second and sixth blade 30th and 110th nodes. The decreases in the critical buckling load are also seen to be when the crack is at the roots and corners of the blades at 1st , 10th , 20th ,40th ,50th , 60th ,70th , 80th ,,90th, 100th 120th and 130th nodes.

5.4.7 Two-story frame structure

Figure 5.44 shows the effect of crack location and crack depth on the first buckling critical load of two-story frame structures and its mode shape. As the crack depth increases, the variation of first buckling critical load becomes significant. The variation in the first buckling critical load when the crack is between 1st and 30th nodes, is centered symmetrically around the 15th node, and between 30th and 60th nodes is centered symmetrically around the 45th node of the FE as seen in Figure 5.44©. The maximum decrease in the buckling load occurs when the crack is either at 10th and 20th nodes (the joint point between the lower and the upper frame) .The decrease in the critical load also occurs when the crack is at 40th and 50th nodes.

5.4.8 Three-story frame structure

Figure 5.45 shows the effect of crack location and crack depth on the first buckling critical load of three-story frame structures and its mode shape. As seen in Figure 5.45©, similar to the effect of the crack shown in Figure 5.44©, variation in the first buckling critical load when the crack is between 1st and 30th nodes is

centered symmetrically around the 15th node. Moreover the similar symmetric canters are seen around 45th and 75th nodes for the crack in the areas between 30th and 60th, 60th and 90th nodes of the FE respectively. The maximum decrease in the first buckling critical load occurs when the crack is either at the connection points between the middle and the upper frame at the 40th and 50th nodes.

5.5 Dynamic stability

The regions of dynamic instability are distinguished as the first, second, third, etc. In this work the first region of instability (near $\Omega = 2\omega$) or it is called the principle region of dynamic stability is studied the most dangerous and has the greatest practical importance. Here Ω and ω are the forcing (disturbing) frequency and the natural frequency respectively. So, the first region of instability is studied by taking the static load parameter $\alpha = 0$, 0.2 and relative crack depth a/b=0.5. The effect of both crack depth and crack location on the forcing (disturbing) frequencies (Ω), which construct the boundaries of unstable regions, are shown as 3D plots in figures 5.47 to 5.62. From these frequencies it can easily be noticed that the unstable region widens as dynamic load parameter β increase and an increase in static load parameter α decreases the frequencies and unstable region occurs at lower frequencies. As seen from the 3D plots, when static load parameter α has the extreme values of 0 and 0.2, the forcing frequencies constructing the lower border of unstable region reach zero values at which dynamic load parameter β corresponds to the values of 2 and 1.6, respectively, no matter where the crack locates.

Figures 5.63 to 5.70, shows the unstable regions having different static load parameters and relative crack ratios. The unstable regions of the frame structure with the static load ($\alpha \neq 0$) is wider than that without static load ($\alpha = 0$).

Figure 5.71, shows the unstable region for the multi-bay frame. When the number of blades decreases the unstable region becomes wider.

Figure 5.72, shows the unstable region for the multi-story frame. When the number of stories decreases the unstable region becomes narrower and shifts to the origin.

Figure 5.73, shows the effect of crack depths. Increase in the relative crack depth reduces the values of frequencies but the differences between the borders of the unstable regions with different crack depths are very small, even for the crack ratio of 0.5.
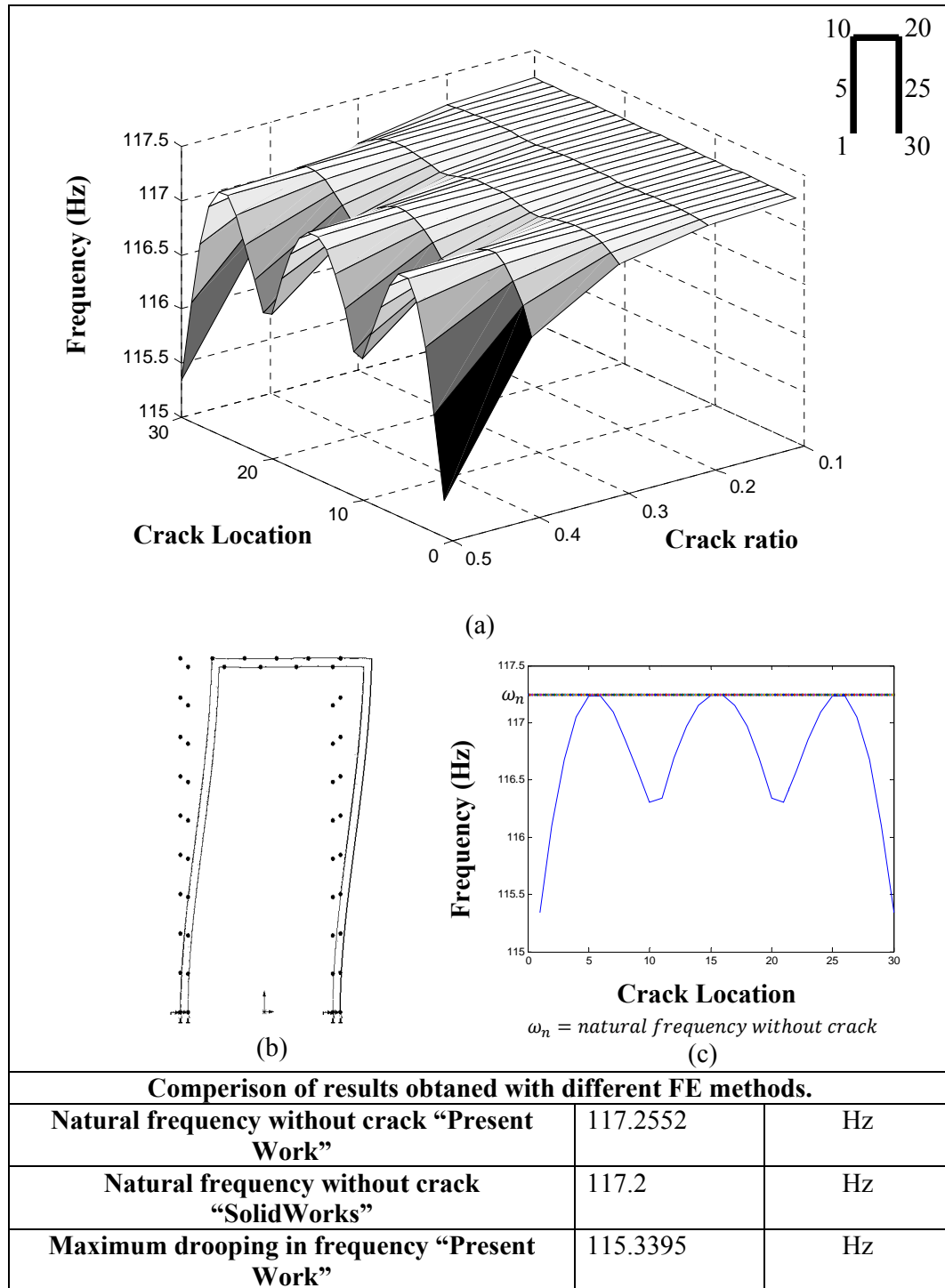
(a)

ω_n

$\omega_n = natural\ frequency\ without\ crack$

(b)

(c)

Comperison of results obtaned with different FE methods.		
Natural frequency without crack "Present Work"	117.2552	Hz
Natural frequency without crack "SolidWorks"	117.2	Hz
Maximum drooping in frequency "Present Work"	115.3395	Hz

Figure 5.6 Crack effect on the first natural frequency of a single frame structure.

    a) Effect of crack ratio and crack location

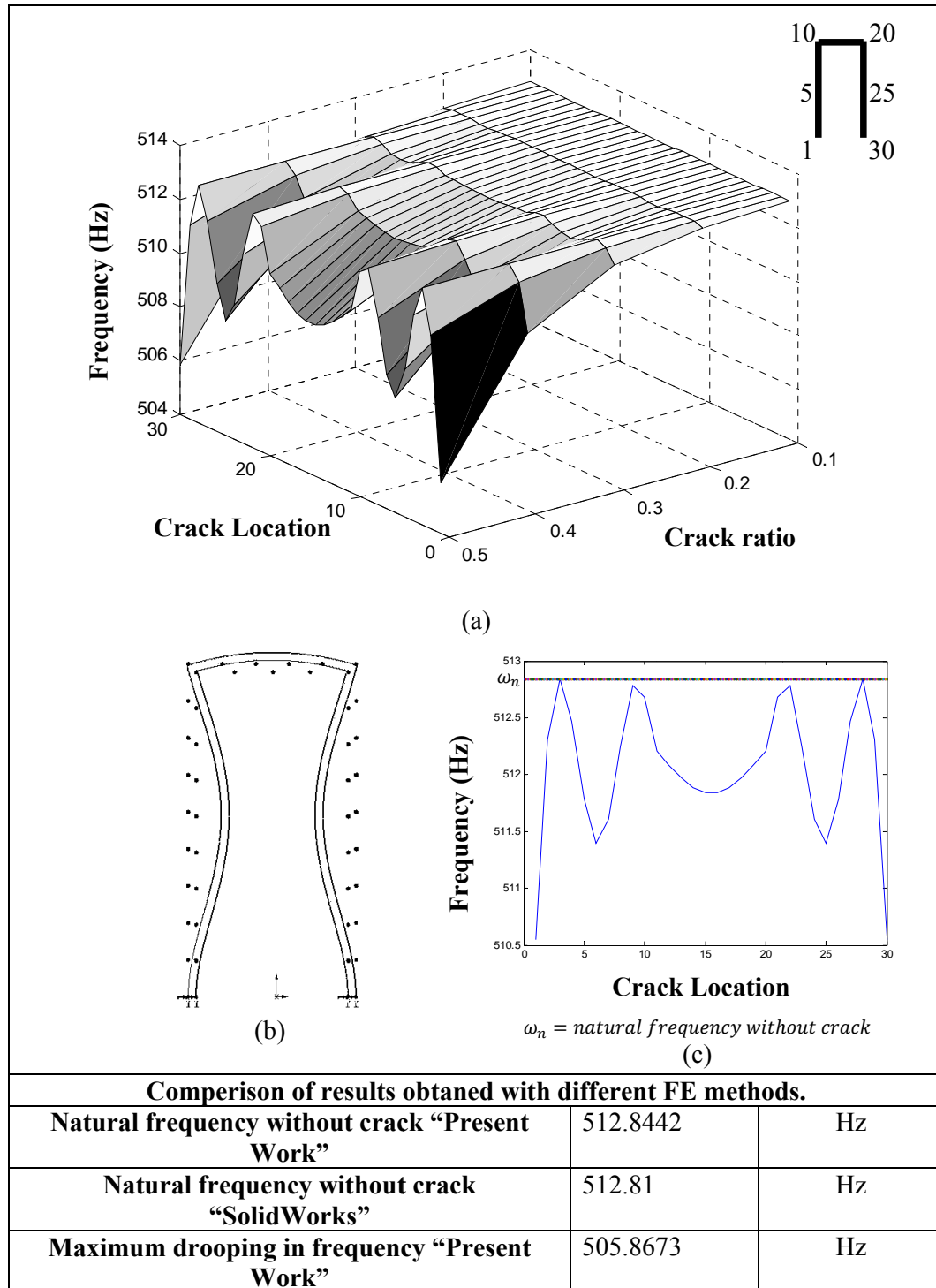   b) First mode shape

    c) Effect of maximum crack ratio 0.5

(a)

(b)

$\omega_n = natural\ frequency\ without\ crack$

(c)

Comperison of results obtaned with different FE methods.		
Natural frequency without crack "Present Work"	512.8442	Hz
Natural frequency without crack "SolidWorks"	512.81	Hz
Maximum drooping in frequency "Present Work"	505.8673	Hz

Figure 5.7 Crack effect on the second natural frequency of a single frame structure.

 a) Effect of crack ratio and crack location

 b) Second mode shape

 c) Effect of maximum crack ratio 0.5
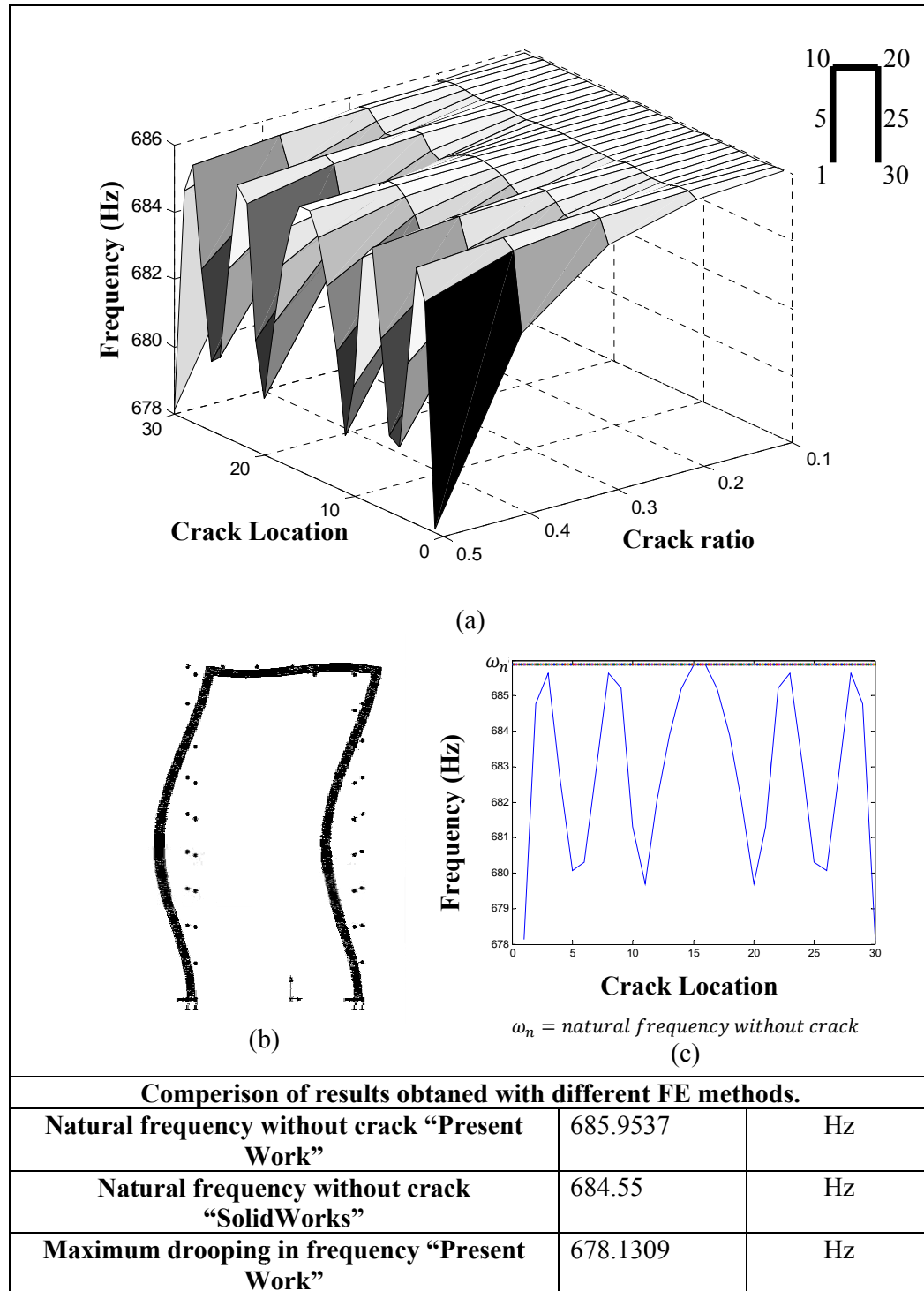
Figure 5.8 Crack effect on the third natural frequency of a single frame structure.

a) Effect of crack ratio and crack location
b) Third mode shape
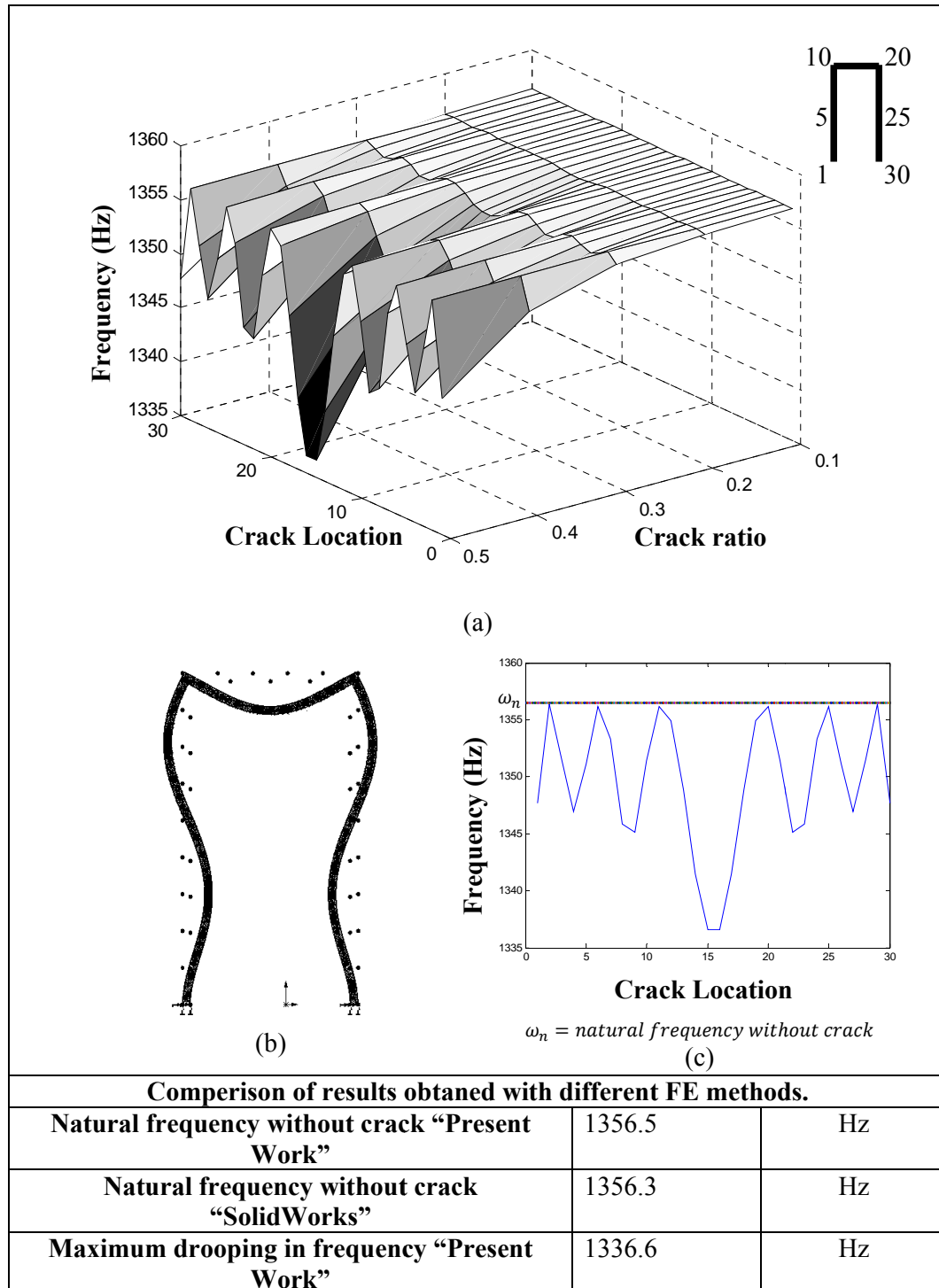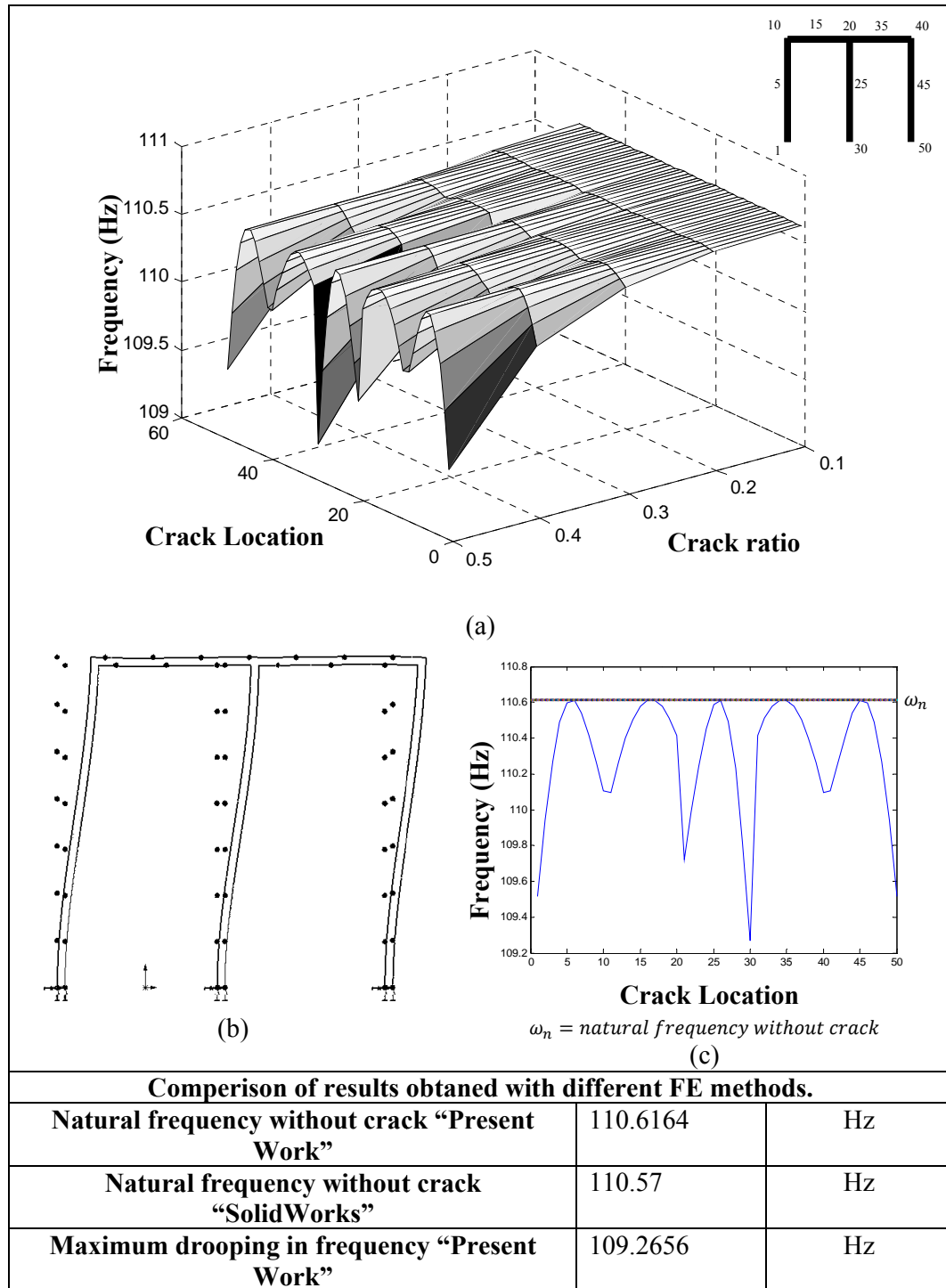c) Effect of maximum crack ratio 0.5

Comperison of results obtaned with different FE methods.		
Natural frequency without crack "Present Work"	685.9537	Hz
Natural frequency without crack "SolidWorks"	684.55	Hz
Maximum drooping in frequency "Present Work"	678.1309	Hz

(a)

(b)

$\omega_n = natural\ frequency\ without\ crack$

(c)

Comperison of results obtaned with different FE methods.		
Natural frequency without crack "Present Work"	1356.5	Hz
Natural frequency without crack "SolidWorks"	1356.3	Hz
Maximum drooping in frequency "Present Work"	1336.6	Hz

Figure 5.9 Crack effect on the fourth natural frequency of a single frame structure.

     a) Effect of crack ratio and crack location

     b) Fourth mode shape

     c) Effect of maximum crack ratio 0.5
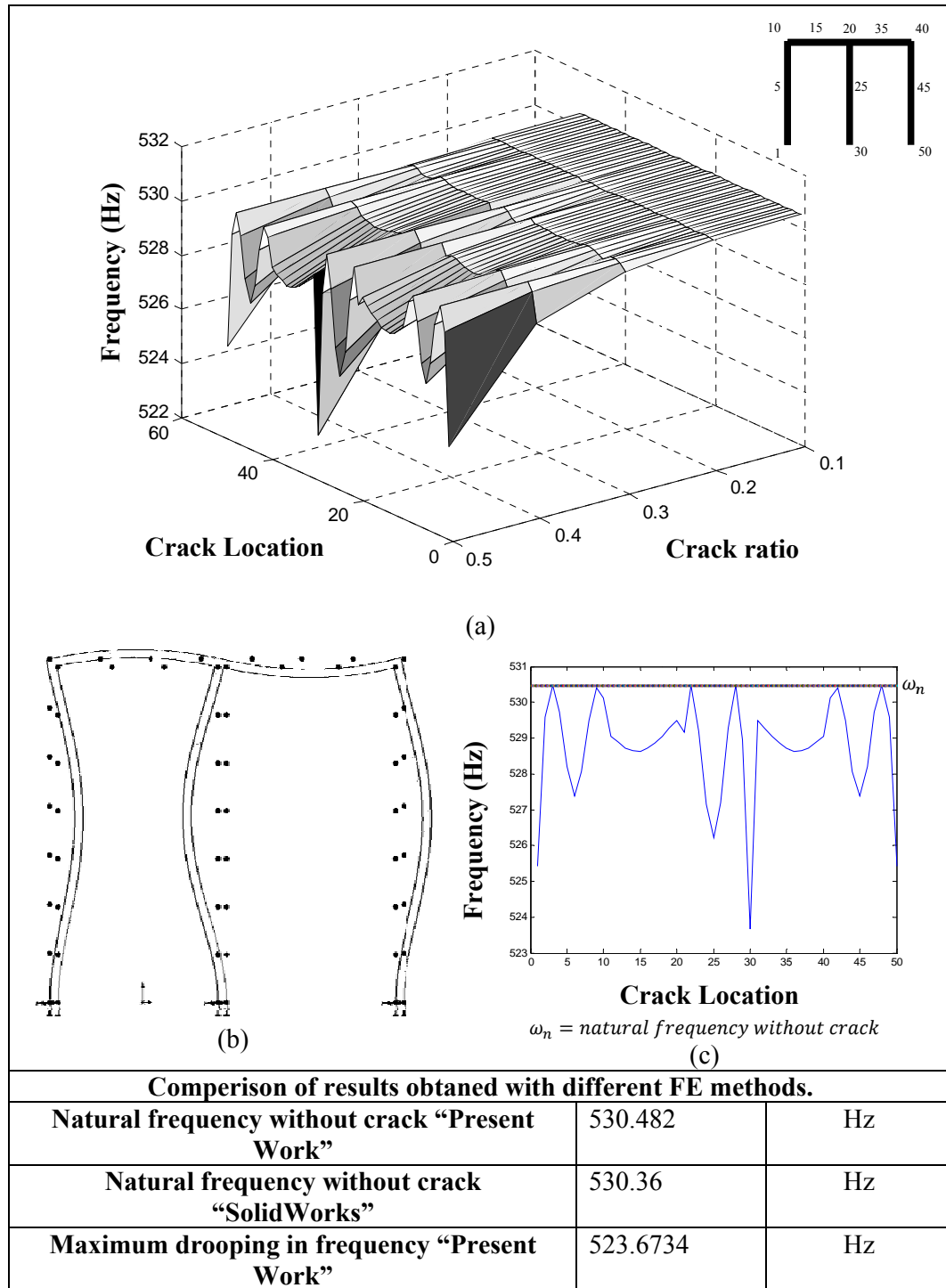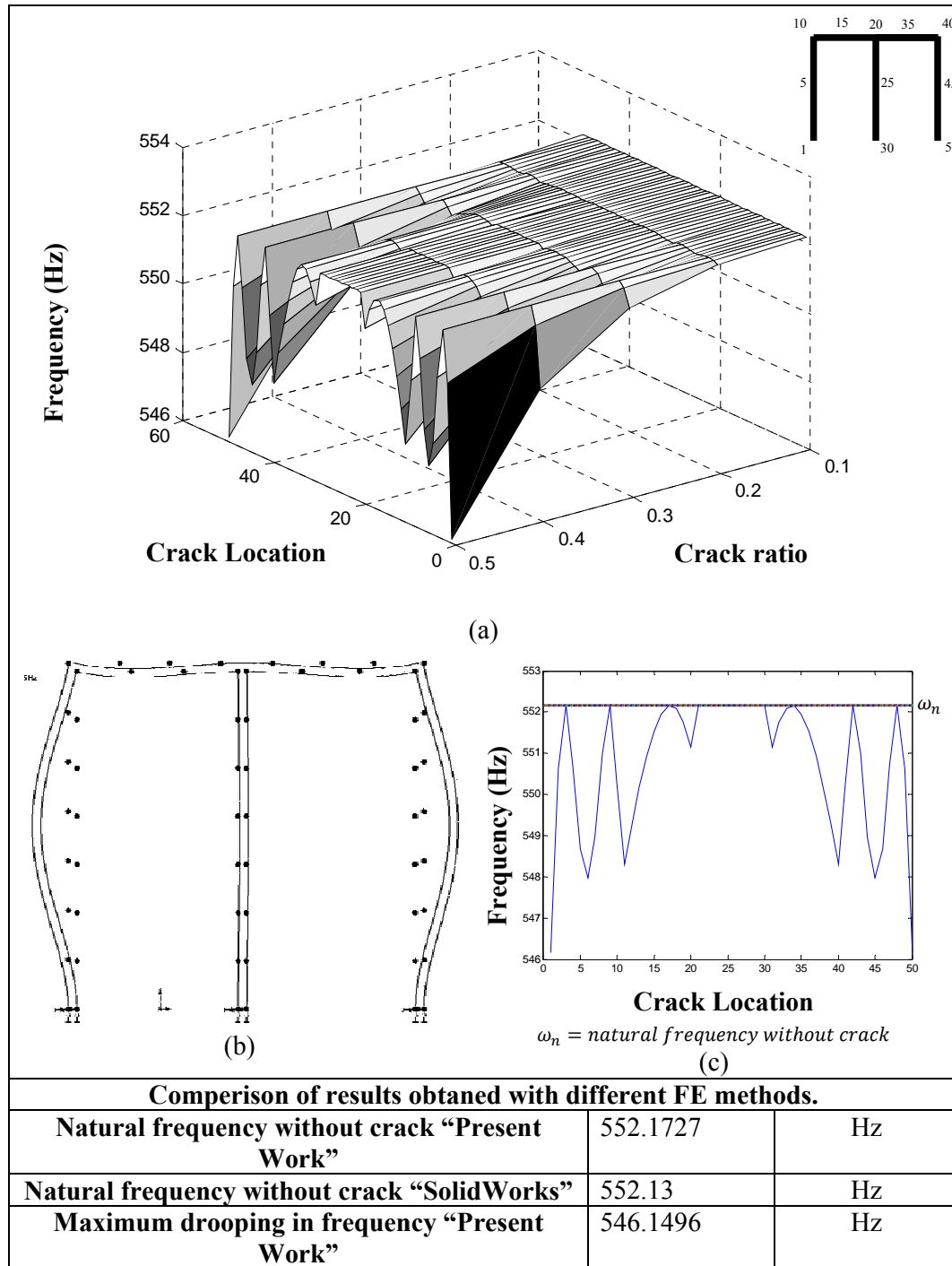
(a)

(b)

(c)

$\omega_n = natural\ frequency\ without\ crack$

Comperison of results obtaned with different FE methods.		
Natural frequency without crack "Present Work"	110.6164	Hz
Natural frequency without crack "SolidWorks"	110.57	Hz
Maximum drooping in frequency "Present Work"	109.2656	Hz

Figure 5.10 Crack effect on the first natural frequency of a two-bay frame structure.

    a) Effect of crack ratio and crack location

    b) First mode shape

    c) Effect of maximum crack ratio 0.5
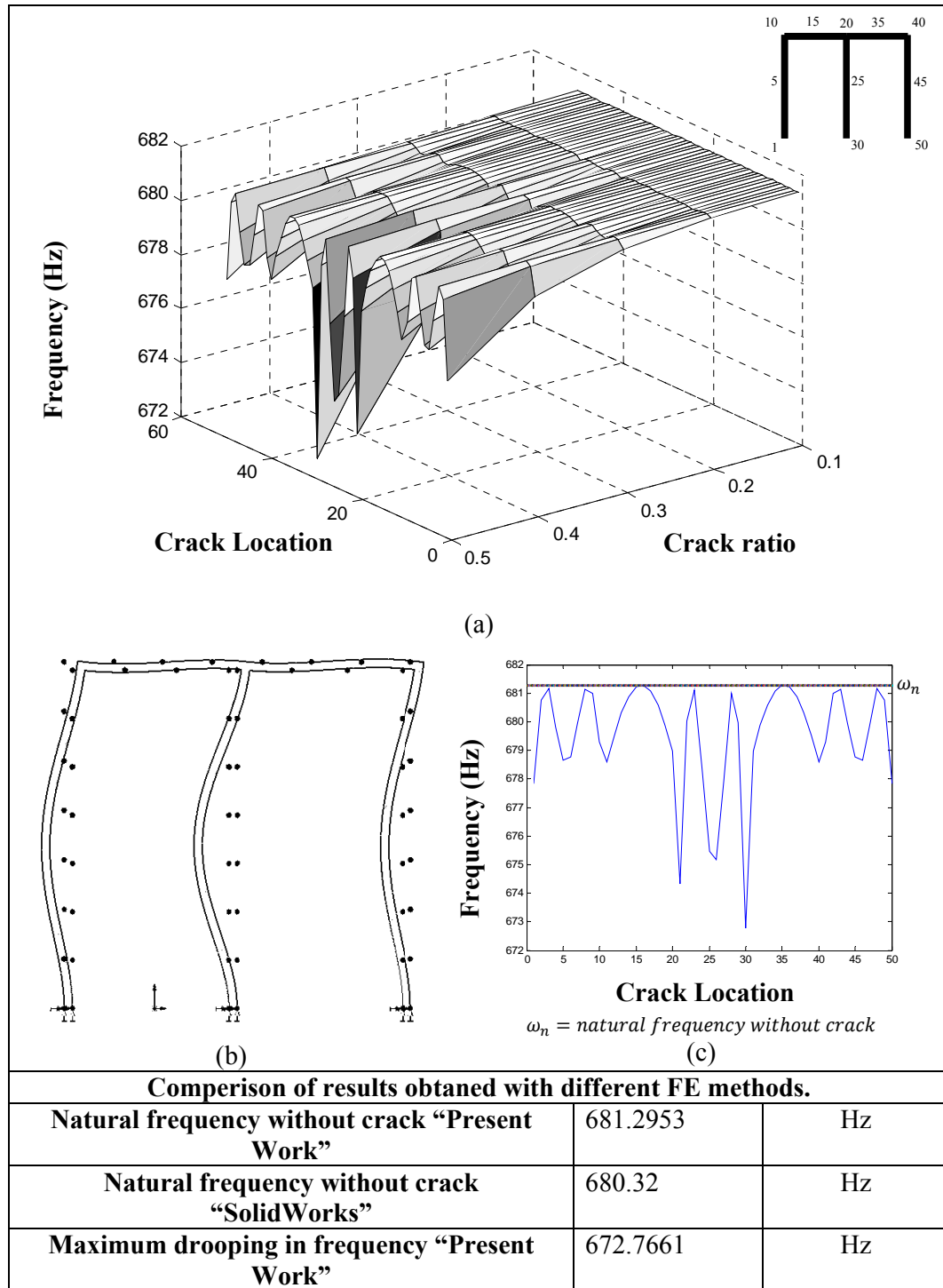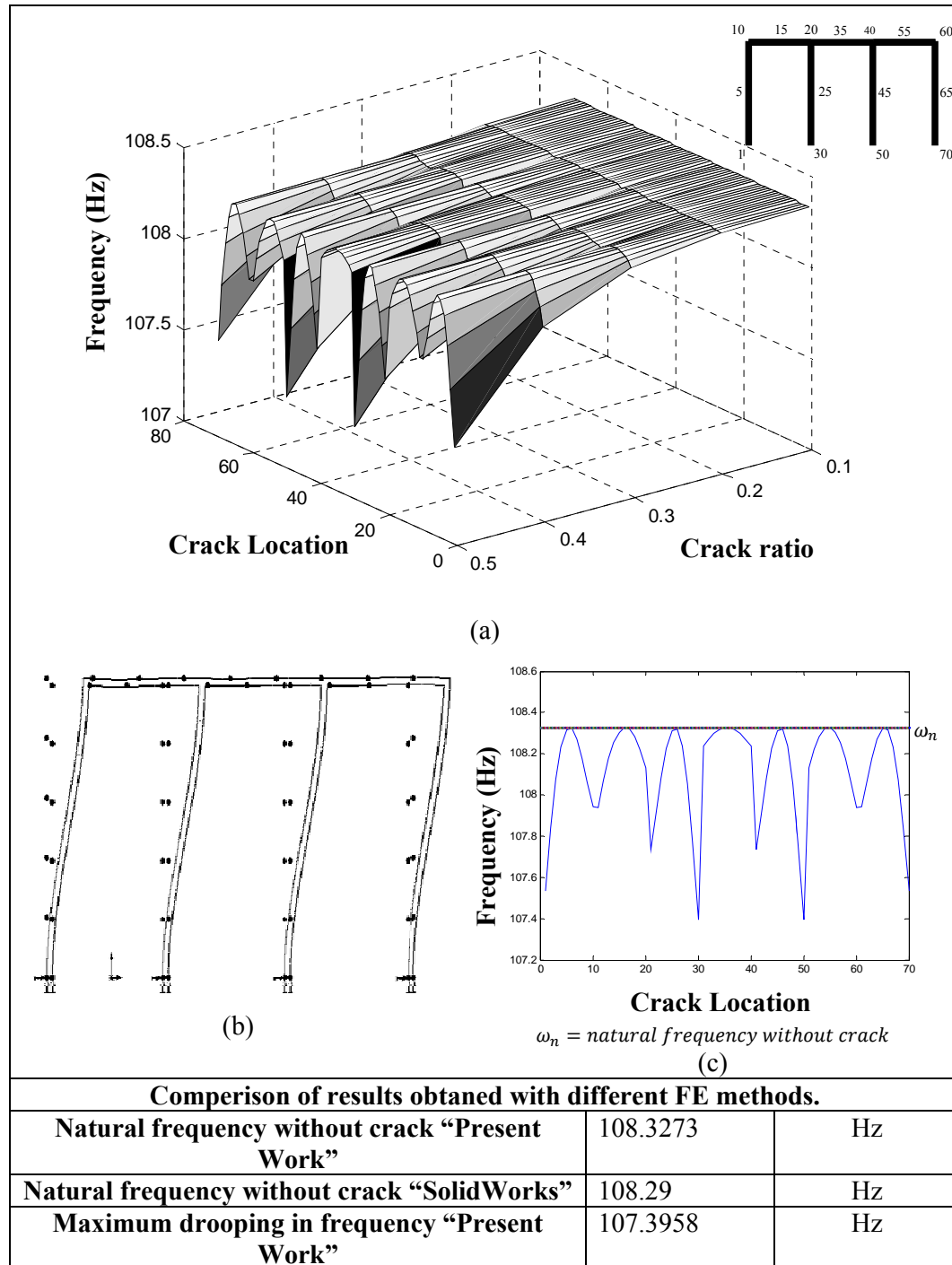
(a)

(b)

$\omega_n = natural\ frequency\ without\ crack$

(c)

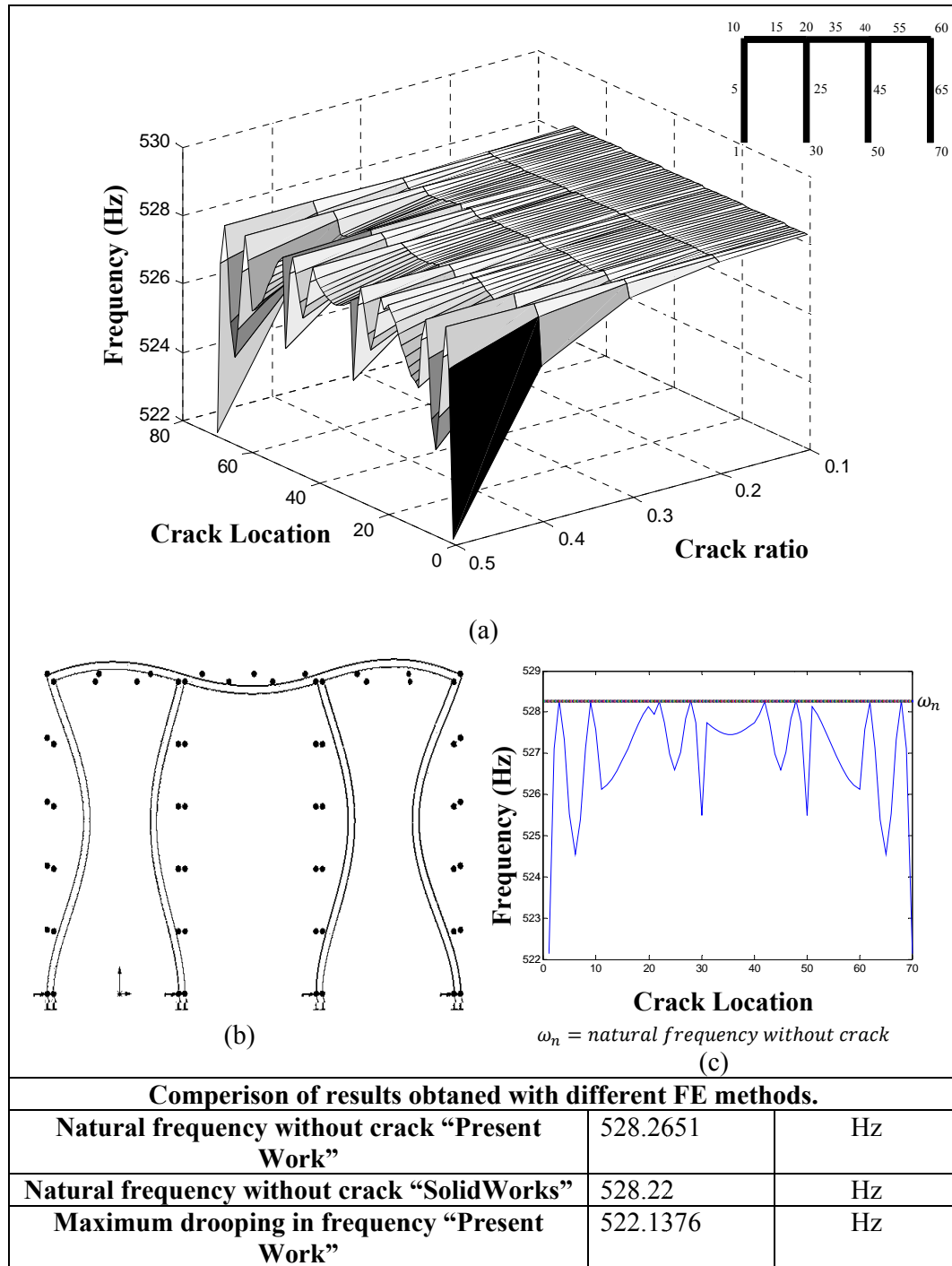| Comperison of results obtaned with different FE methods.		
Natural frequency without crack "Present Work"	530.482	Hz
Natural frequency without crack "SolidWorks"	530.36	Hz
Maximum drooping in frequency "Present Work"	523.6734	Hz

Figure 5.11 Crack effect on the second natural frequency of a two-bay frame structure.

    a)   Effect of crack ratio and crack location

    b)   Second mode shape

    c)   Effect of maximum crack ratio 0.5

(a)

(b)

$\omega_n = natural\ frequency\ without\ crack$

(c)

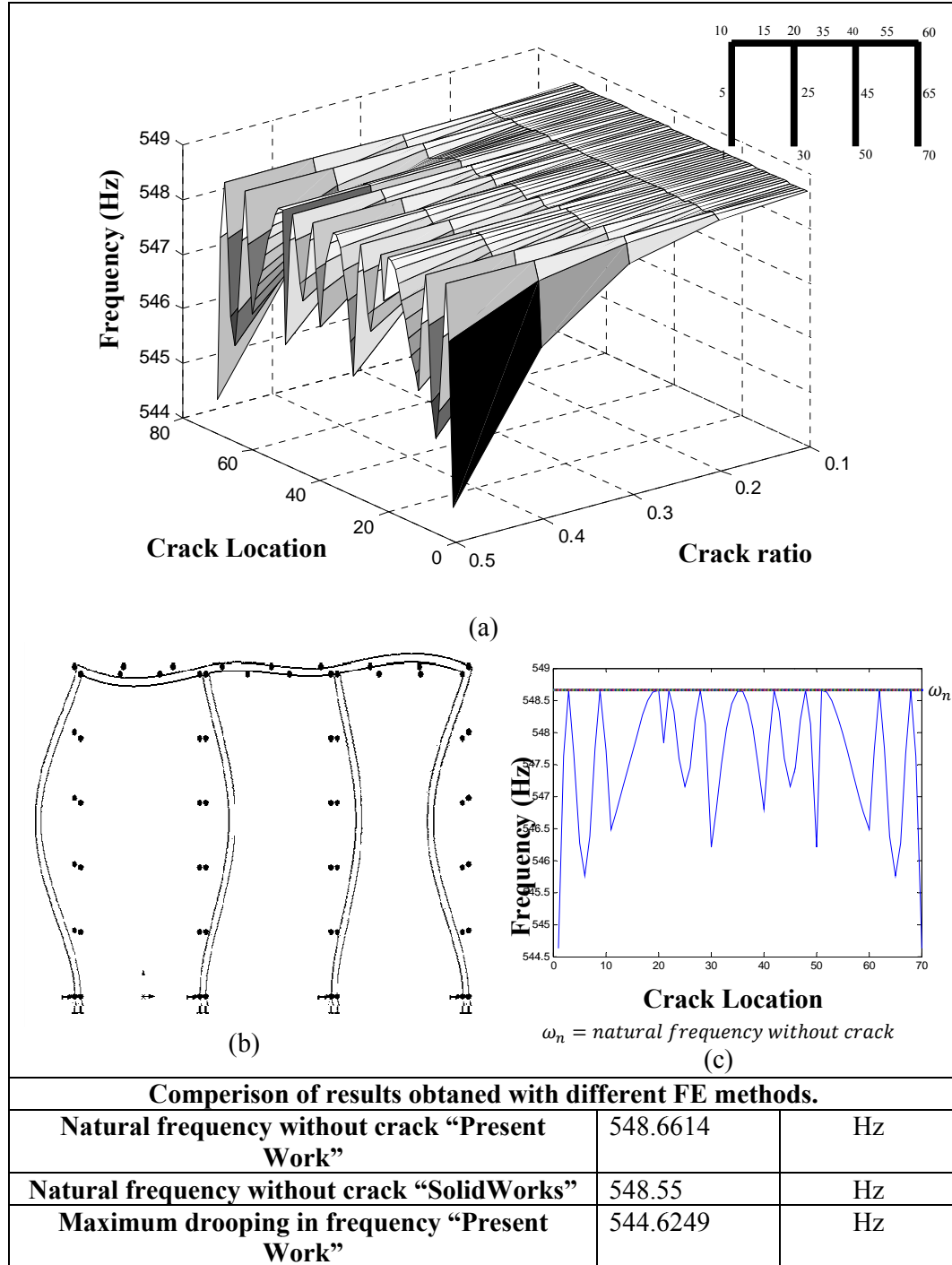| Comperison of results obtaned with different FE methods.		
Natural frequency without crack "Present Work"	552.1727	Hz
Natural frequency without crack "SolidWorks"	552.13	Hz
Maximum drooping in frequency "Present Work"	546.1496	Hz

Figure 5.12 Crack effect on the third natural frequency of a two-bay frame structure.

    a) Effect of crack ratio and crack location

    b) Third mode shape

    c) Effect of maximum crack ratio 0.5

(a)

(b)

$\omega_n = natural\ frequency\ without\ crack$

(c)

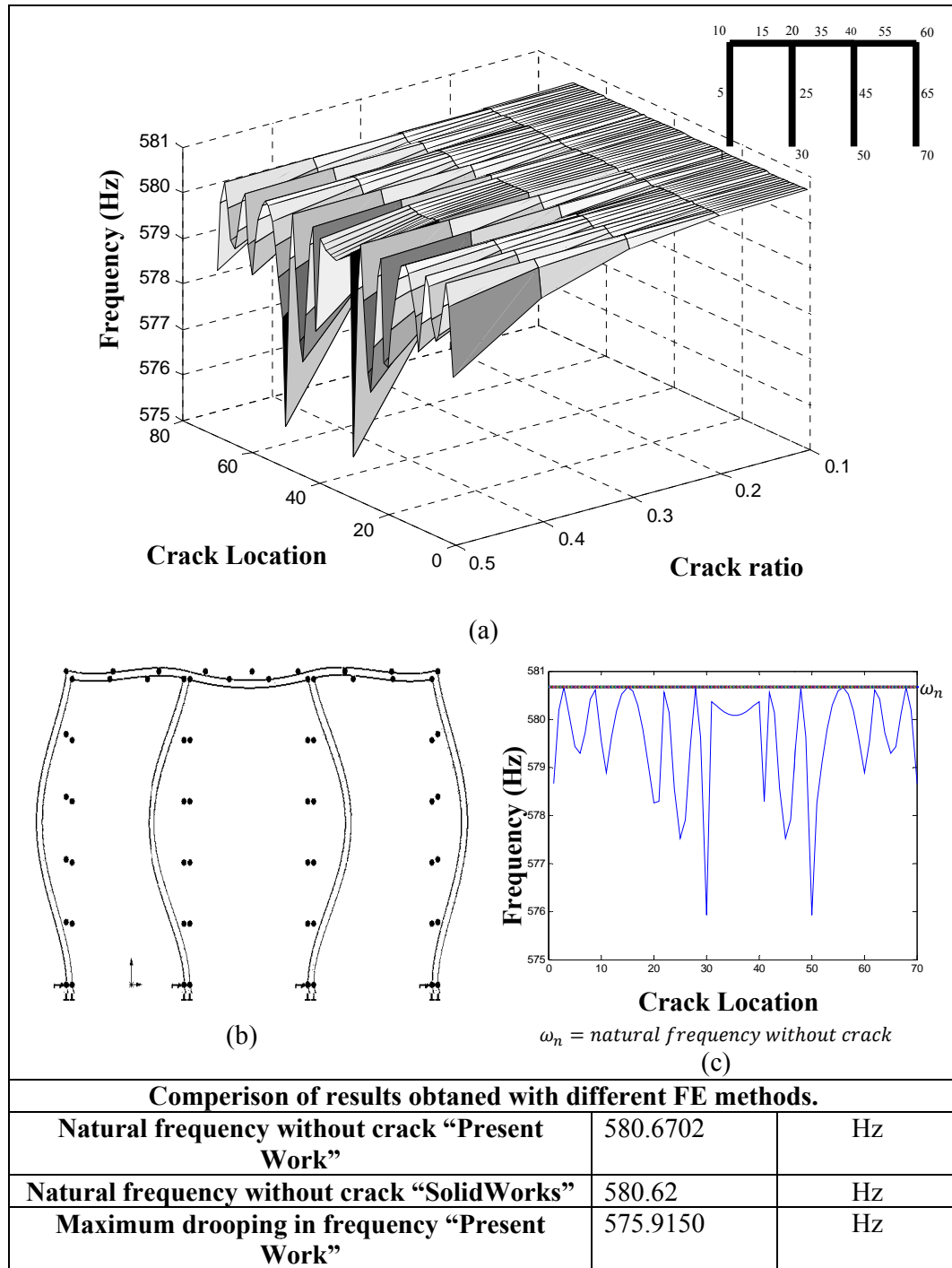| Comperison of results obtaned with different FE methods.		
Natural frequency without crack "Present Work"	681.2953	Hz
Natural frequency without crack "SolidWorks"	680.32	Hz
Maximum drooping in frequency "Present Work"	672.7661	Hz

Figure 5.13 Crack effect on the fourth natural frequency of a two-bay frame structure.

    a)   Effect of crack ratio and crack location

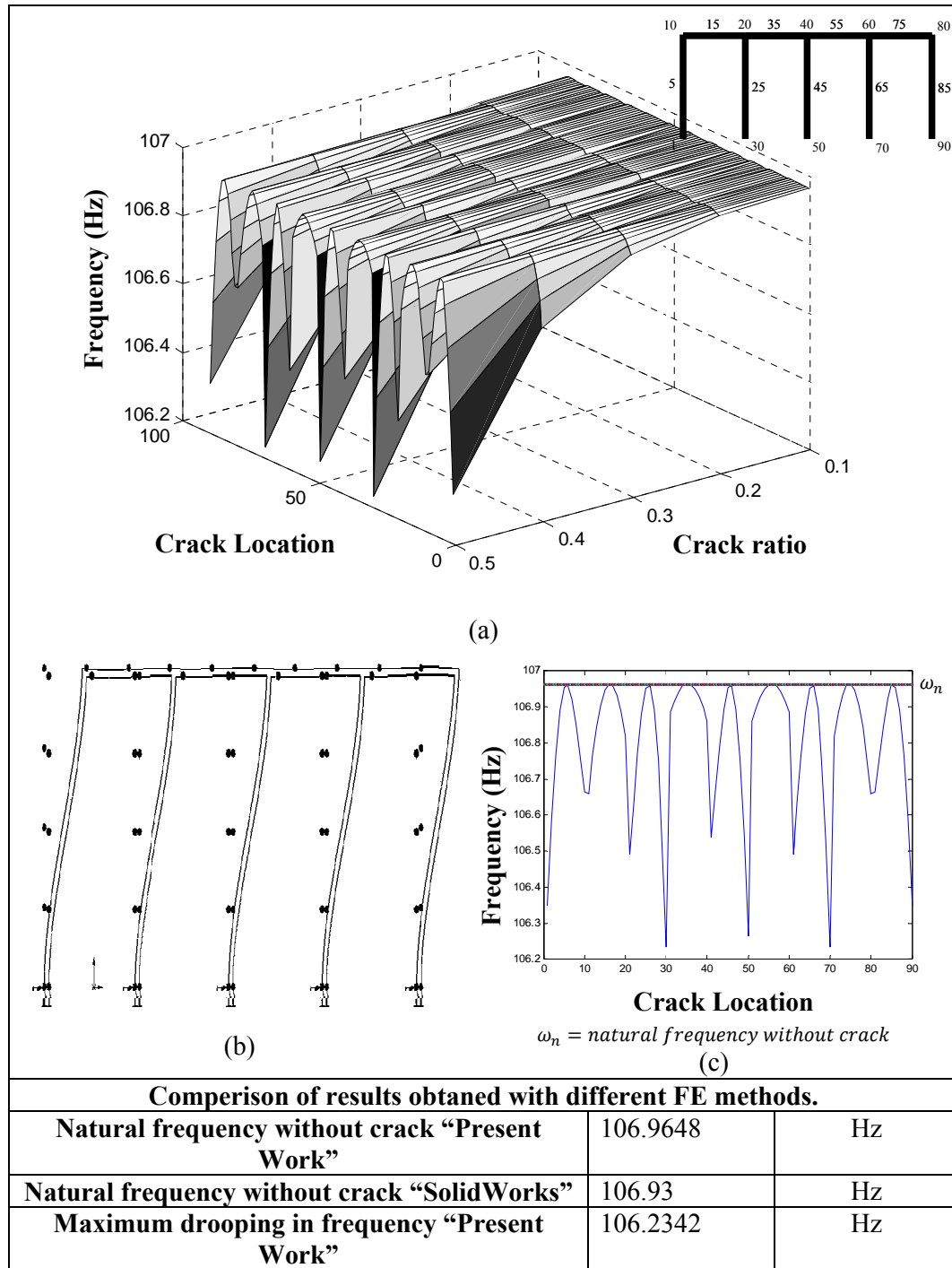   b)   Fourth mode shape

    c)   Effect of maximum crack ratio 0.5

(a)

(b)

$\omega_n = natural\ frequency\ without\ crack$

(c)

Comperison of results obtaned with different FE methods.		
Natural frequency without crack "Present Work"	108.3273	Hz
Natural frequency without crack "SolidWorks"	108.29	Hz
Maximum drooping in frequency "Present Work"	107.3958	Hz

Figure 5.14 Crack effect on the first natural frequency of a three-bay frame structure.
  a) Effect of crack ratio and crack location
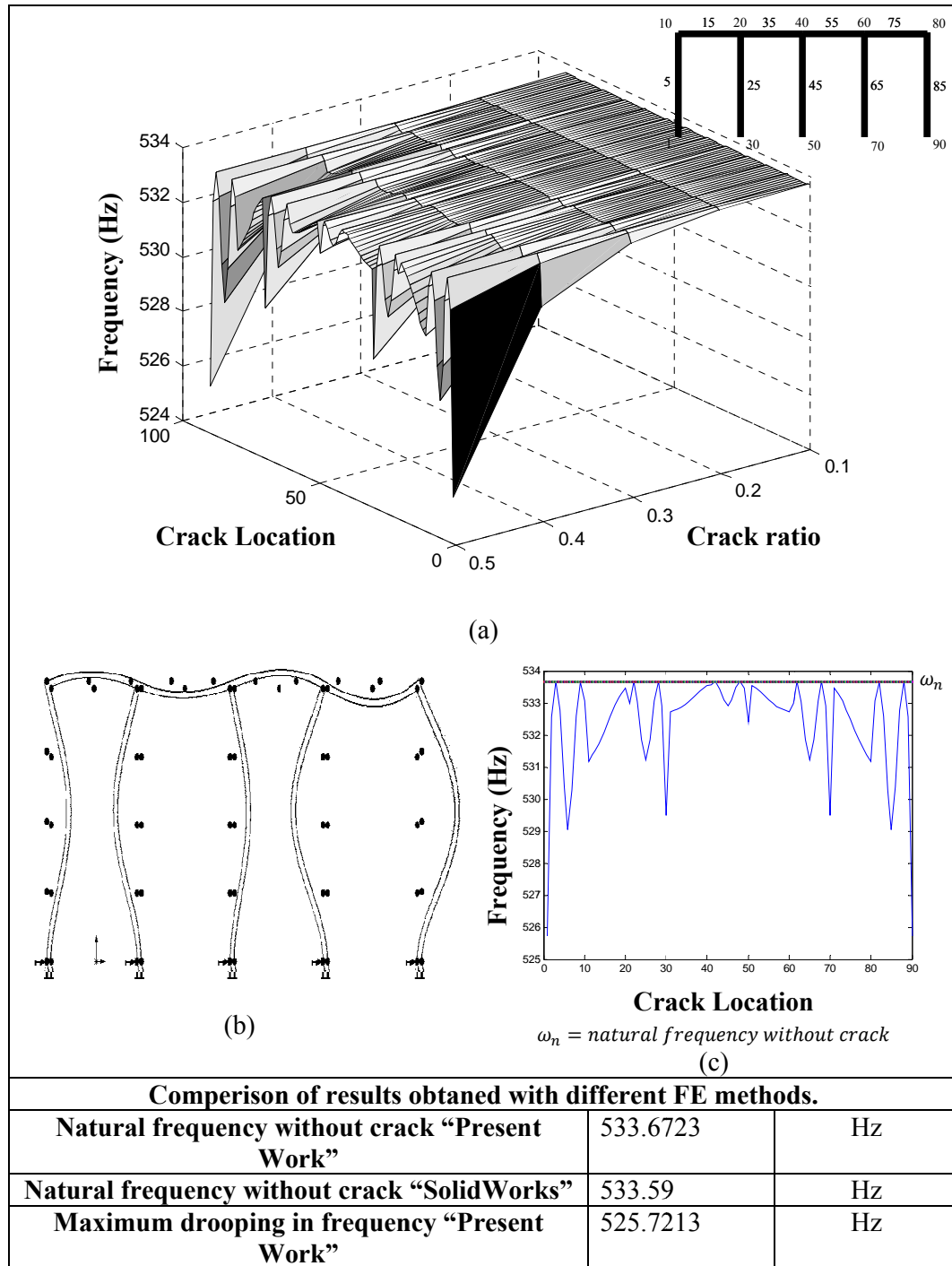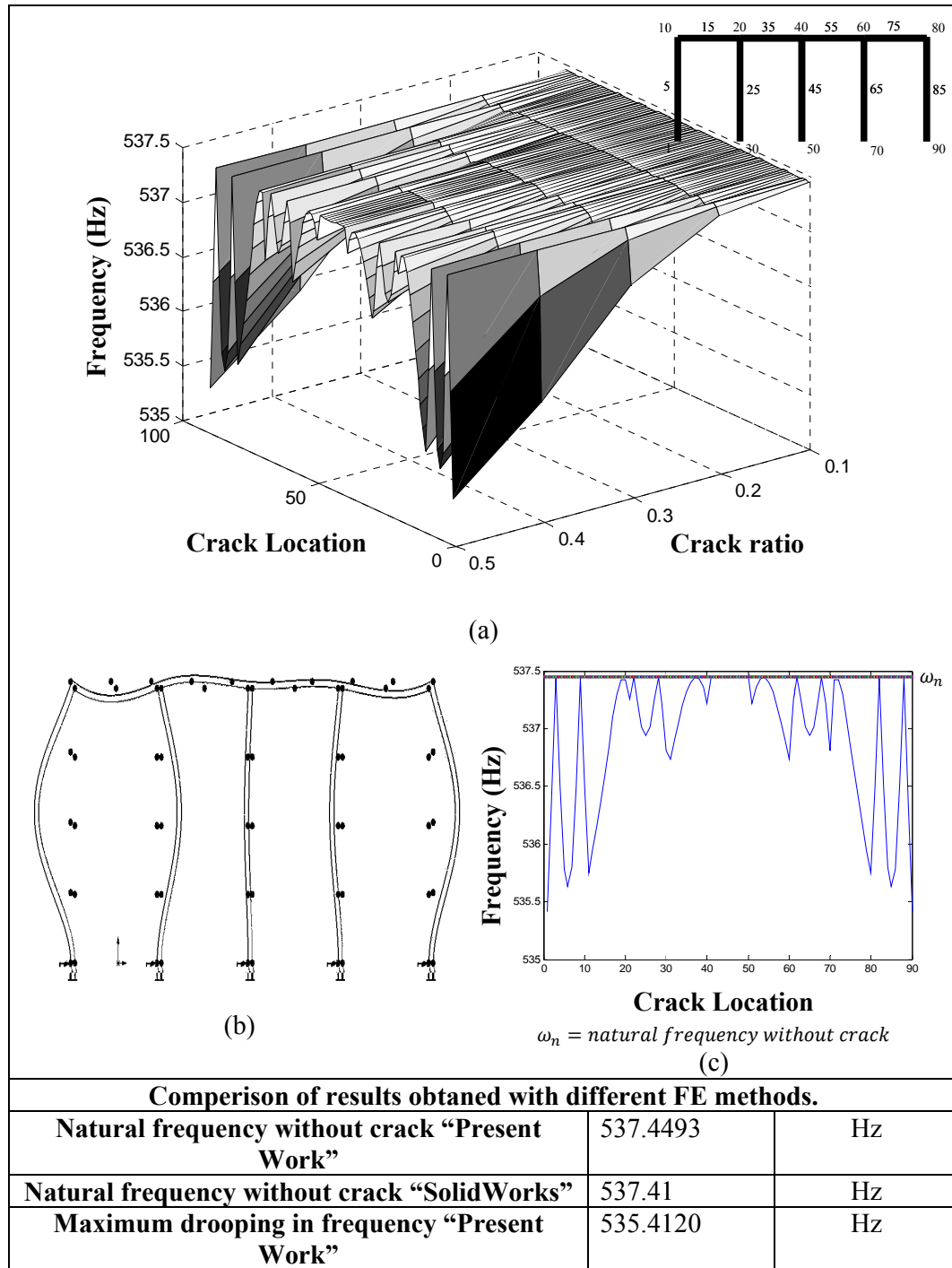 b) First mode shape
  c) Effect of maximum crack ratio 0.5

(a)

(b)

(c)

$\omega_n = natural\ frequency\ without\ crack$

Comperison of results obtaned with different FE methods.		
Natural frequency without crack "Present Work"	528.2651	Hz
Natural frequency without crack "SolidWorks"	528.22	Hz
Maximum drooping in frequency "Present Work"	522.1376	Hz

Figure 9.15 Crack effect on the second natural frequency of a three-bay frame structure.
   a) Effect of crack ratio and crack location
   b) Second mode shape
   c) Effect of maximum crack ratio 0.5
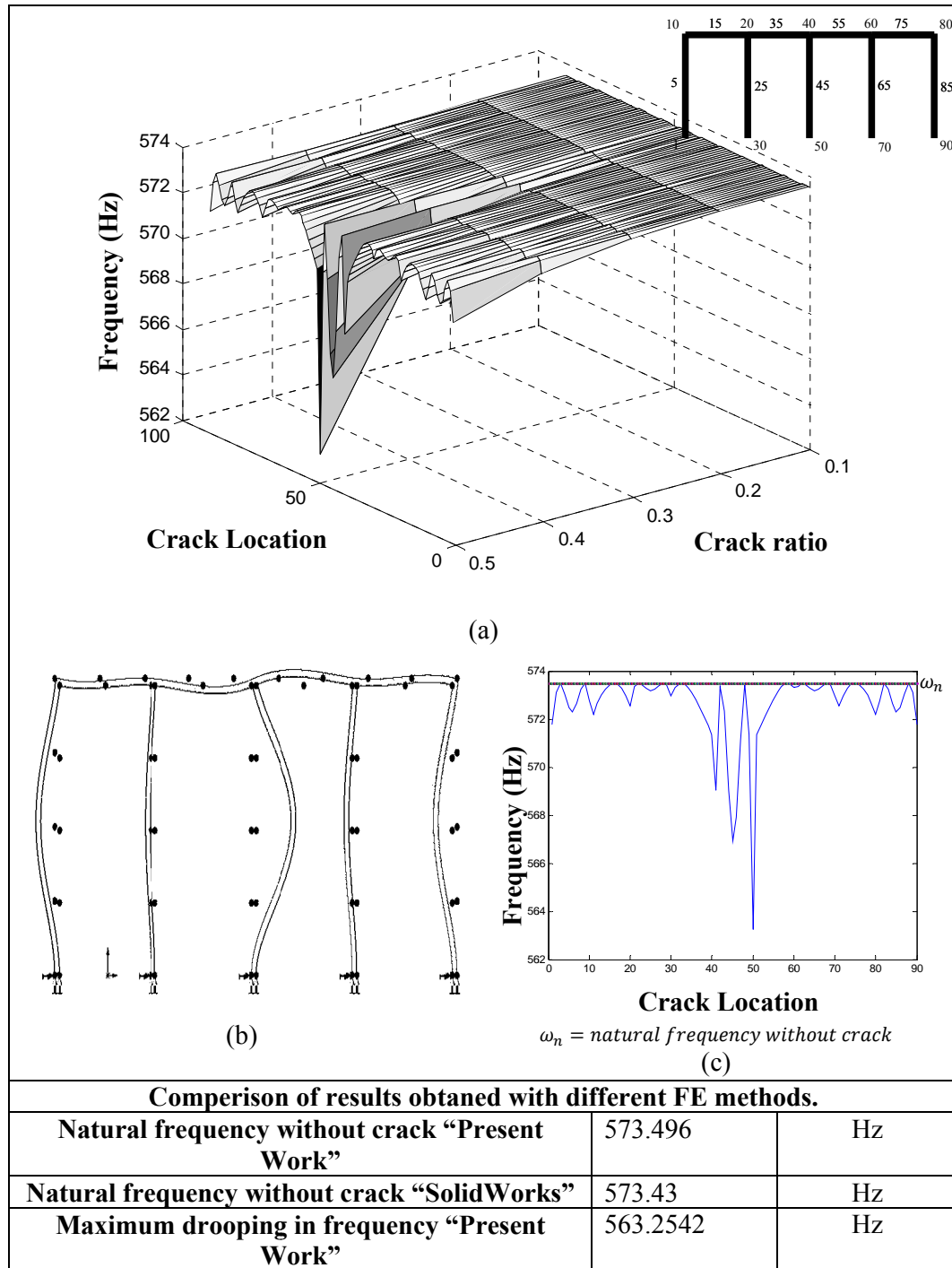
(a)

(b)

$\omega_n = natural\ frequency\ without\ crack$

(c)

Comperison of results obtaned with different FE methods.		
Natural frequency without crack "Present Work"	548.6614	Hz
Natural frequency without crack "SolidWorks"	548.55	Hz
Maximum drooping in frequency "Present Work"	544.6249	Hz

Figure 5.16 Crack effect on the third natural frequency of a three-bay frame structure.

    a)   Effect of crack ratio and crack location

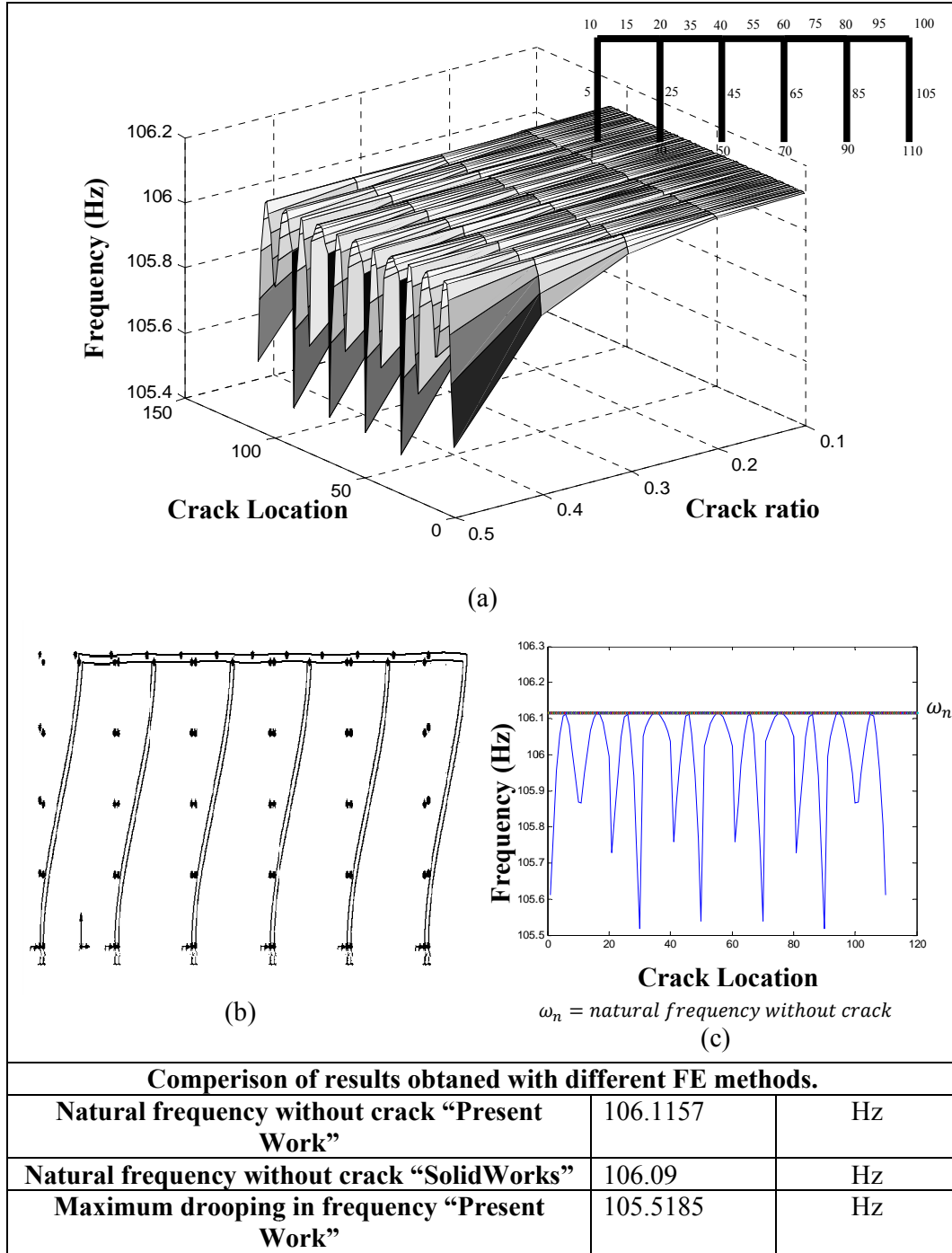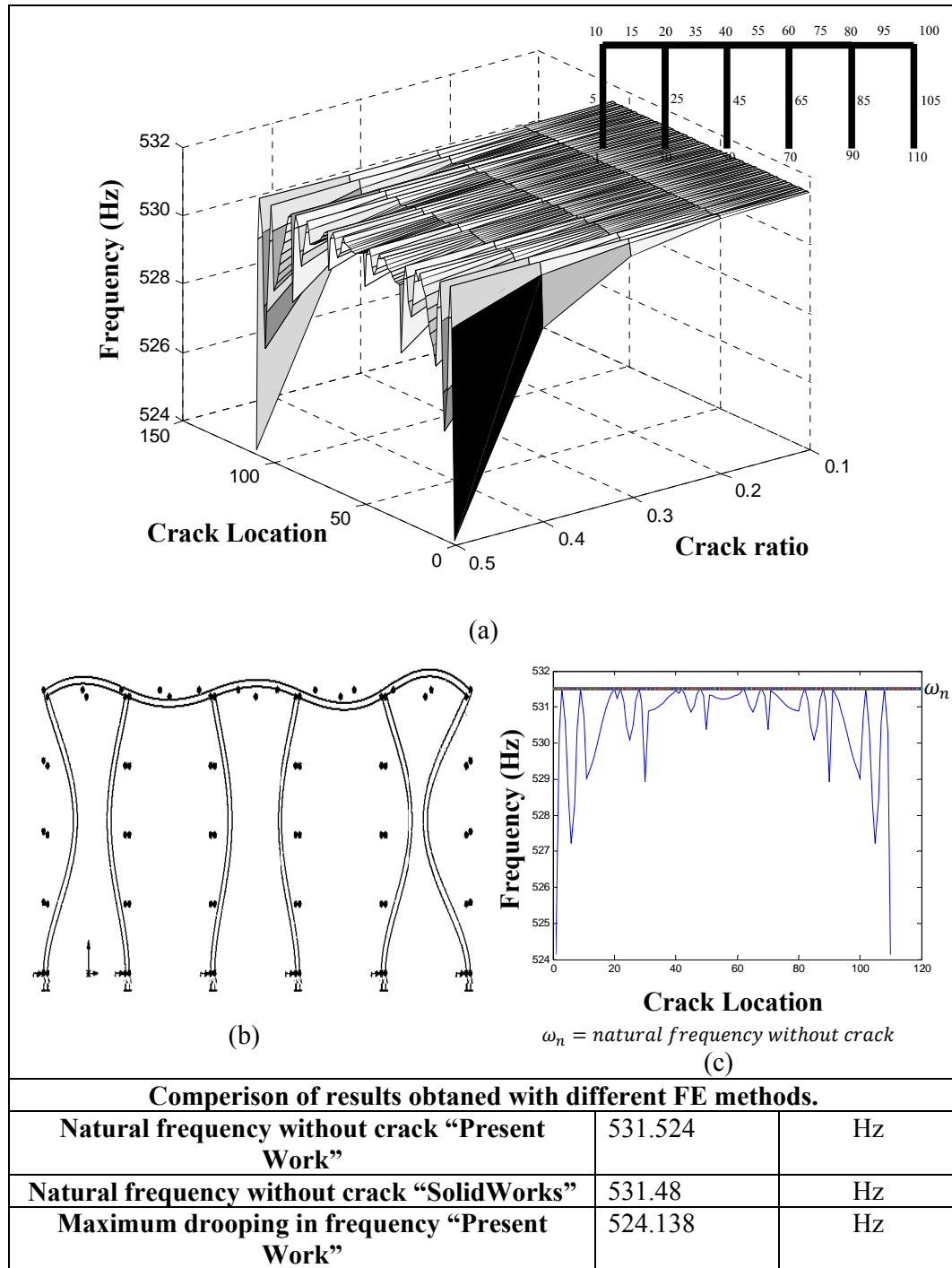   b)   Third mode shape

    c)   Effect of maximum crack ratio 0.5

(a)

(b)

$\omega_n = natural\ frequency\ without\ crack$

(c)

Comperison of results obtaned with different FE methods.		
Natural frequency without crack "Present Work"	580.6702	Hz
Natural frequency without crack "SolidWorks"	580.62	Hz
Maximum drooping in frequency "Present Work"	575.9150	Hz

Figure 5.17 Crack effect on the fourth natural frequency of a three-bay frame structure.

    a) Effect of crack ratio and crack location

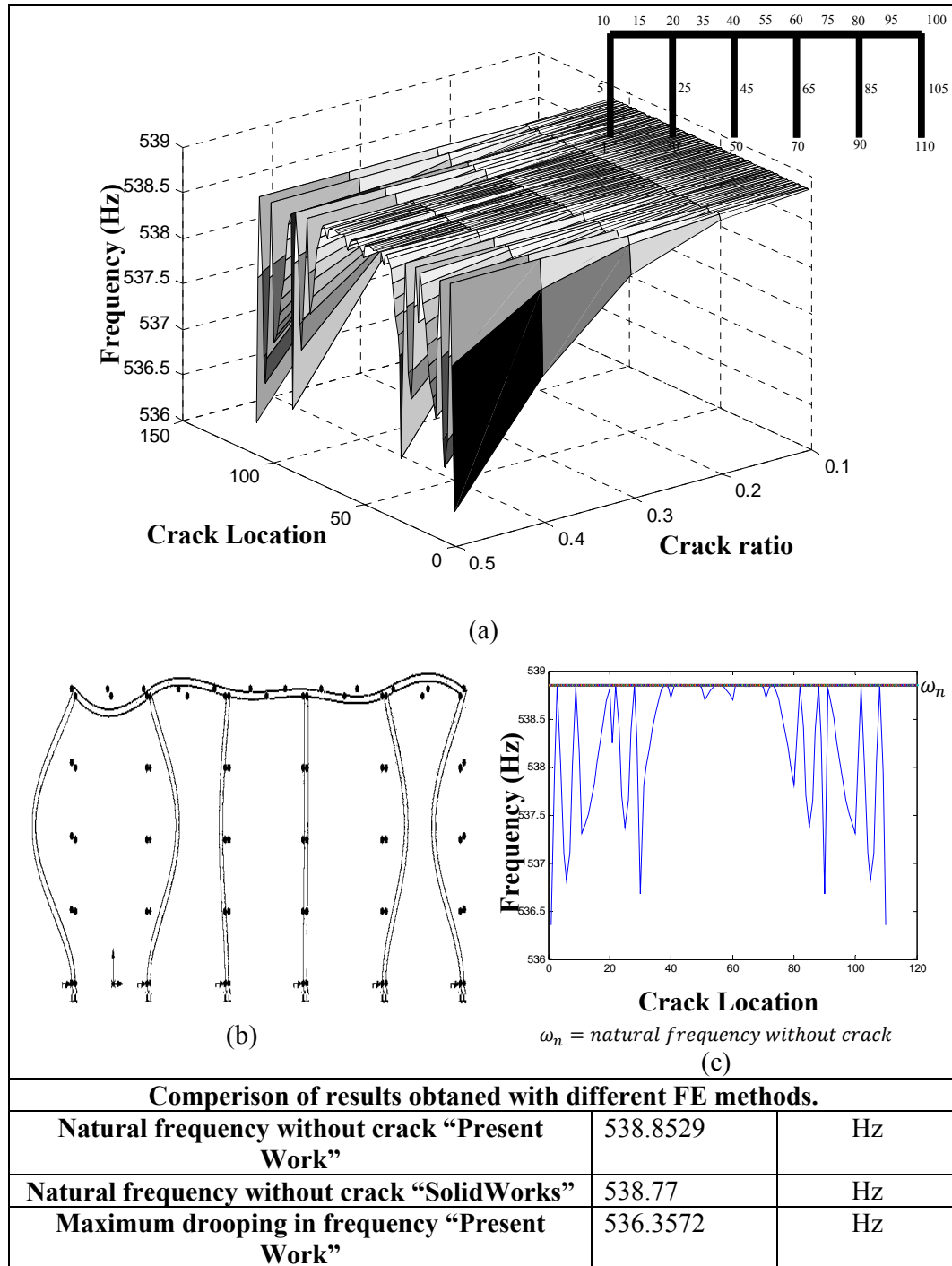   b) Fourth mode shape

    c) Effect of maximum crack ratio 0.5

(a)

(b)

(c)

$\omega_n = natural\ frequency\ without\ crack$

Comperison of results obtaned with different FE methods.		
Natural frequency without crack "Present Work"	106.9648	Hz
Natural frequency without crack "SolidWorks"	106.93	Hz
Maximum drooping in frequency "Present Work"	106.2342	Hz

Figure 5.18 Crack effect on the first natural frequency of a four-bay frame structure.
a) Effect of crack ratio and crack location
b) First mode shape
c) Effect of maximum crack ratio 0.5

(a)

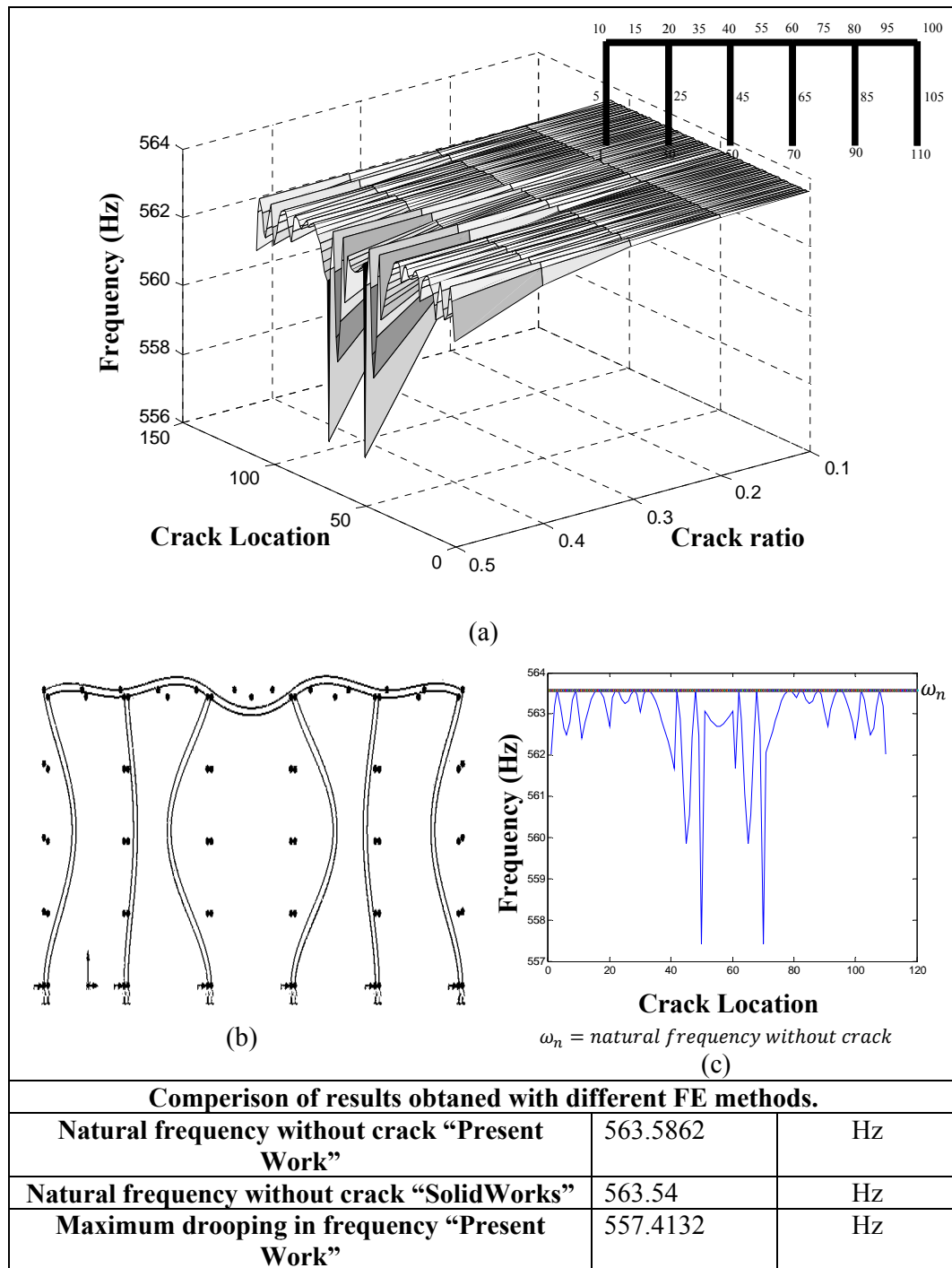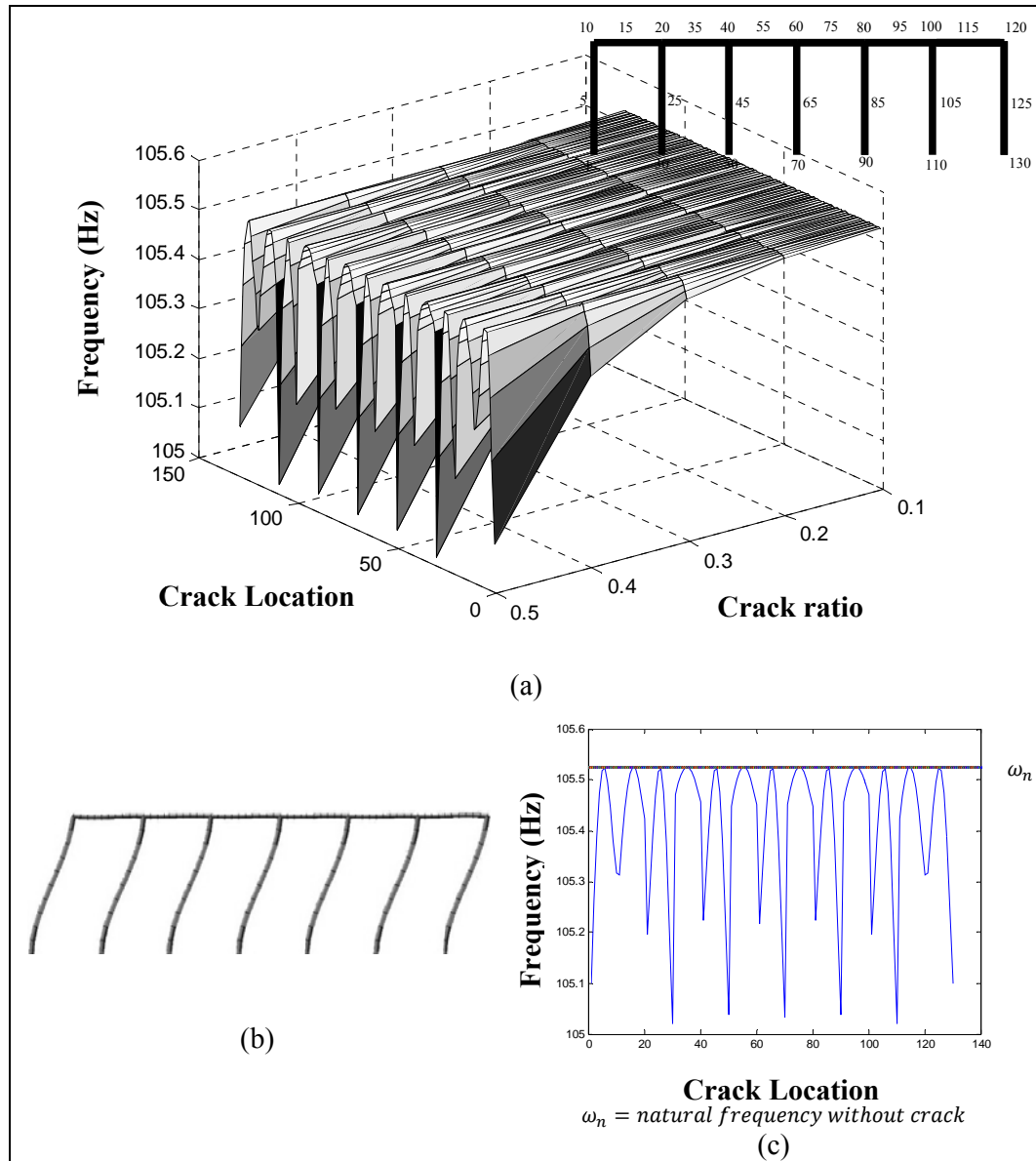

(b)

$\omega_n = natural\ frequency\ without\ crack$

(c)

Comperison of results obtaned with different FE methods.		
Natural frequency without crack "Present Work"	533.6723	Hz
Natural frequency without crack "SolidWorks"	533.59	Hz
Maximum drooping in frequency "Present Work"	525.7213	Hz

Figure 5.19 Crack effect on the second natural frequency of a four-bay frame structure.

    a) Effect of crack ratio and crack location

    b) Second mode shape

    c) Effect of maximum crack ratio 0.5

(a)

(b)

$\omega_n = natural\ frequency\ without\ crack$

(c)

Comperison of results obtaned with different FE methods.		
Natural frequency without crack "Present Work"	537.4493	Hz
Natural frequency without crack "SolidWorks"	537.41	Hz
Maximum drooping in frequency "Present Work"	535.4120	Hz

Figure 5.20 Crack effect on the third natural frequency of a four-bay frame structure.

  a) Effect of crack ratio and crack location

  b) Third mode shape

  c) Effect of maximum crack ratio 0.5
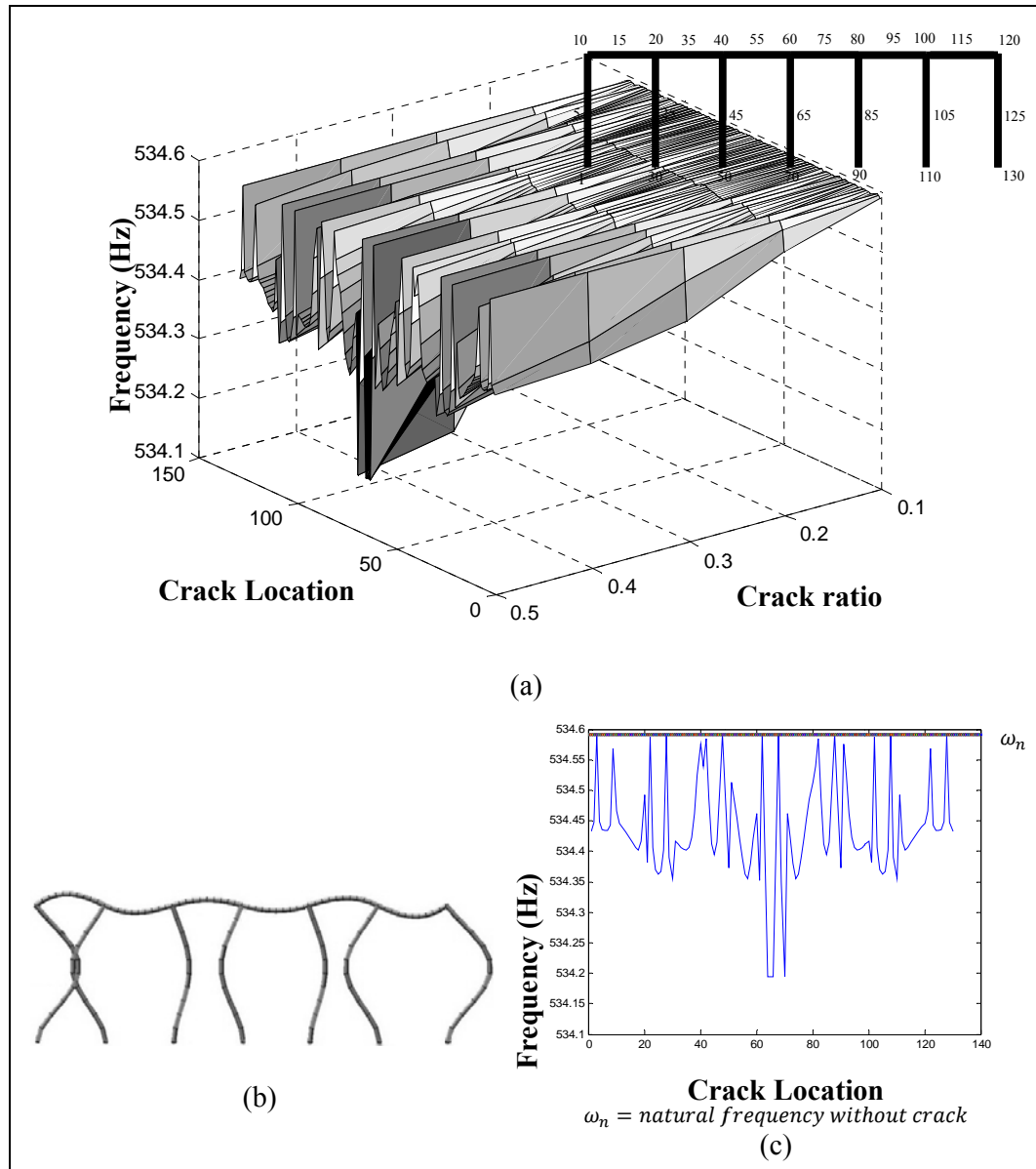
(a)

(b)

$\omega_n = natural\ frequency\ without\ crack$

(c)

Comperison of results obtaned with different FE methods.		
Natural frequency without crack "Present Work"	573.496	Hz
Natural frequency without crack "SolidWorks"	573.43	Hz
Maximum drooping in frequency "Present Work"	563.2542	Hz

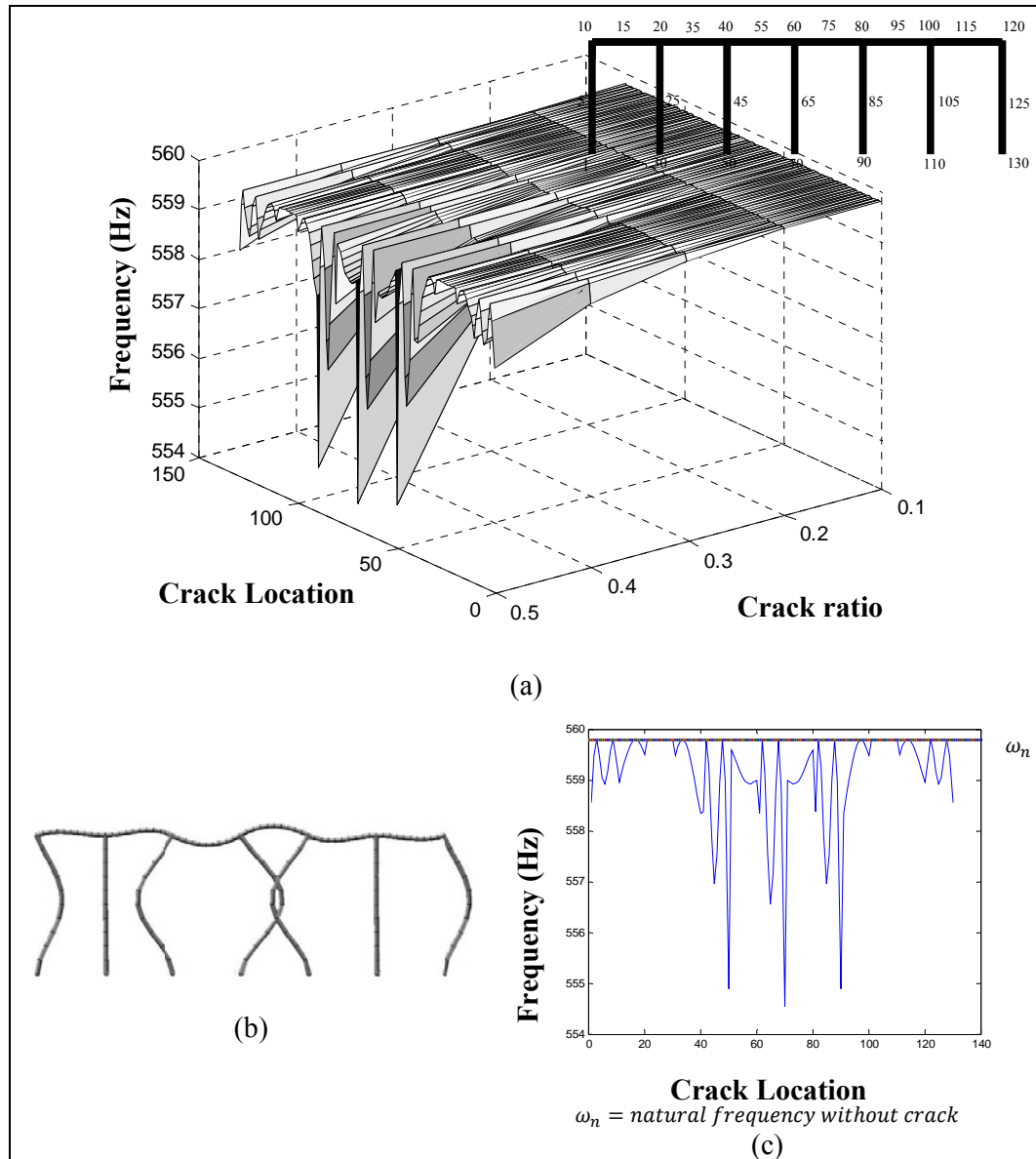Figure 5.21 Crack effect on the fourth natural frequency of a four-bay frame structure.

    a)   Effect of crack ratio and crack location

    b)   Fourth mode shape

    c)   Effect of maximum crack ratio 0.5

(a)

(b)

(c)

$\omega_n = natural\ frequency\ without\ crack$

Comperison of results obtaned with different FE methods.		
Natural frequency without crack "Present Work"	106.1157	Hz
Natural frequency without crack "SolidWorks"	106.09	Hz
Maximum drooping in frequency "Present Work"	105.5185	Hz

Figure 5.22 Crack effect on the first natural frequency of a five-bay frame structure.

    a)   Effect of crack ratio and crack location

    b)   First mode shape

    c)   Effect of maximum crack ratio 0.5

(a)

(b)

(c)

$\omega_n = natural\ frequency\ without\ crack$

Comperison of results obtaned with different FE methods.		
Natural frequency without crack "Present Work"	531.524	Hz
Natural frequency without crack "SolidWorks"	531.48	Hz
Maximum drooping in frequency "Present Work"	524.138	Hz

Figure 5.23 Crack effect on the second natural frequency of a five-bay frame structure.

    a)   Effect of crack ratio and crack location

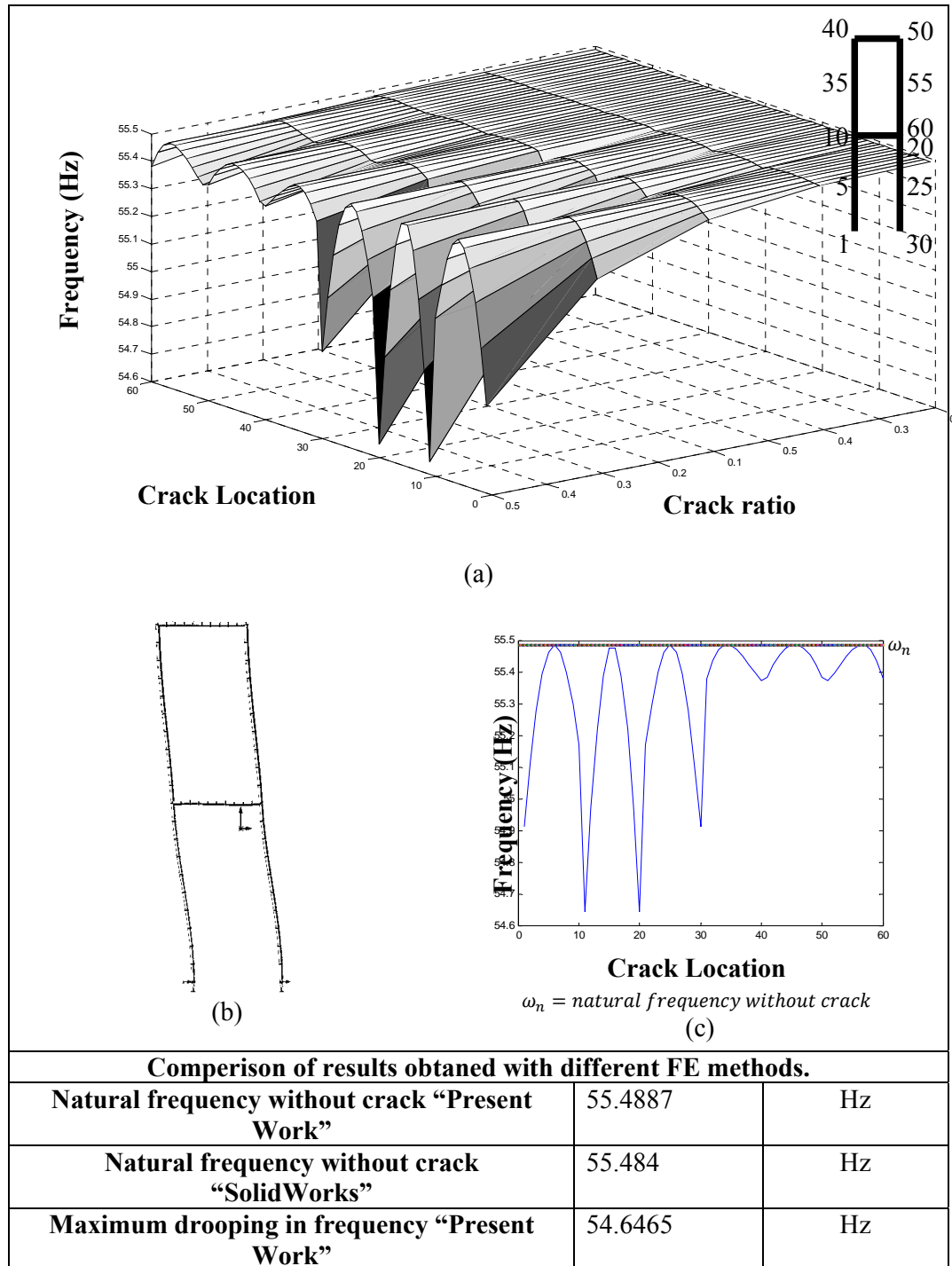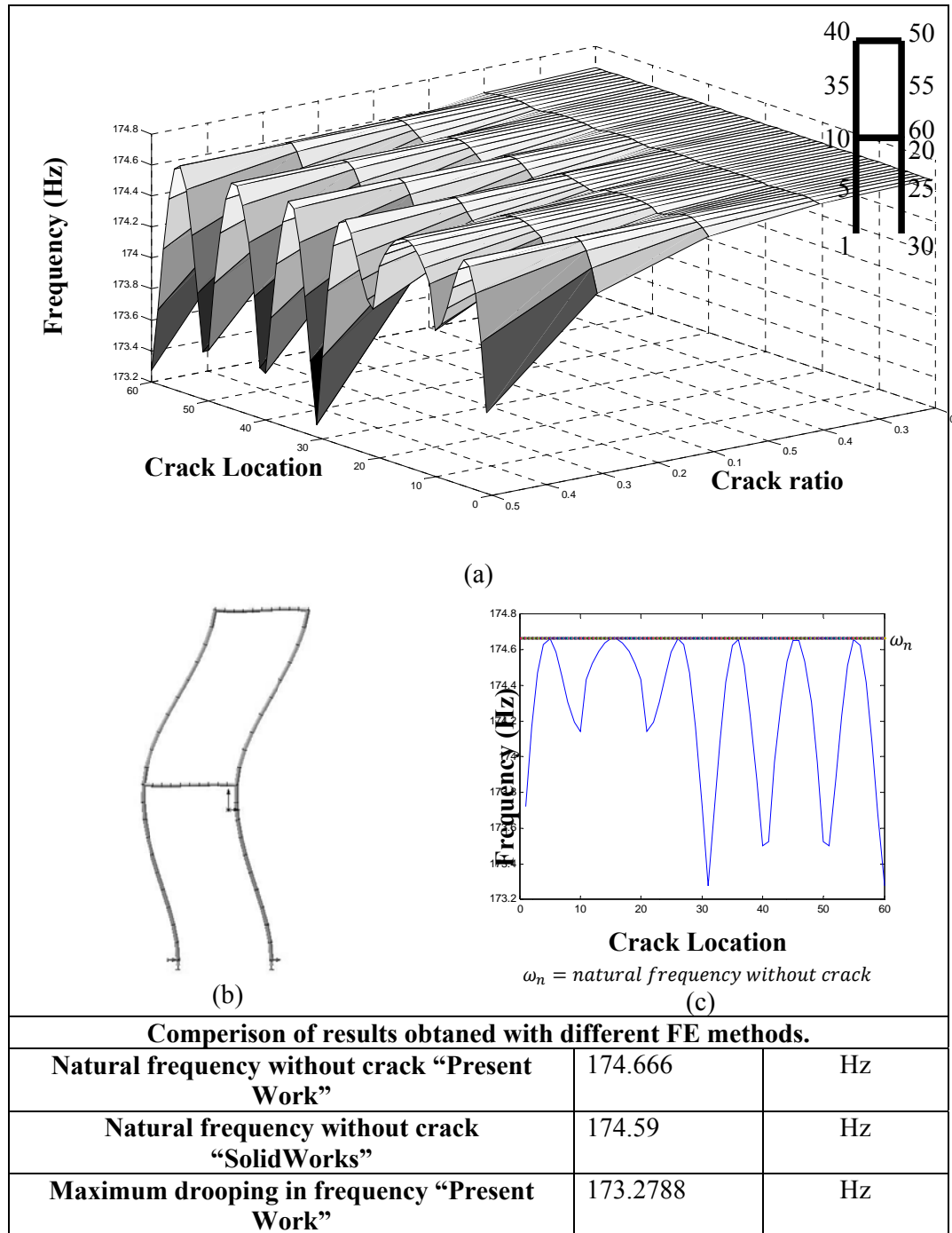   b)   Second mode shape

    c)   Effect of maximum crack ratio 0.5

(a)

(b)

$\omega_n = natural\ frequency\ without\ crack$

(c)

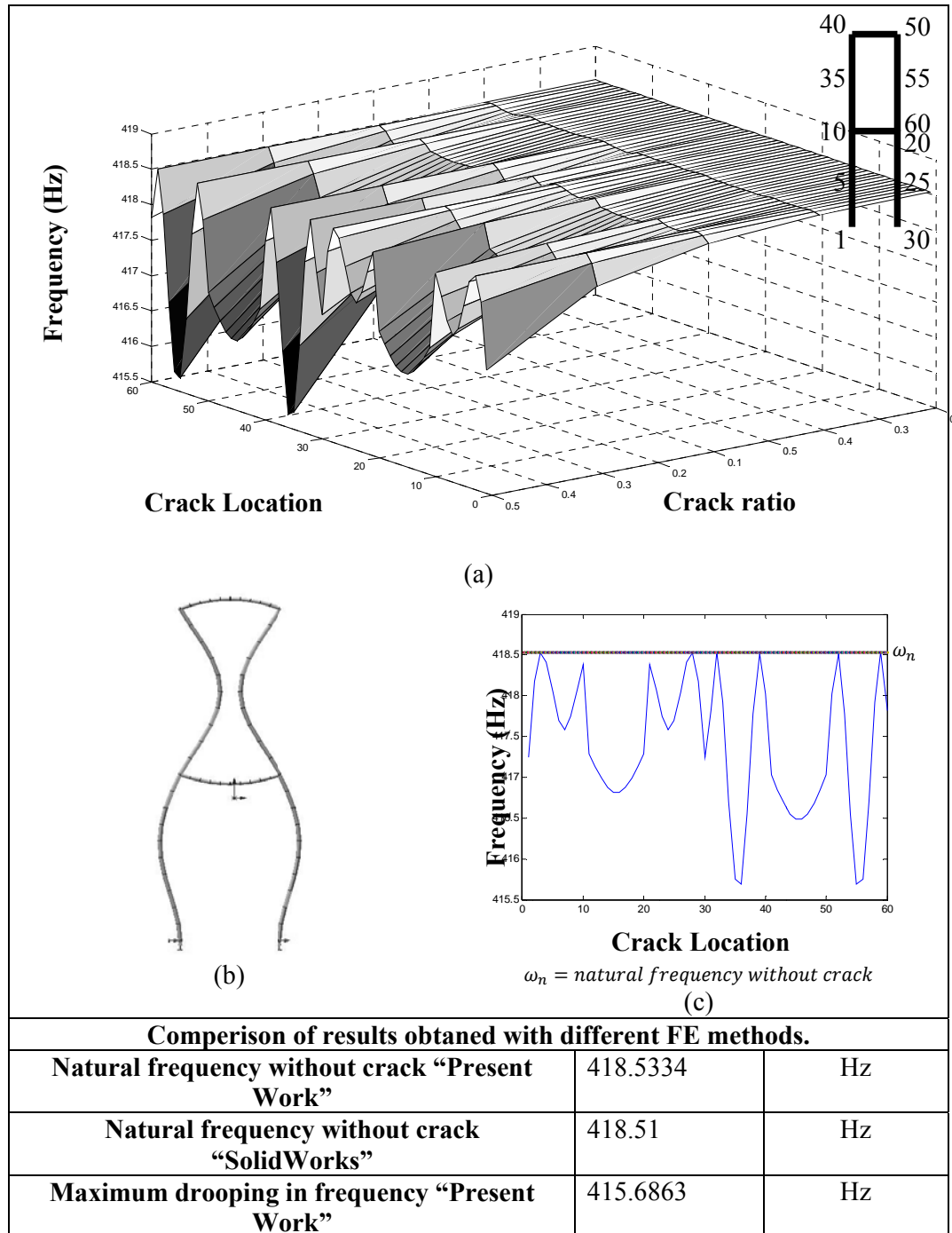| Comperison of results obtaned with different FE methods.		
Natural frequency without crack "Present Work"	538.8529	Hz
Natural frequency without crack "SolidWorks"	538.77	Hz
Maximum drooping in frequency "Present Work"	536.3572	Hz

Figure 5.24 Crack effect on the third natural frequency of a five-bay frame structure.

  a) Effect of crack ratio and crack location

  b) Third mode shape

  c) Effect of maximum crack ratio 0.5

(a)

(b)

$\omega_n = natural\ frequency\ without\ crack$

(c)

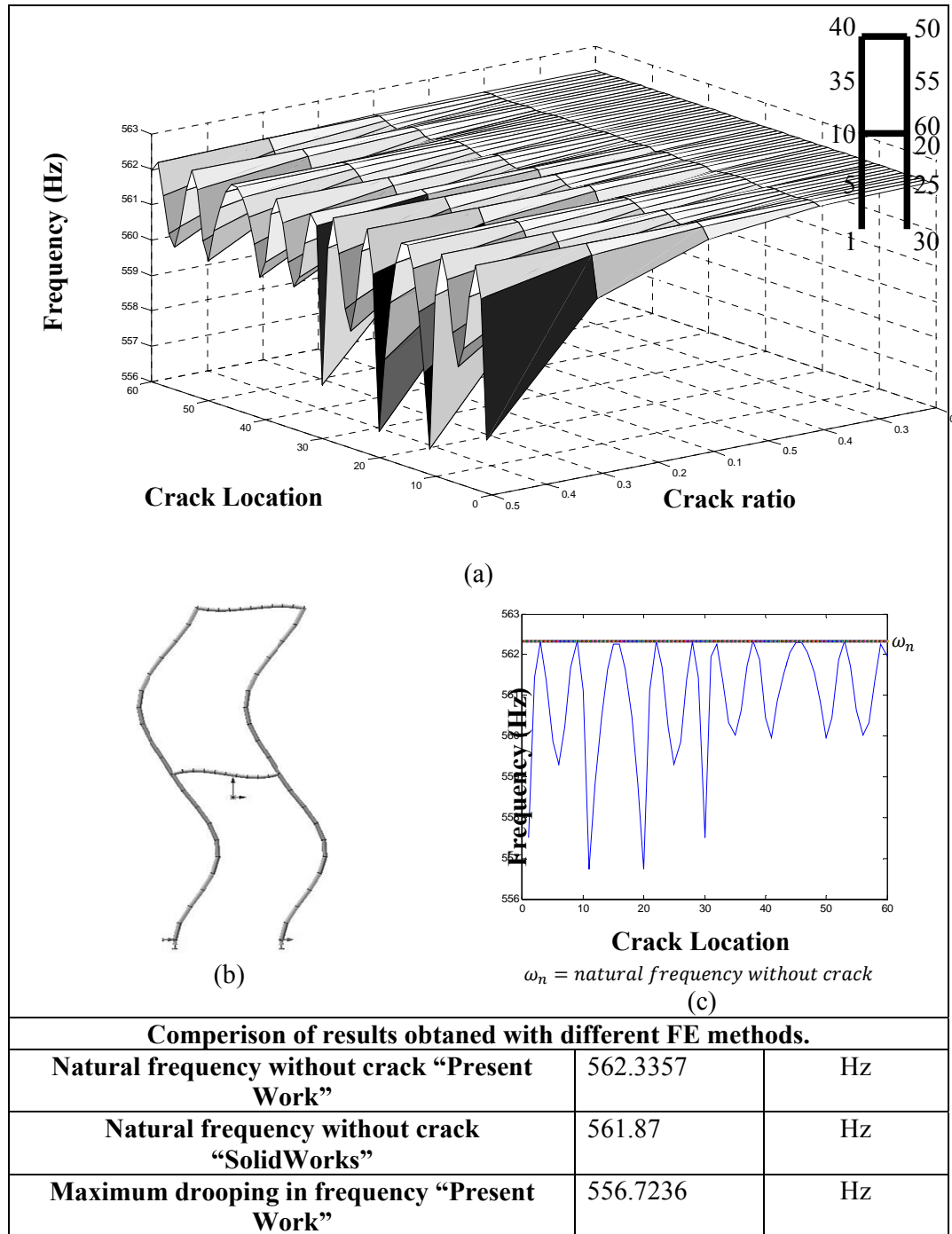| Comperison of results obtaned with different FE methods.		
Natural frequency without crack "Present Work"	563.5862	Hz
Natural frequency without crack "SolidWorks"	563.54	Hz
Maximum drooping in frequency "Present Work"	557.4132	Hz

Figure 5.25 Crack effect on the fourth natural frequency of a five-bay frame structure.

    a) Effect of crack ratio and crack location

    b) Fourth mode shape

    c) Effect of maximum crack ratio 0.5 .
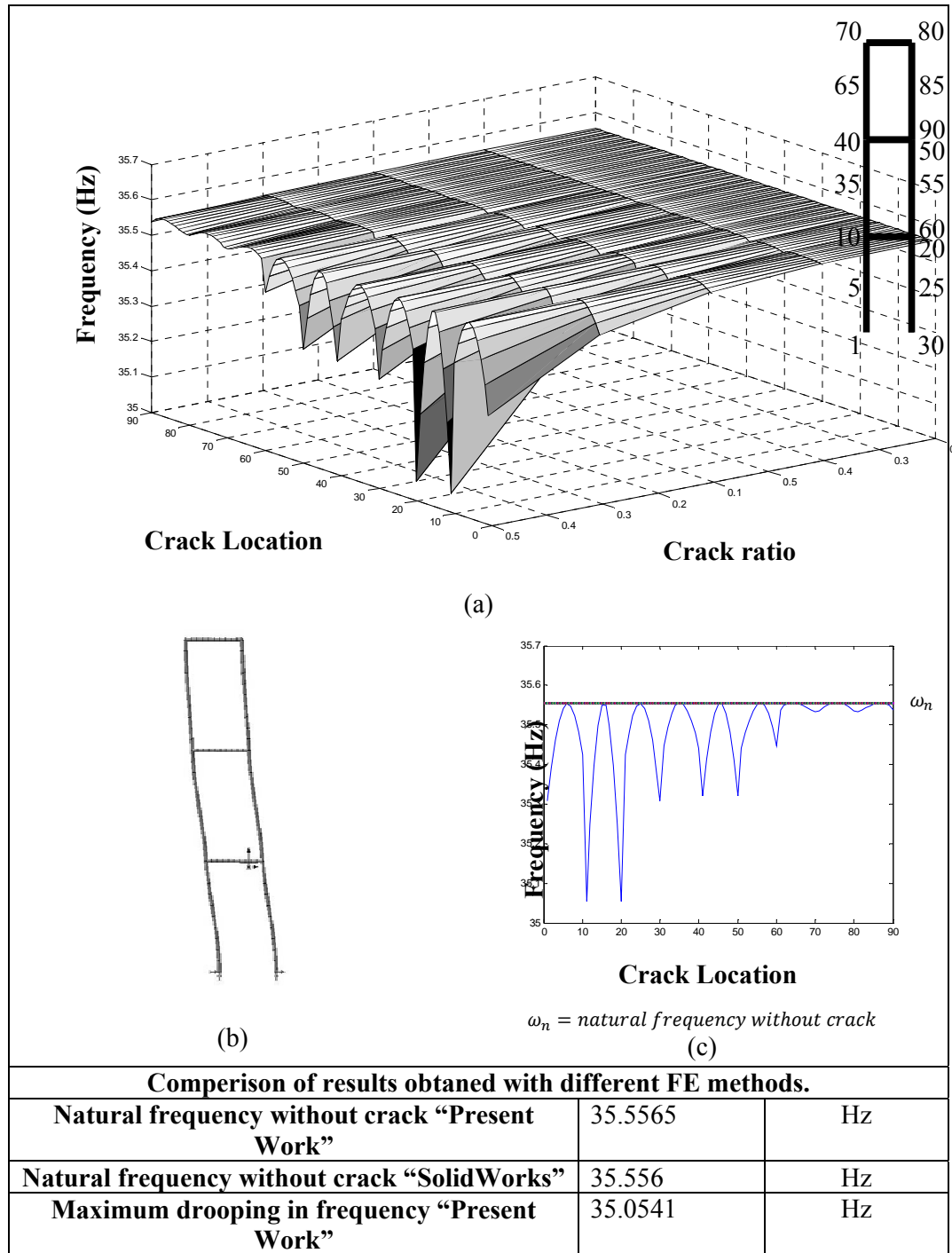
(a)

(b)

$\omega_n = natural\ frequency\ without\ crack$

(c)

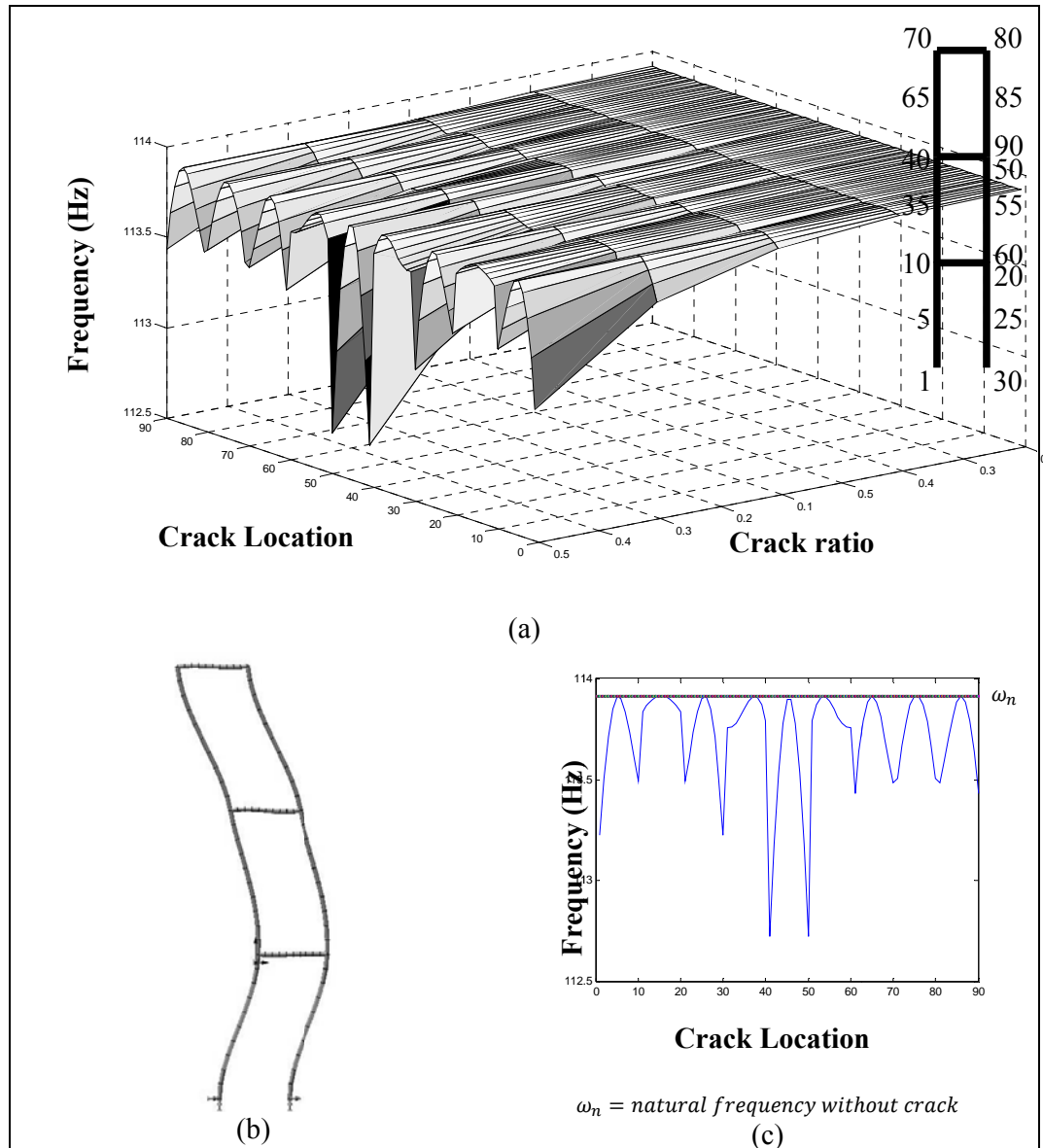| Comperison of results obtaned with different FE methods.		
Natural frequency without crack "Present Work"	105.5260	Hz
Natural frequency without crack "SolidWorks"	105.5	Hz
Maximum drooping in frequency "Present Work"	105.0202	Hz

Figure 5.26 Crack effect on the first natural frequency of a six-bay frame structure.

    a) Effect of crack ratio and crack location

    b) First mode shape

    c) Effect of maximum crack ratio 0.5

(a)

(b)

Crack Location
$\omega_n = natural\ frequency\ without\ crack$

(c)
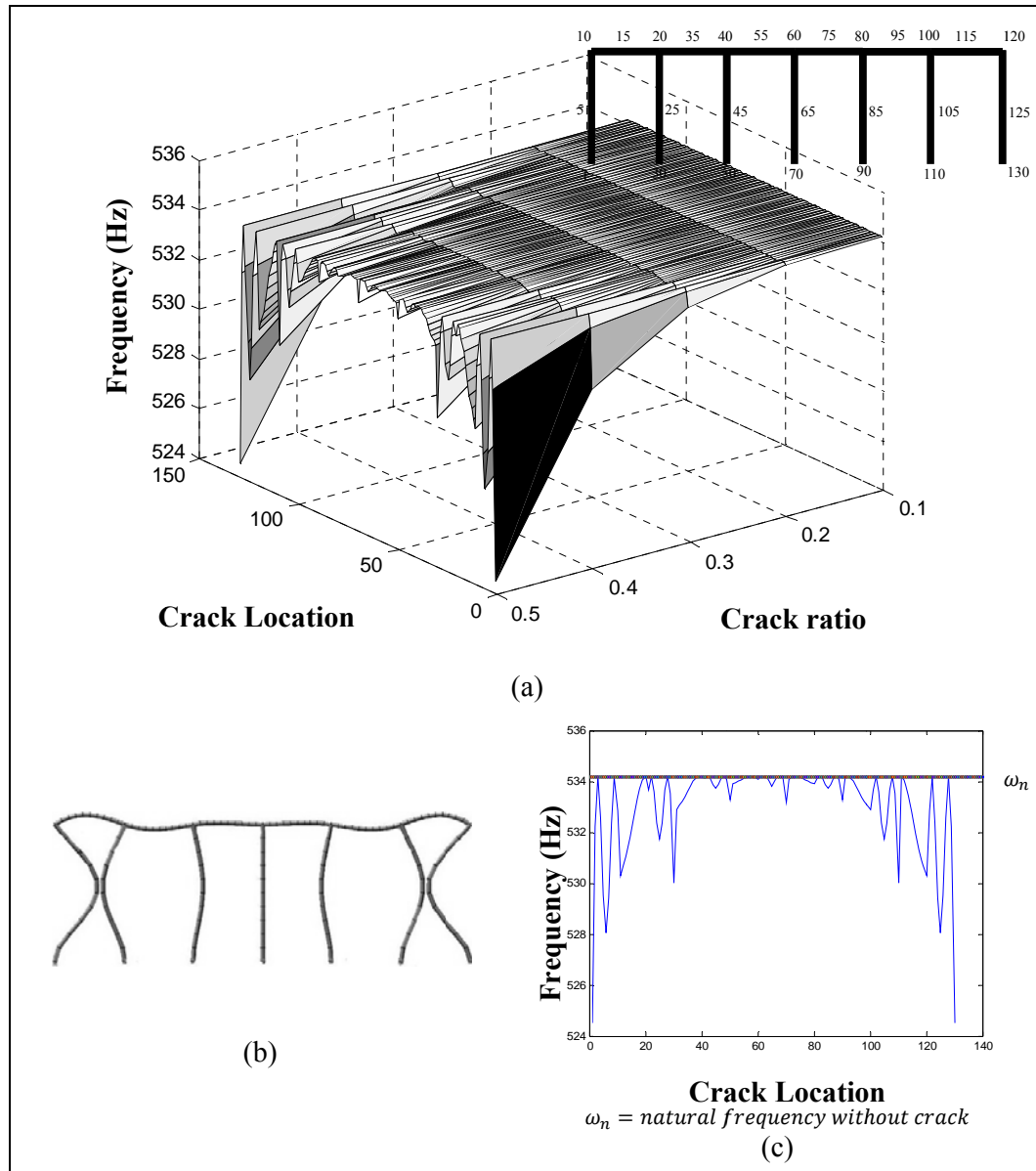
Comperison of results obtaned with different FE methods.		
Natural frequency without crack "Present Work"	534.1947	Hz
Natural frequency without crack "SolidWorks"	534.15	Hz
Maximum drooping in frequency "Present Work"	534.5177	Hz

Figure 5.27 Crack effect on the second natural frequency of a six-bay frame structure.

a)   Effect of crack ratio and crack location

b)   Second mode shape

c)   Effect of maximum crack ratio 0.5

(a)

(b)

(c)

$\omega_n = natural\ frequency\ without\ crack$

Comperison of results obtaned with different FE methods.		
Natural frequency without crack "Present Work"	534.592	Hz
Natural frequency without crack "SolidWorks"	534.52	Hz
Maximum drooping in frequency "Present Work"	534.194	Hz

Figure 5.28 Crack effect on the third natural frequency of a six-bay frame structure.

  a)   Effect of crack ratio and crack location
  b)   Third mode shape
  c)   Effect of maximum crack ratio 0.5.

(a)

(b)

(c)

$\omega_n = natural\ frequency\ without\ crack$

Comperison of results obtained with different FE methods.		
Natural frequency without crack "Present Work"	559.7982	Hz
Natural frequency without crack "SolidWorks"	559.74	Hz
Maximum drooping in frequency "Present Work"	554.5409	Hz

Figure 5.29 Crack effect on the fourth natural frequency of a six-bay frame structure.

    a) Effect of crack ratio and crack location

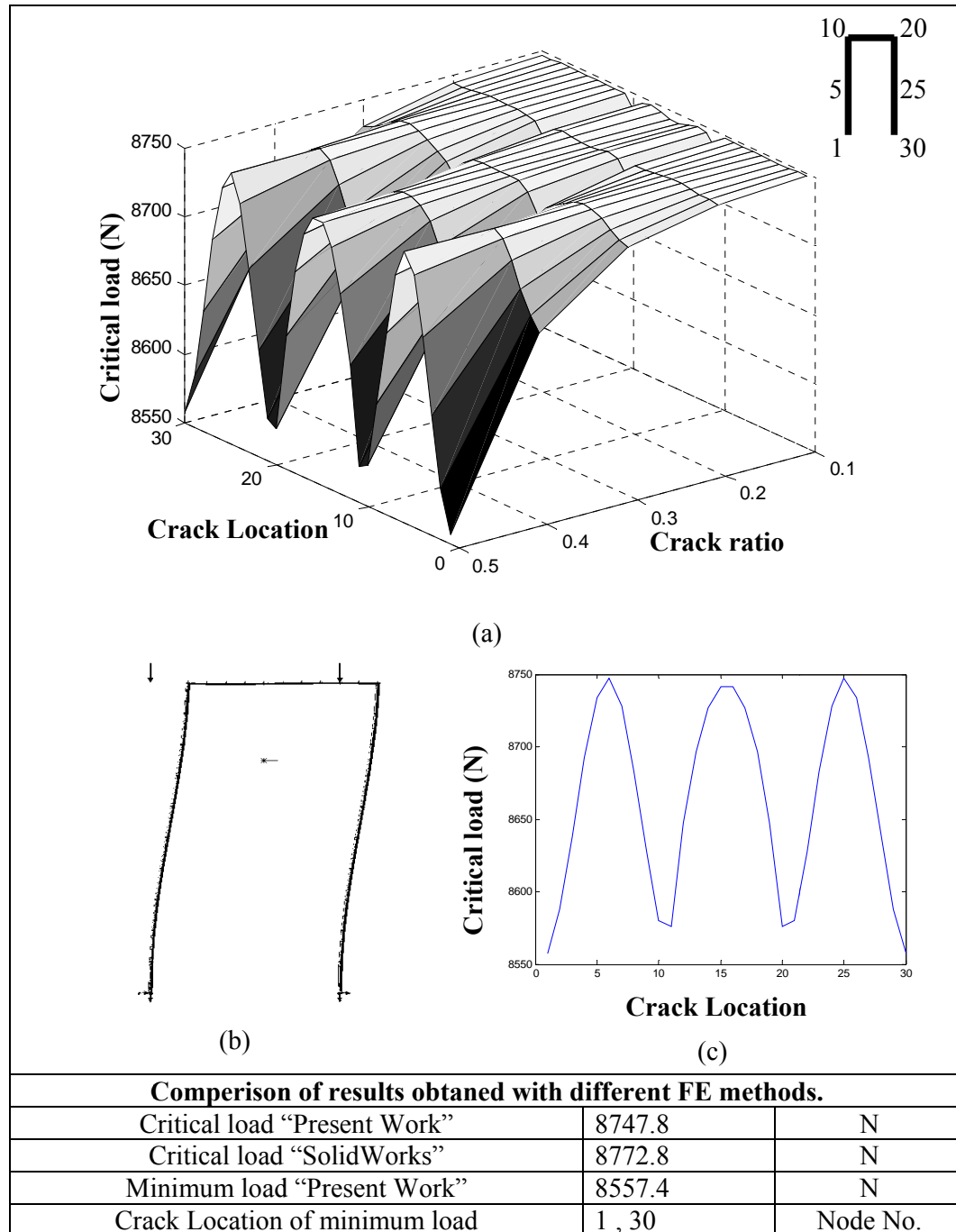   b) Fourth mode shape

    c) Effect of maximum crack ratio 0.5.

(a)

(b)

$\omega_n = natural\ frequency\ without\ crack$

(c)

Comperison of results obtaned with different FE methods.		
Natural frequency without crack "Present Work"	55.4887	Hz
Natural frequency without crack "SolidWorks"	55.484	Hz
Maximum drooping in frequency "Present Work"	54.6465	Hz

Figure 5.30 Crack effect on the first natural frequency of a two-story frame structure.

    a)   Effect of crack ratio and crack location

    b)   First mode shape

    c)   Effect of maximum crack ratio 0.5
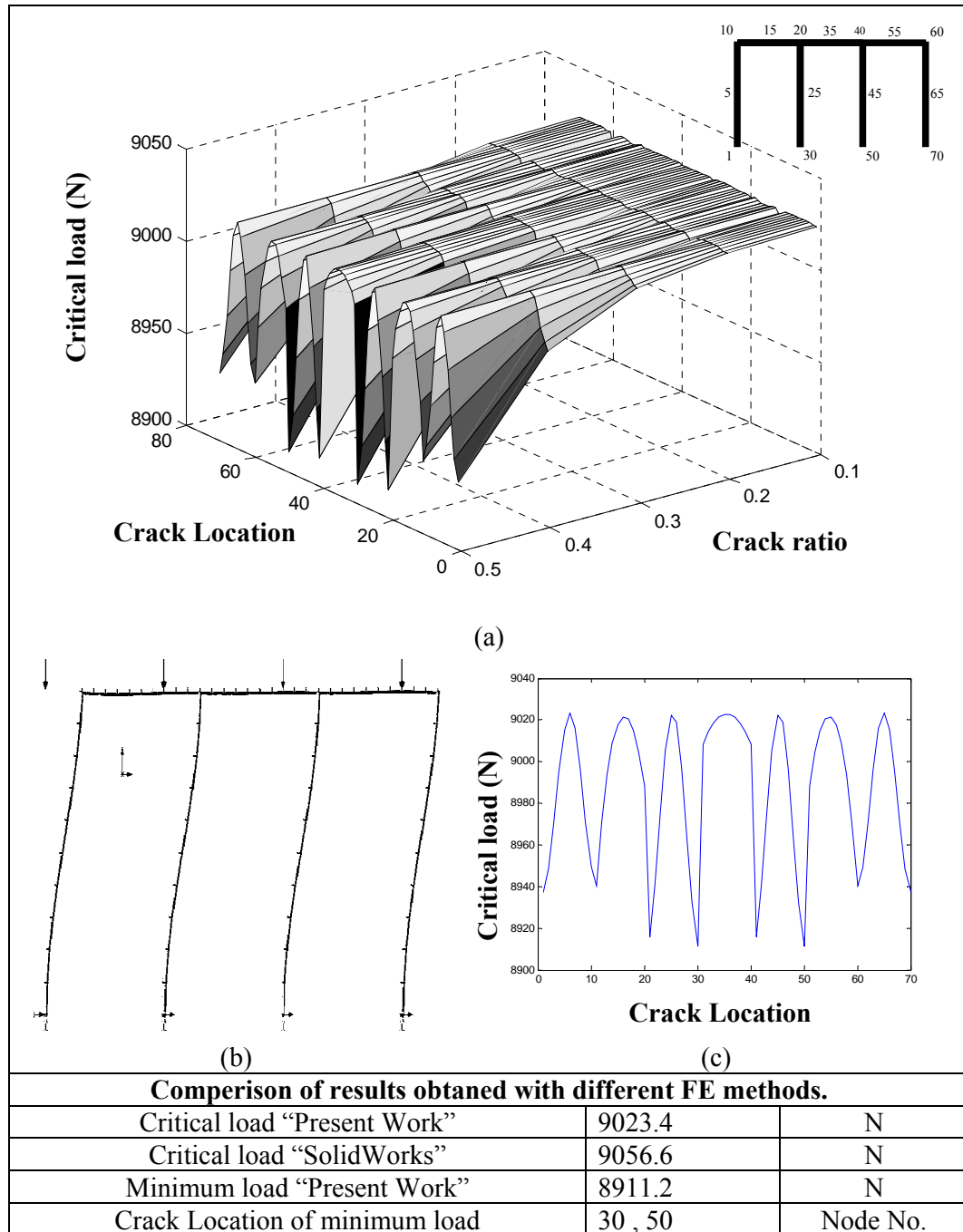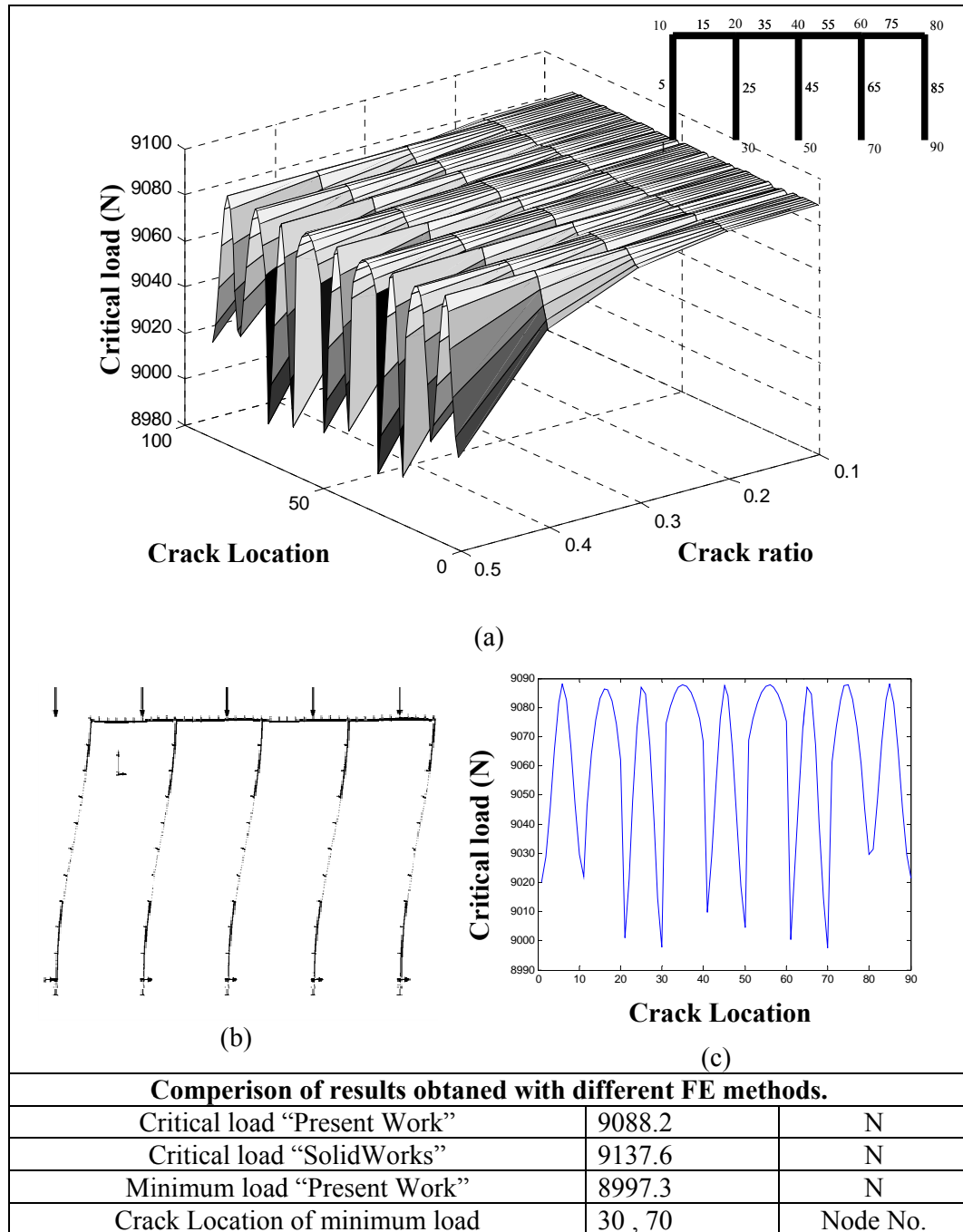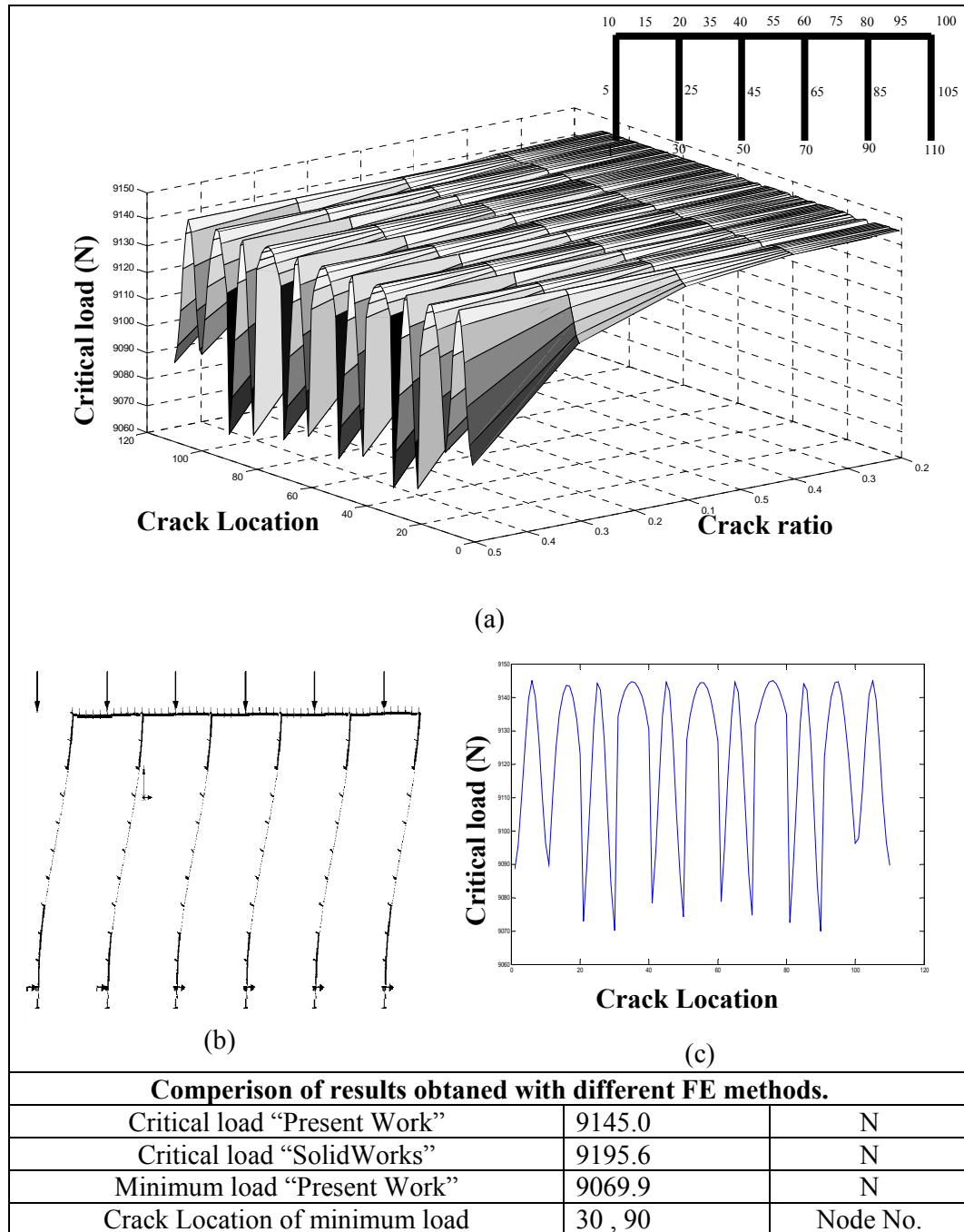
(a)

(b)   (c)

$\omega_n = natural\ frequency\ without\ crack$

Comperison of results obtaned with different FE methods.		
Natural frequency without crack "Present Work"	174.666	Hz
Natural frequency without crack "SolidWorks"	174.59	Hz
Maximum drooping in frequency "Present Work"	173.2788	Hz

Figure 5.31 Crack effect on the second natural frequency of a two-story frame structure.
a)   Effect of crack ratio and crack location
b)   Second mode shape
c)   Effect of maximum crack ratio 0.5

(a)

(b)

Crack Location

$\omega_n = natural\ frequency\ without\ crack$

(c)

Comperison of results obtaned with different FE methods.		
Natural frequency without crack "Present Work"	418.5334	Hz
Natural frequency without crack "SolidWorks"	418.51	Hz
Maximum drooping in frequency "Present Work"	415.6863	Hz

Figure 5.32 Crack effect on the third natural frequency of a two-story frame structure.

    a)   Effect of crack ratio and crack location

    b)   Third mode shape
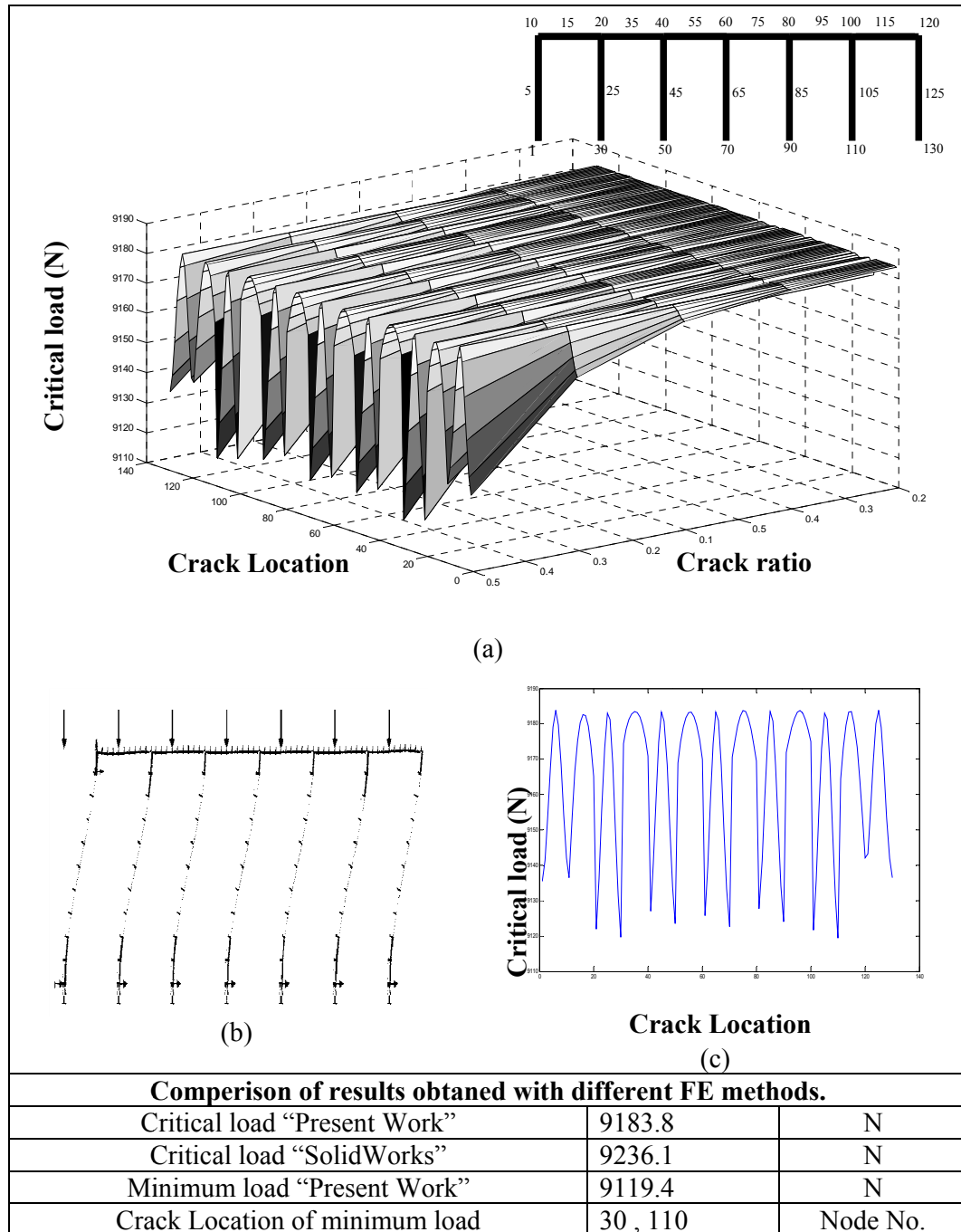
    c)   Effect of maximum crack ratio 0.5

(a)

(b)

$\omega_n = natural\ frequency\ without\ crack$

(c)

Comperison of results obtaned with different FE methods.		
Natural frequency without crack "Present Work"	562.3357	Hz
Natural frequency without crack "SolidWorks"	561.87	Hz
Maximum drooping in frequency "Present Work"	556.7236	Hz

Figure 5.33 Crack effect on the fourth natural frequency of a two-story frame structure.

a) Effect of crack ratio and crack location

b) Fourth mode shape

c) Effect of maximum crack ratio 0.5

(a)

(b)

Crack Location

$\omega_n = natural\ frequency\ without\ crack$

(c)

Comperison of results obtaned with different FE methods.		
Natural frequency without crack "Present Work"	35.5565	Hz
Natural frequency without crack "SolidWorks"	35.556	Hz
Maximum drooping in frequency "Present Work"	35.0541	Hz

Figure 5.34 Crack effect on the first natural frequency of a three-story frame structure.

    a)   Effect of crack ratio and crack location

    b)   First mode shape
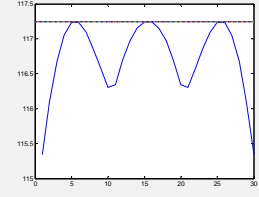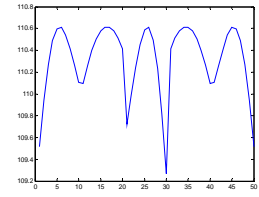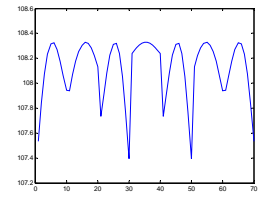
    c)   Effect of maximum crack ratio 0.5

(a)

(b)

$\omega_n = natural\ frequency\ without\ crack$

(c)

Comperison of results obtaned with different FE methods.		
Natural frequency without crack "Present Work"	113.9145	Hz
Natural frequency without crack "SolidWorks"	113.89	Hz
Maximum drooping in frequency "Present Work"	112.7249	Hz

Figure 5.35 Crack effect on the second natural frequency of a three-story frame structure.

    a)   Effect of crack ratio and crack location

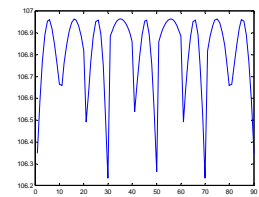   b)   Second mode shape

    c)   Effect of maximum crack ratio 0.5

(a)

(b)

$\omega_n = natural\ frequency\ without\ crack$

(c)

Comperison of results obtaned with different FE methods.		
Natural frequency without crack "Present Work"	196.7334	Hz
Natural frequency without crack "SolidWorks"	196.67	Hz
Maximum drooping in frequency "Present Work"	195.7384	Hz
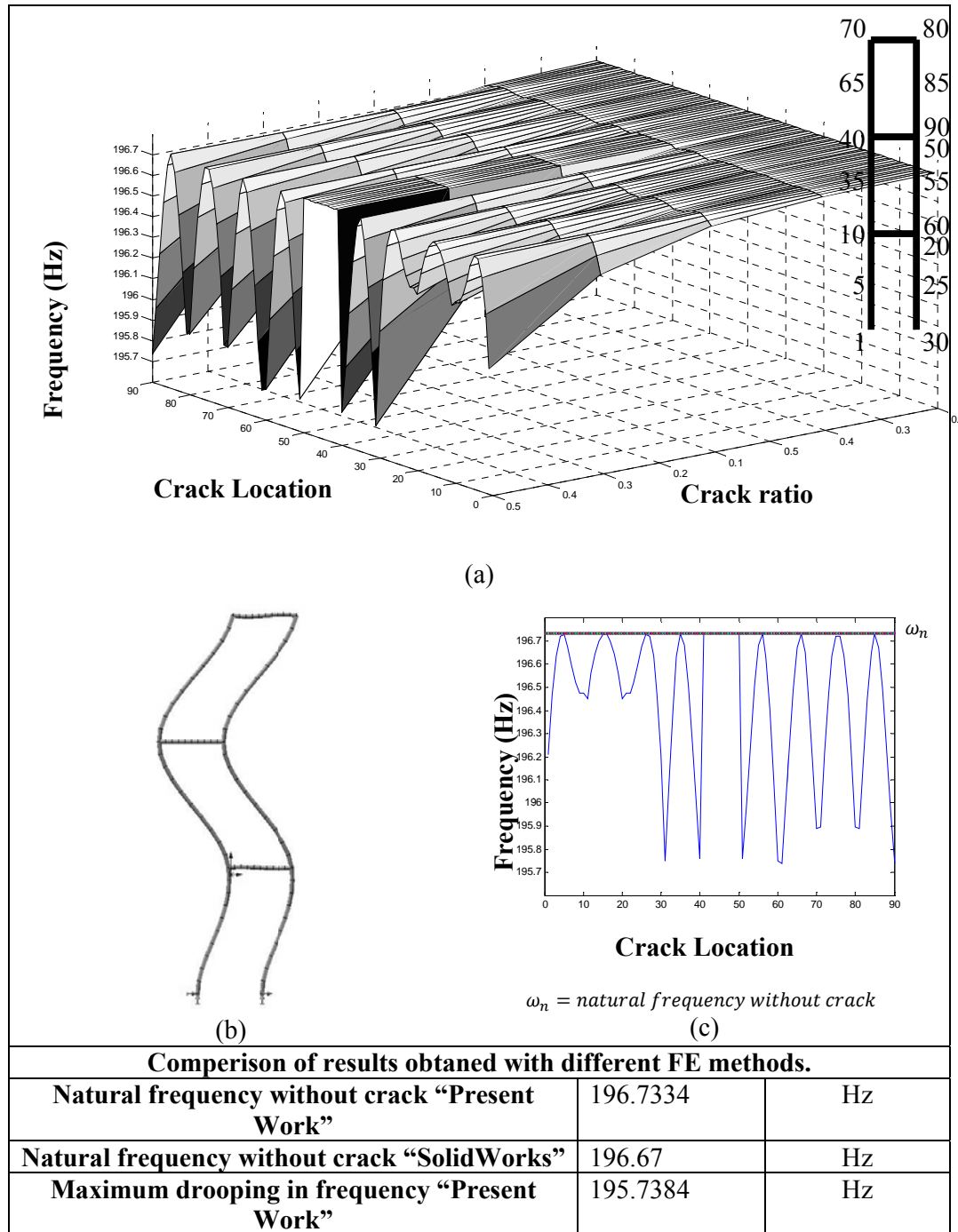
Figure 5.36 Crack effect on the third natural frequency of a three-story frame structure.

    a)   Effect of crack ratio and crack location

    b)   Third mode shape

    c)   Effect of maximum crack ratio 0.5

(a)

(b)

$\omega_n = natural\ frequency\ without\ crack$

(c)

Comperison of results obtaned with different FE methods.		
Natural frequency without crack "Present Work"	393.3456	Hz
Natural frequency without crack "SolidWorks"	393.32	Hz
Maximum drooping in frequency "Present Work"	391.5365	Hz
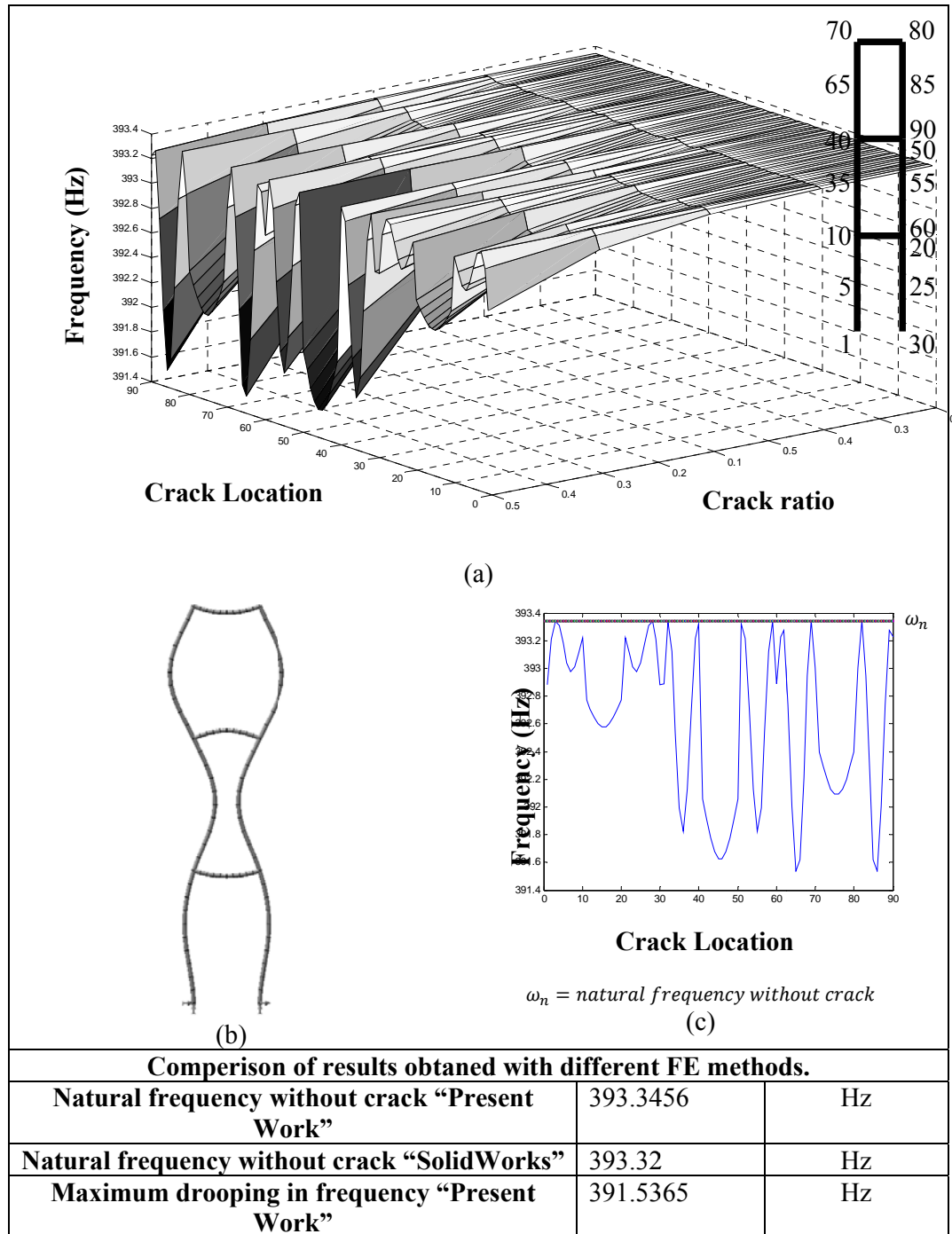
Figure 5.37 Crack effect on the fourth natural frequency of a three-story frame structure.

a)   Effect of crack ratio and crack location

b)   Fourth mode shape

c)   Effect of maximum crack ratio 0.5

(a)

(b)

(c)

Comperison of results obtaned with different FE methods.		
Critical load "Present Work"	8747.8	N
Critical load "SolidWorks"	8772.8	N
Minimum load "Present Work"	8557.4	N
Crack Location of minimum load	1 , 30	Node No.

Figure 5.38 Crack effect on the first critical buckling load of a single frame structure.

    a)   Effect of crack ratio and crack location

    b)   First mode shape

    c)   Effect of maximum crack ratio 0.5

(a)

(b)

(c)

Comperison of results obtaned with different FE methods.		
Critical load "Present Work"	8848	N
Critical load "SolidWorks"	8881.5	N
Minimum load "Present Work"	8687.6	N
Crack Location of minimum load	30	Node No.
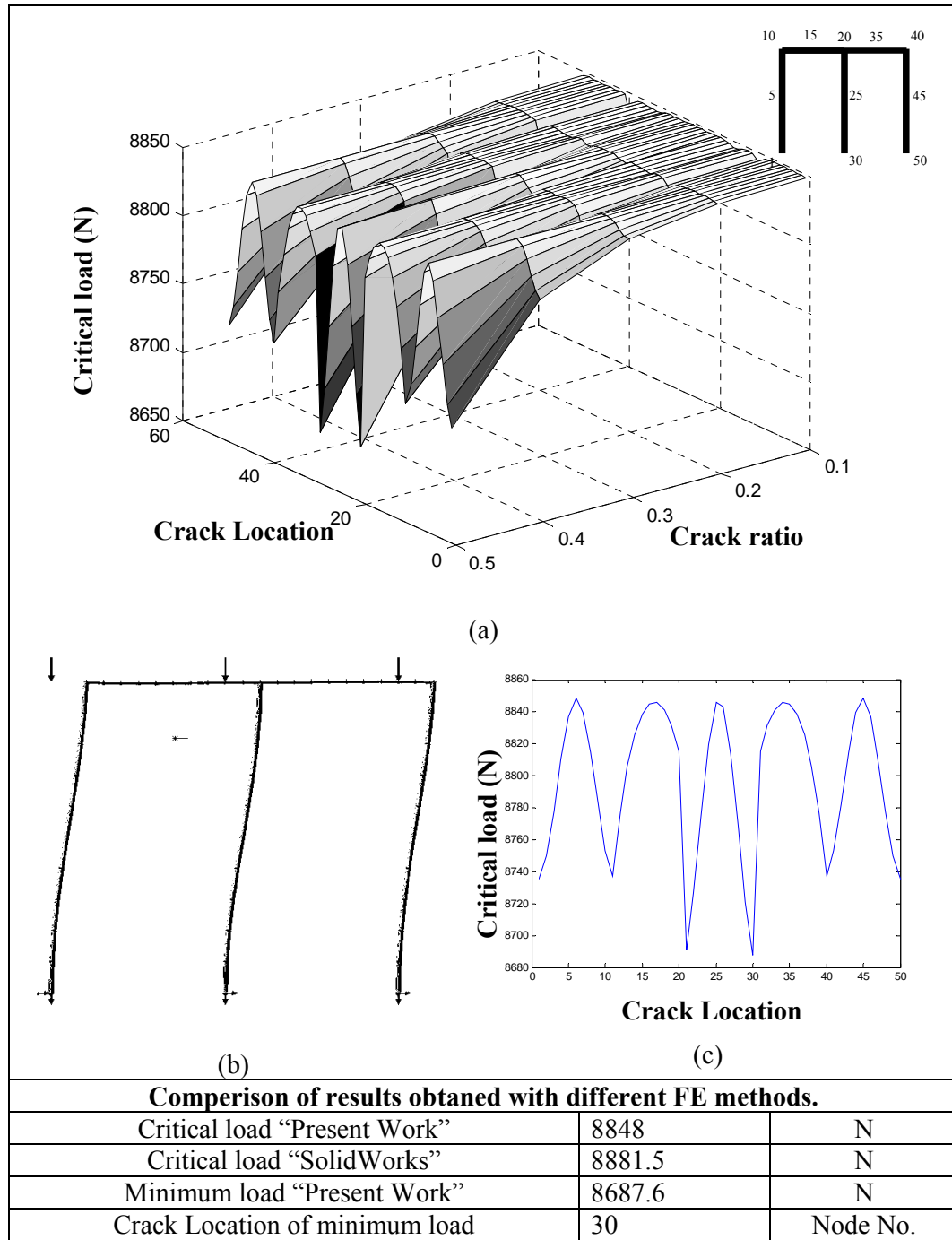
Figure 5.39 Crack effect on the first critical buckling load of a two-bay frame structure.

    a)   Effect of crack ratio and crack location

    b)   First mode shape

    c)   Effect of maximum crack ratio 0.5

(a)

(b)

(c)

Comperison of results obtaned with different FE methods.		
Critical load "Present Work"	9023.4	N
Critical load "SolidWorks"	9056.6	N
Minimum load "Present Work"	8911.2	N
Crack Location of minimum load	30 , 50	Node No.

Figure 5.40 Crack effect on the first critical buckling load of a three-bay frame structure.

    a)   Effect of crack ratio and crack location

    b)   First mode shape

    c)   Effect of maximum crack ratio 0.5

(a)

(b)

(c)

Comperison of results obtaned with different FE methods.		
Critical load "Present Work"	9088.2	N
Critical load "SolidWorks"	9137.6	N
Minimum load "Present Work"	8997.3	N
Crack Location of minimum load	30 , 70	Node No.

Figure 5.41 Crack effect on the first critical buckling load of a four-bay frame structure.

    a)   Effect of crack ratio and crack location

    b)   First mode shape

    c)   Effect of maximum crack ratio 0.5

(a)

(b)

(c)

Comperison of results obtaned with different FE methods.		
Critical load "Present Work"	9145.0	N
Critical load "SolidWorks"	9195.6	N
Minimum load "Present Work"	9069.9	N
Crack Location of minimum load	30 , 90	Node No.

Figure 5.42 Crack effect on the first critical buckling load of a five-bay frame structure.

  a) Effect of crack ratio and crack location
  b) First mode shape
  c) Effect of maximum crack ratio 0.5

(a)

(b)

(c)

Comperison of results obtaned with different FE methods.		
Critical load "Present Work"	9183.8	N
Critical load "SolidWorks"	9236.1	N
Minimum load "Present Work"	9119.4	N
Crack Location of minimum load	30 , 110	Node No.

Figure 5.43 Crack effect on the first critical buckling load of a six-bay frame structure.

    a)   Effect of crack ratio and crack location

    b)   First mode shape

    c)   Effect of maximum crack ratio 0.5

(a)

(b)

(c)
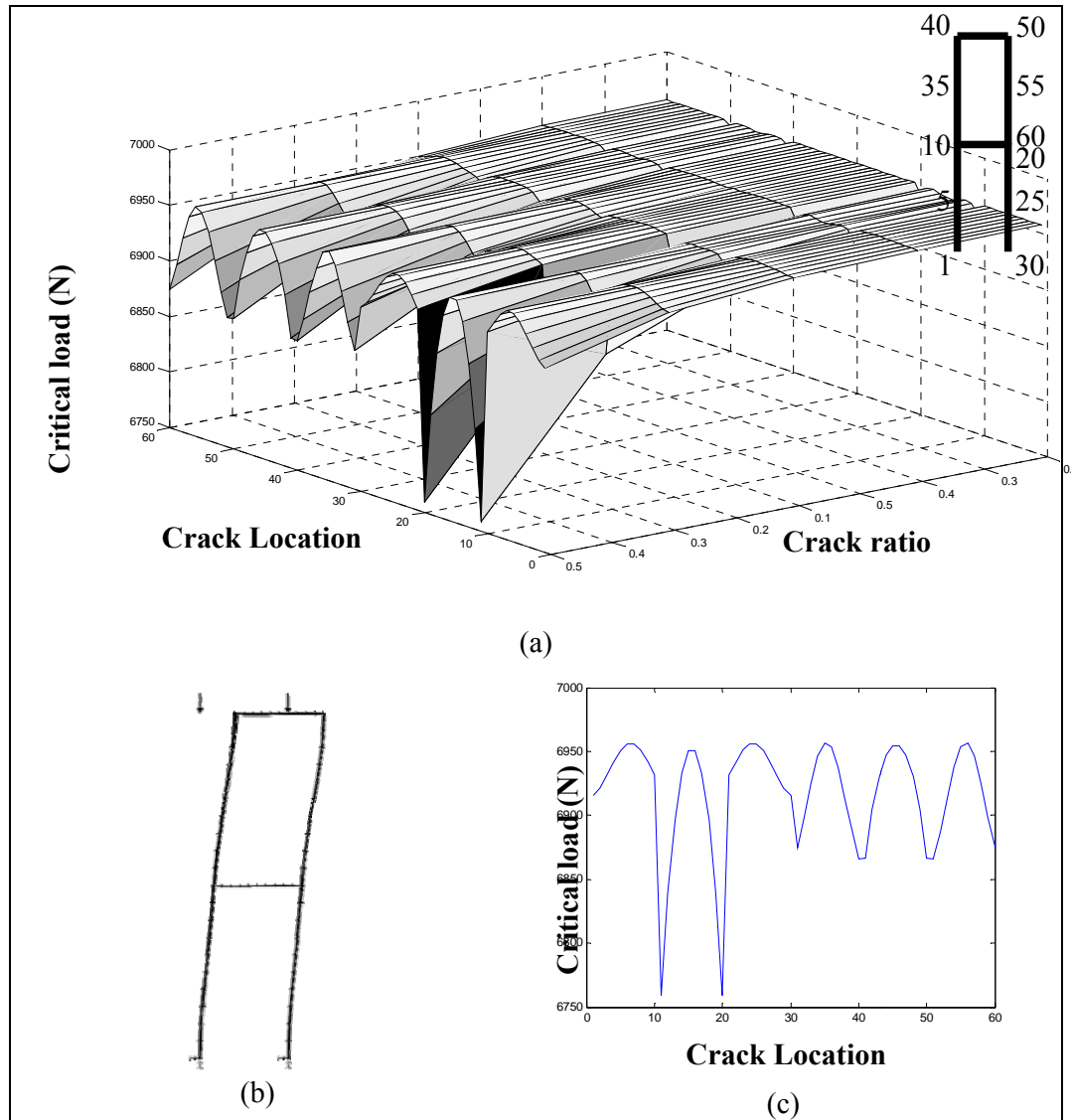
Comperison of results obtaned with different FE methods.		
Critical load "Present Work"	6957.2	N
Critical load "SolidWorks"	6997.9	N
Minimum load "Present Work"	6759.3	N
Crack Location of minimum load	10 , 20	Node No.

Figure 5.44 Crack effect on the first critical buckling load of a two-story frame structure.

    a)   Effect of crack ratio and crack location

    b)   First mode shape

    c)   Effect of maximum crack ratio 0.5

(a)

(b)

(c)
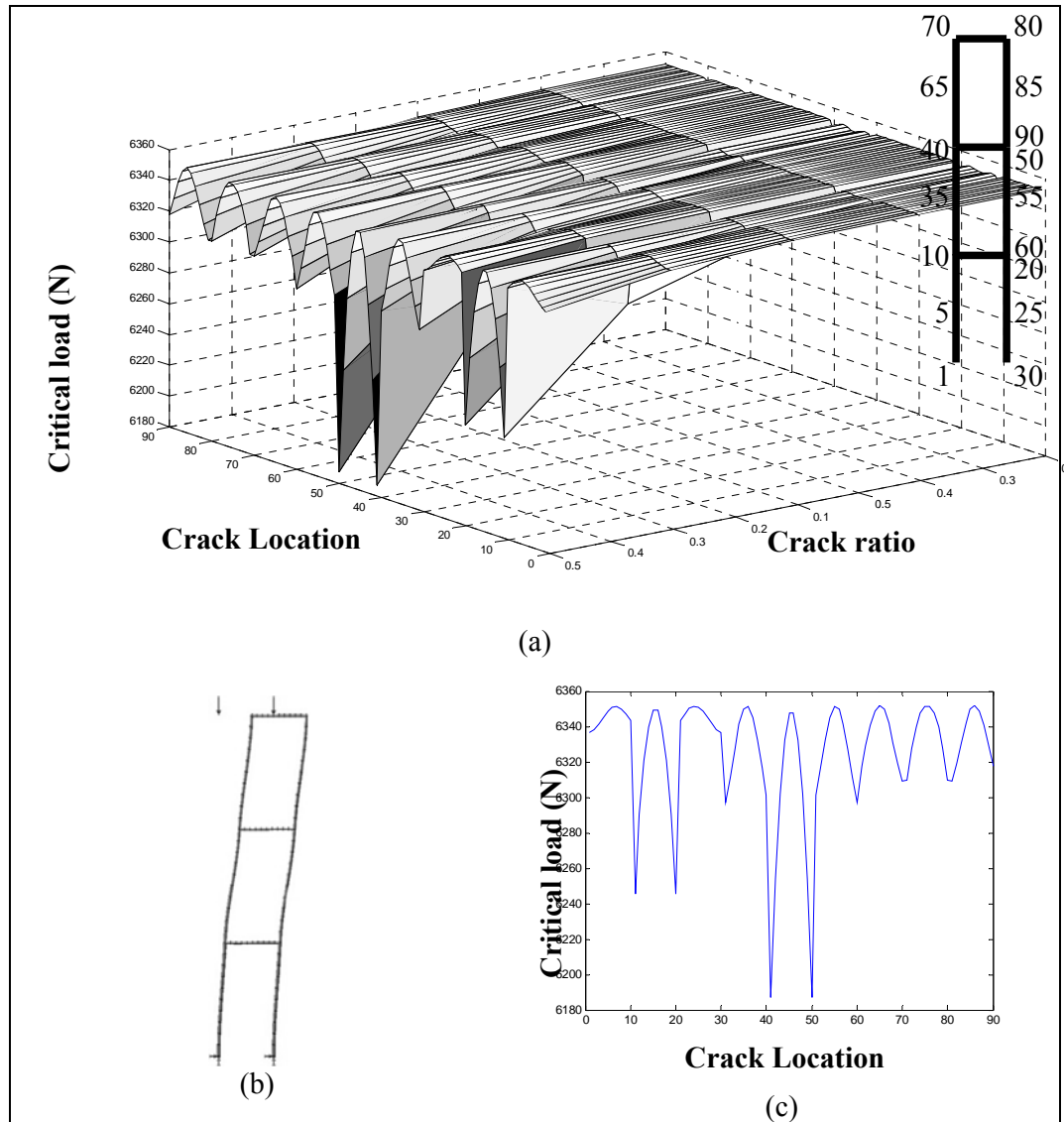
Comperison of results obtaned with different FE methods.		
Critical load "Present Work"	6352.1	N
Critical load "SolidWorks"	6411.5	N
Minimum load "Present Work"	6187.1	N
Crack Location of minimum load	40 , 50	Node No.

Figure 5.45 Crack effect on the first critical buckling load of a three-story frame structure.

a)   Effect of crack ratio and crack location

b)   First mode shape

c)   Effect of maximum crack ratio 0.5
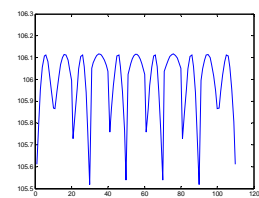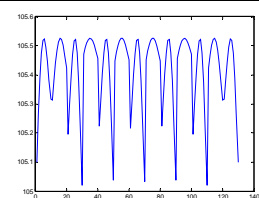
	frames	Frequency at the crack ratio 0.5	Location of Max. decrease in roots	Location of Max. decrease in corners
Single	1 2		1,2	1,2
Two-bay	1 2 3		2	2
Three-bay	1 2 3 4		2,3	2,3
Four-bay	1 2 3 4 5		2,4	2,4
five-bay	1 2 3 4 5 6		2,5	2,5
Six-bay	1 2 3 4 5 6 7		2,6	2,6
			2 , n-1	**2 , n-1**

Figure 5.46 Location of Maximum Decreases in the First Natural Frequency in Multi-Bay   Frames.
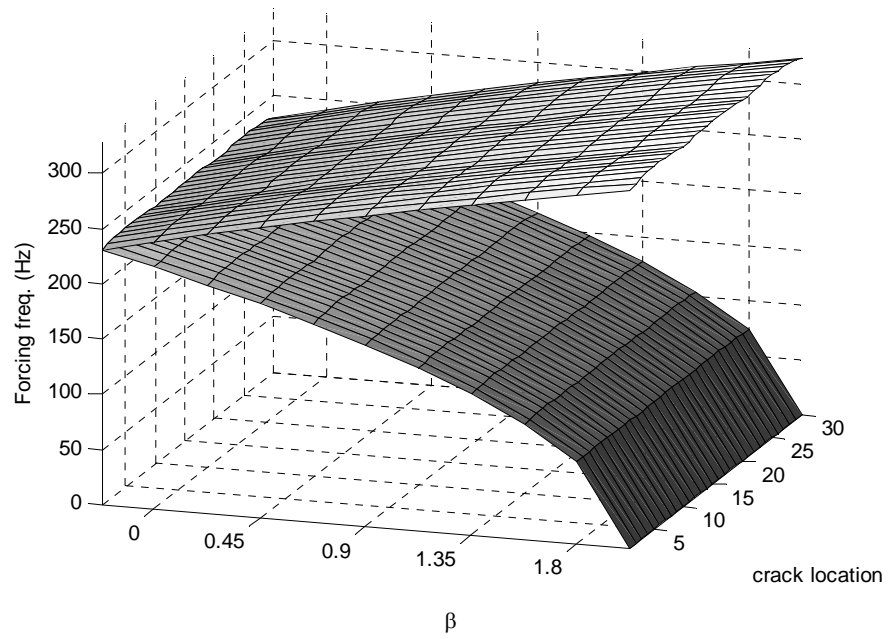
Figure 5.47 Dynamic Stability of Single Frame structure (α=0)
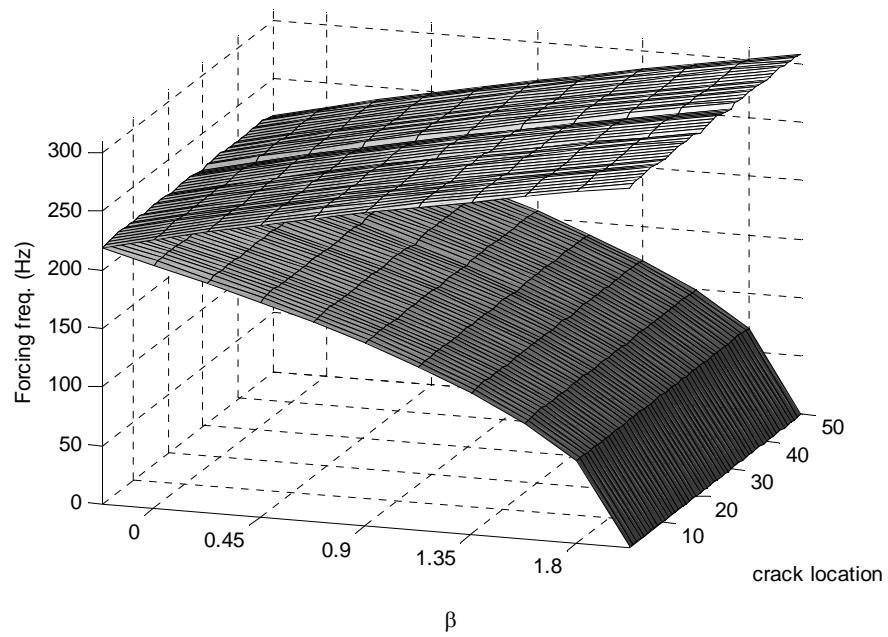
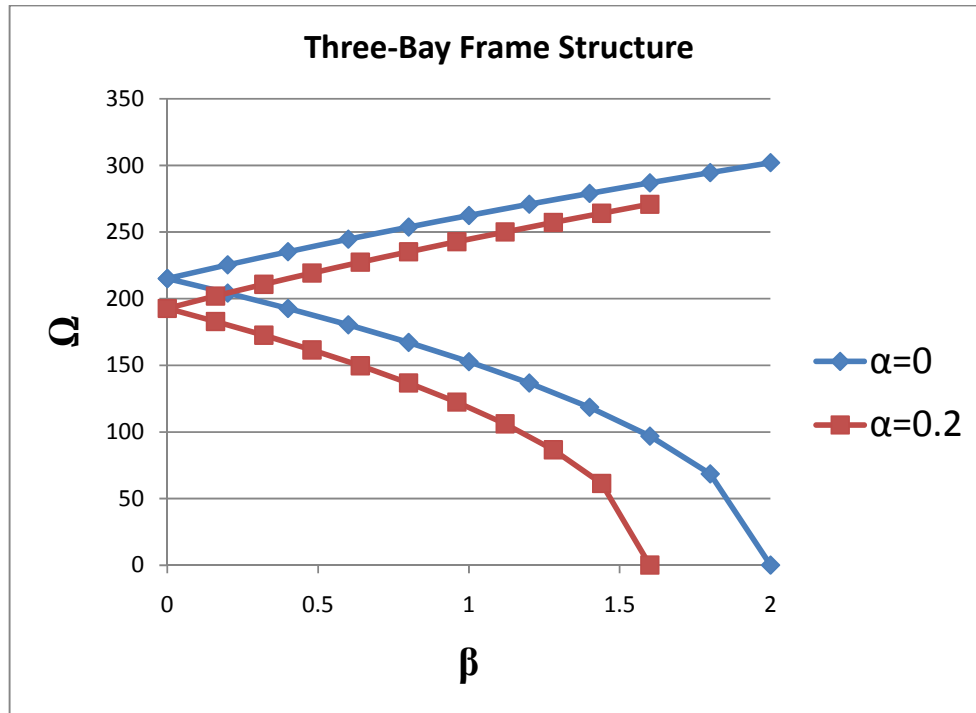Figure 5.48 Dynamic Stability of two-bay Frame structure (α=0)
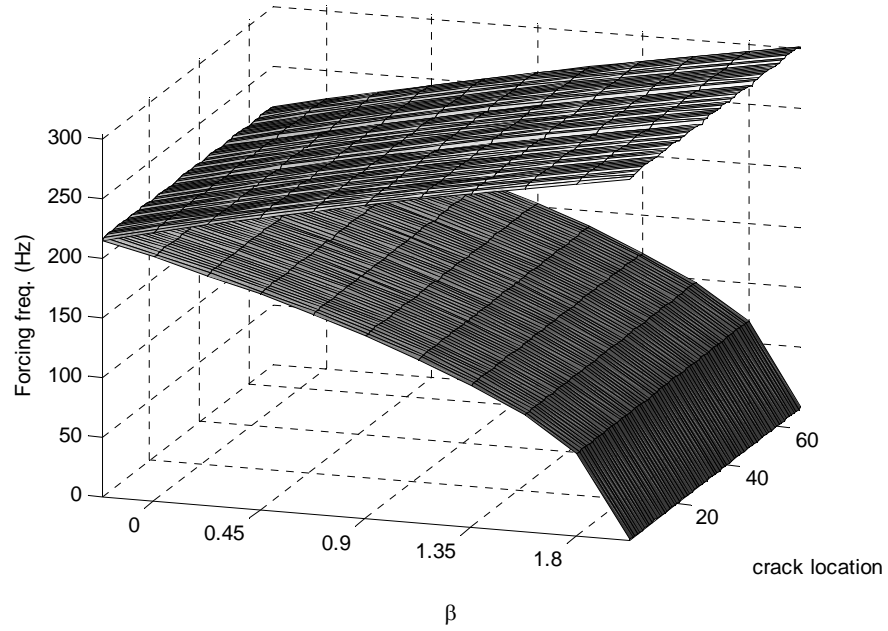
Figure 5.49 Dynamic Stability of three-bay Frame structure (α=0)
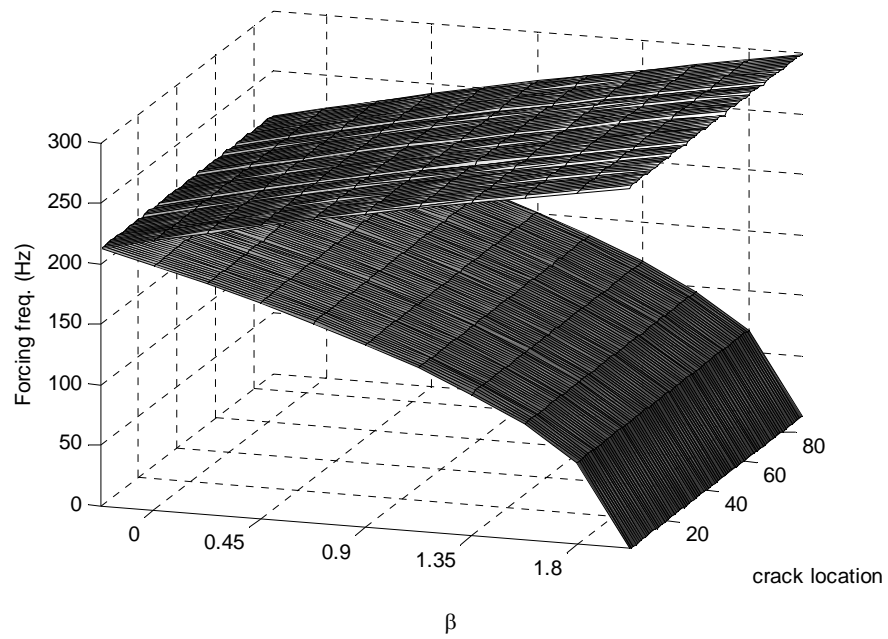
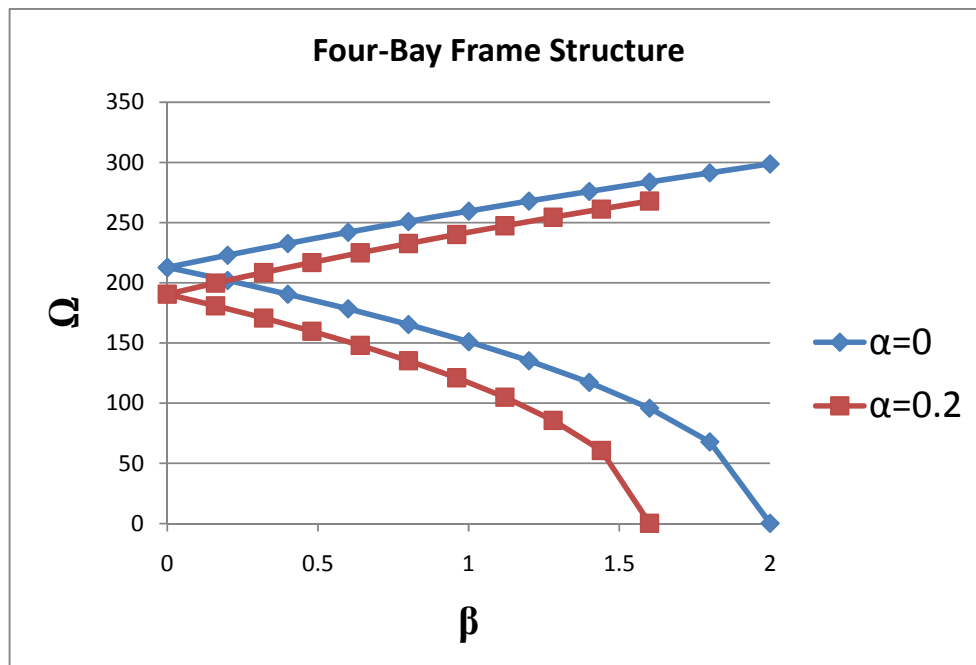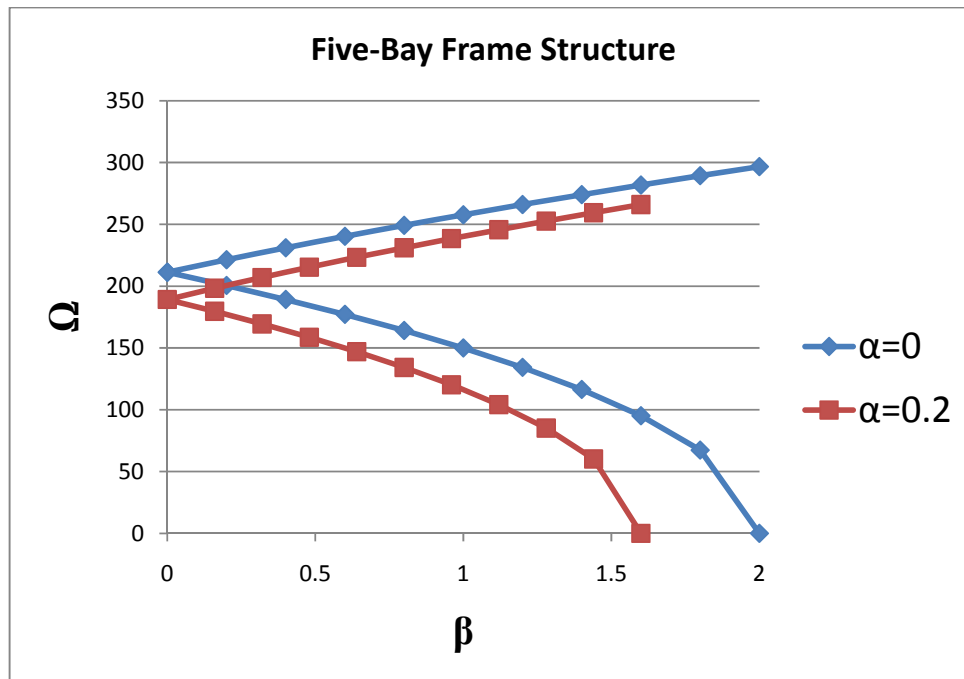Figure 5.50 Dynamic Stability of four-bay Frame structure (α=0)
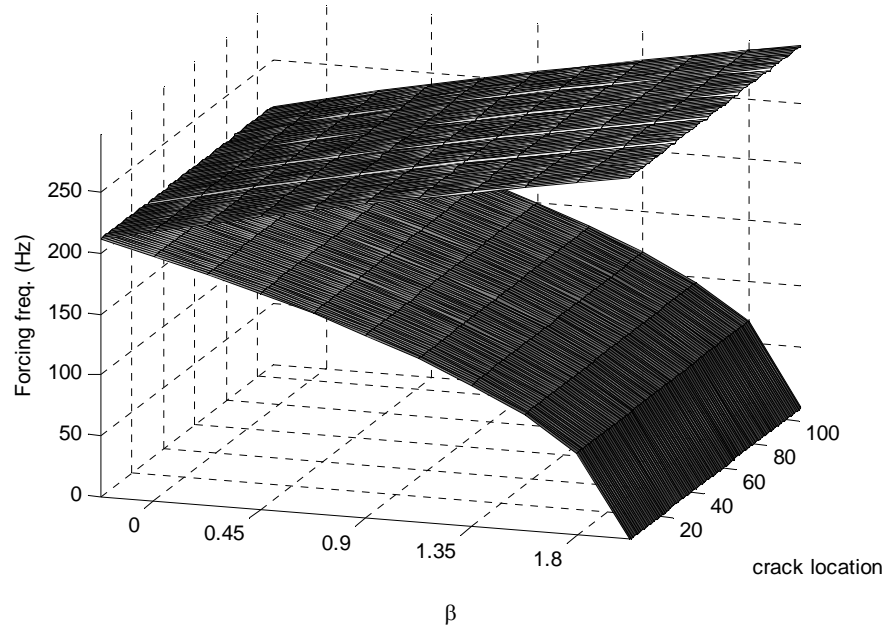
Figure 5.51 Dynamic Stability of five-bay Frame structure (α=0)
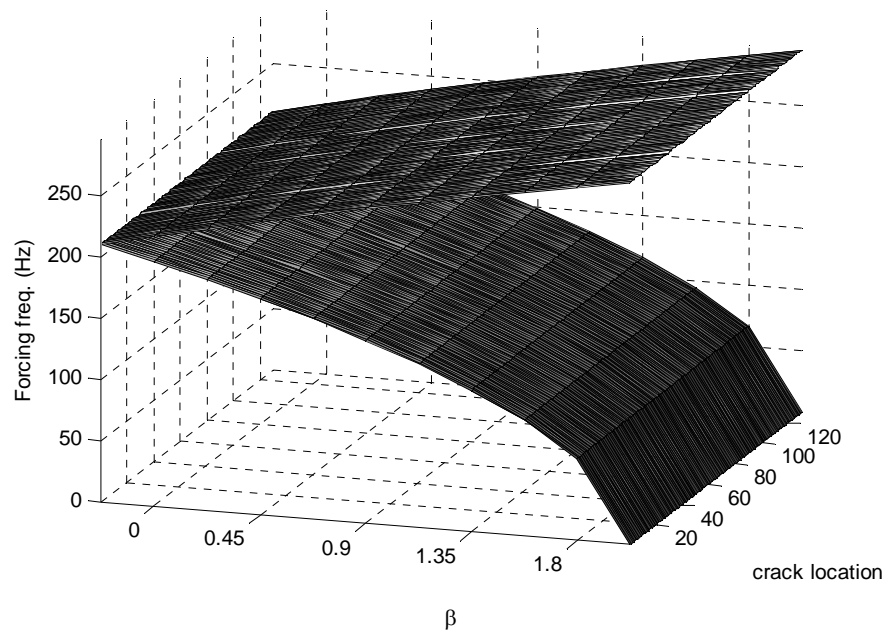
Figure 5.52 Dynamic Stability of six-bay Frame structure (α=0)
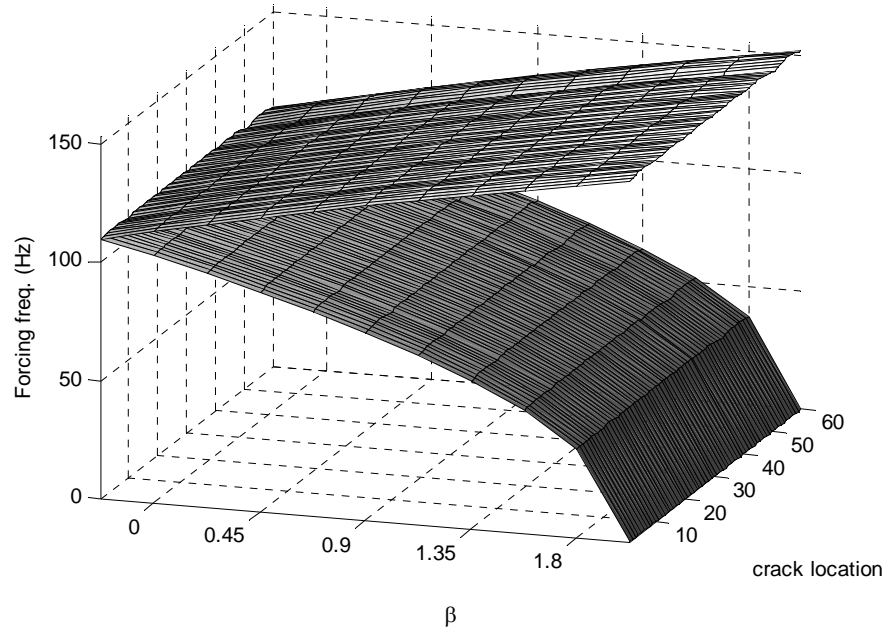
Figure 5.53 Dynamic Stability of two-story Frame structure (α=0)
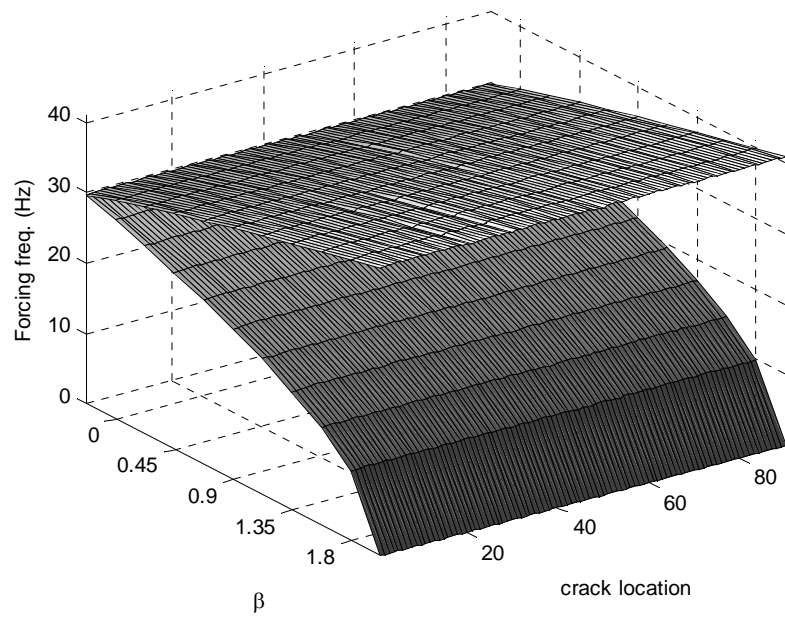
Figure 5.54 Dynamic Stability of three-story Frame structure (α=0)
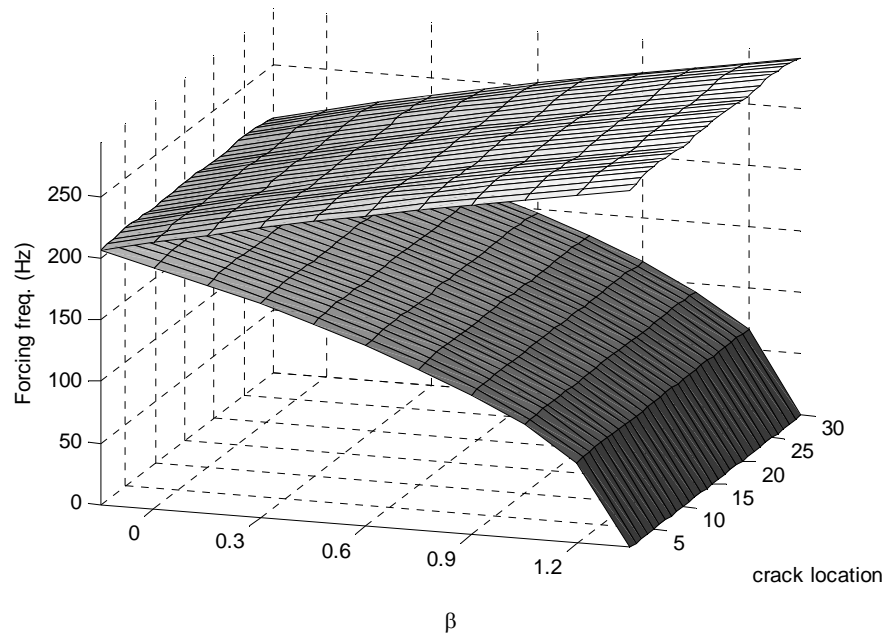
Figure 5.55 Dynamic Stability of single Frame structure (α=0.2)
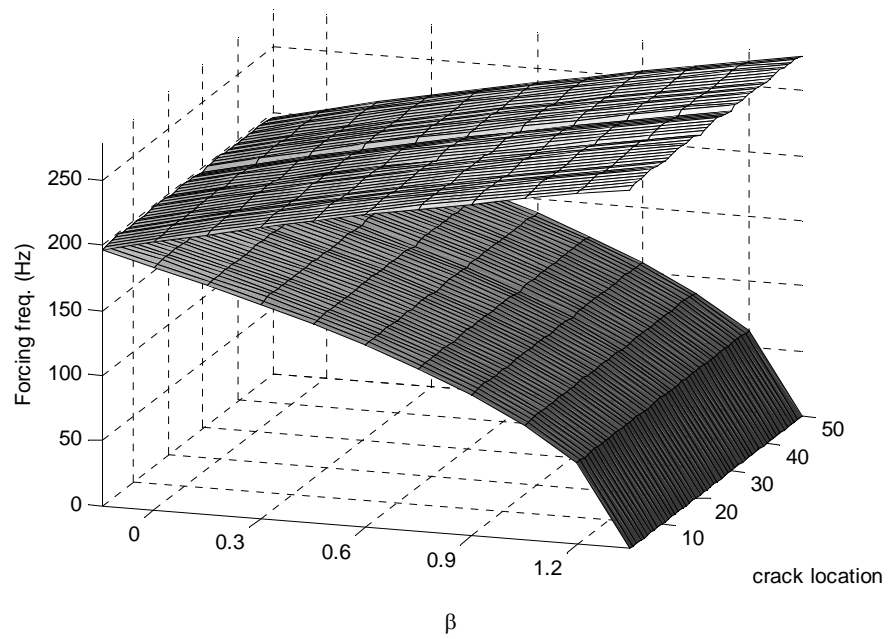
Figure 5.56 Dynamic Stability of two-bay Frame structure (α=0.2)
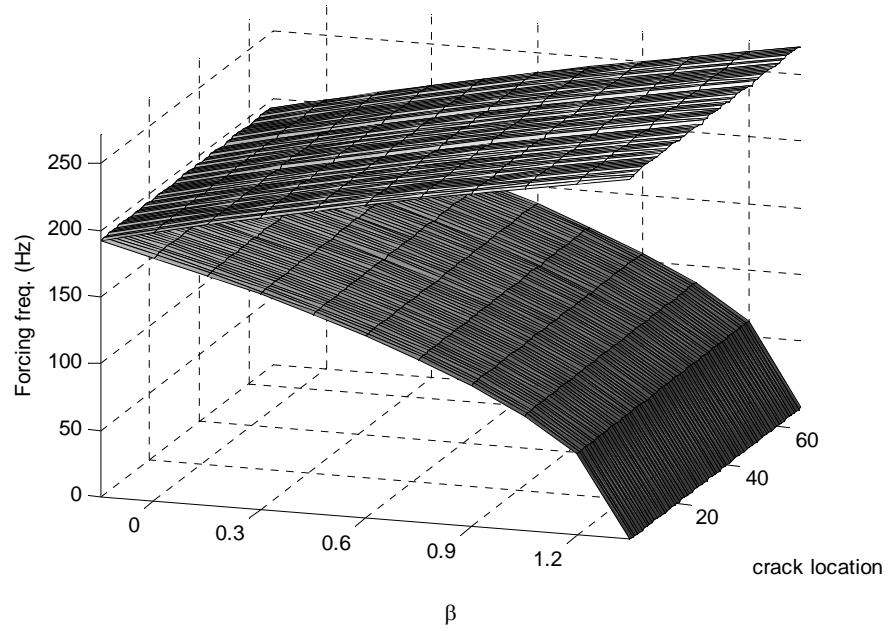
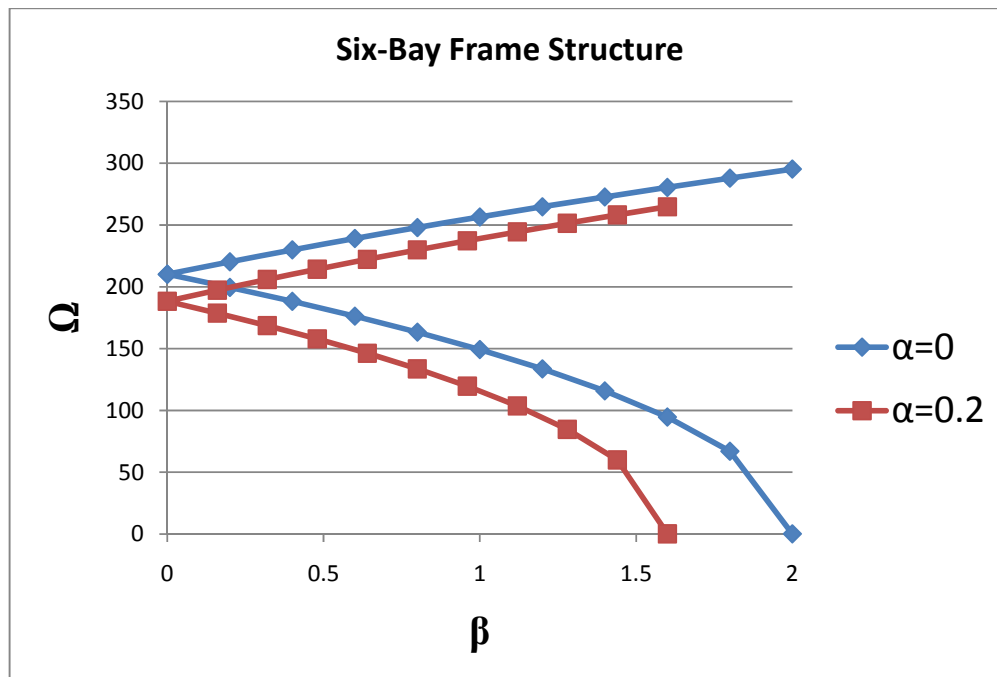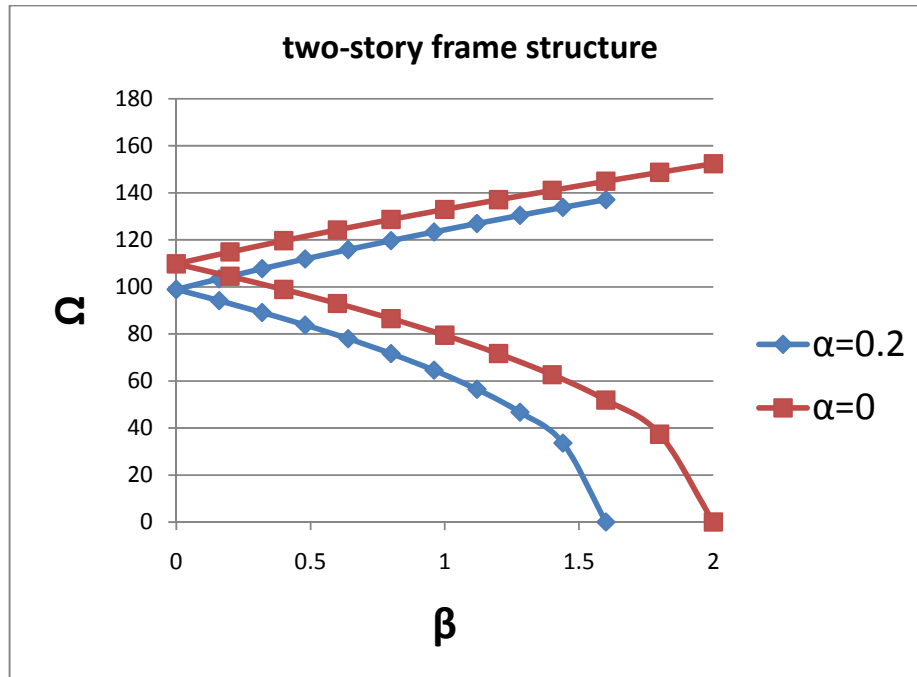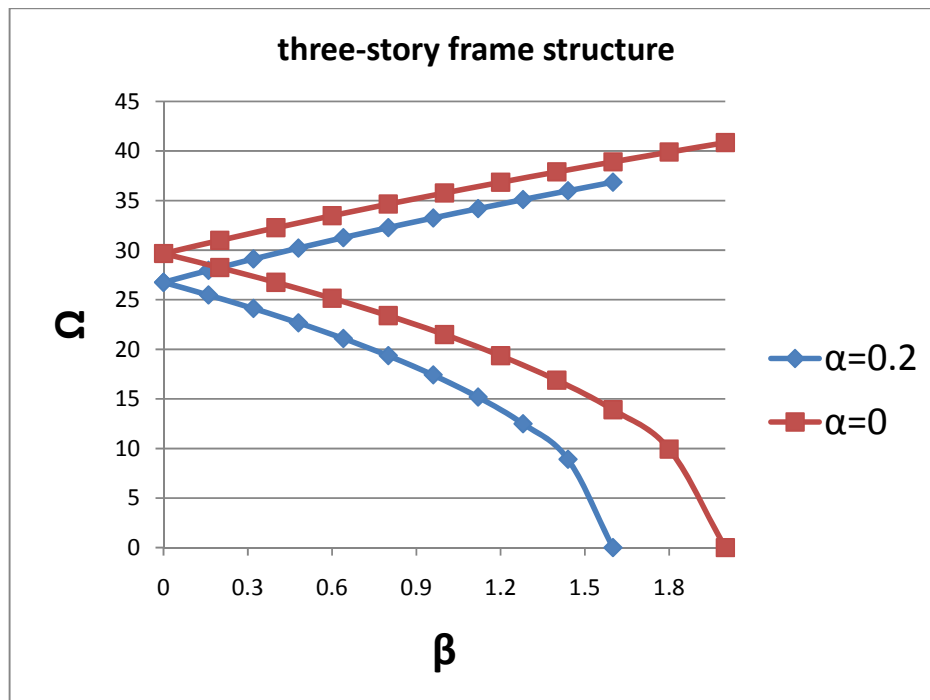Figure 5.57 Dynamic Stability of three-bay Frame structure (α=0.2)
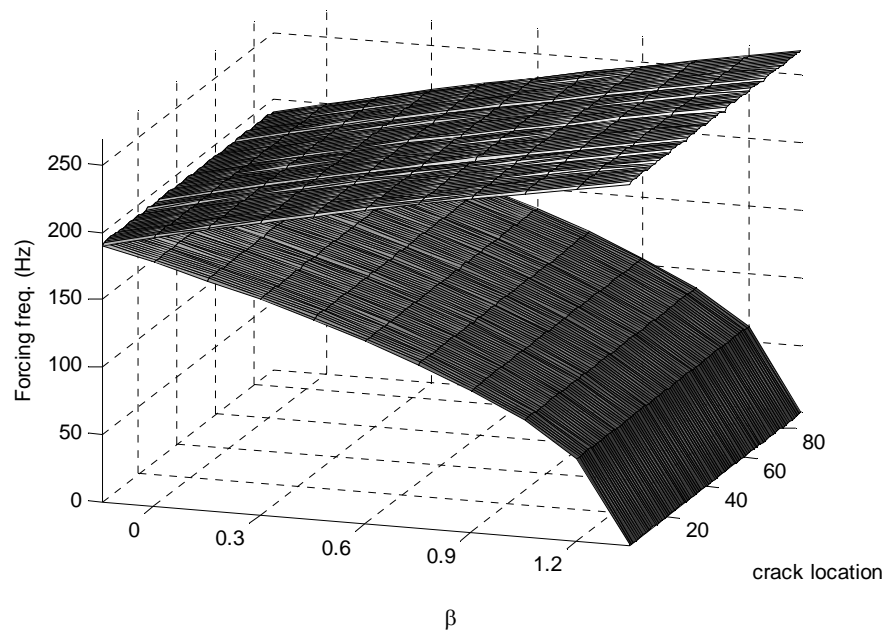
Figure 5.58 Dynamic Stability of four-bay Frame structure (α=0.2)
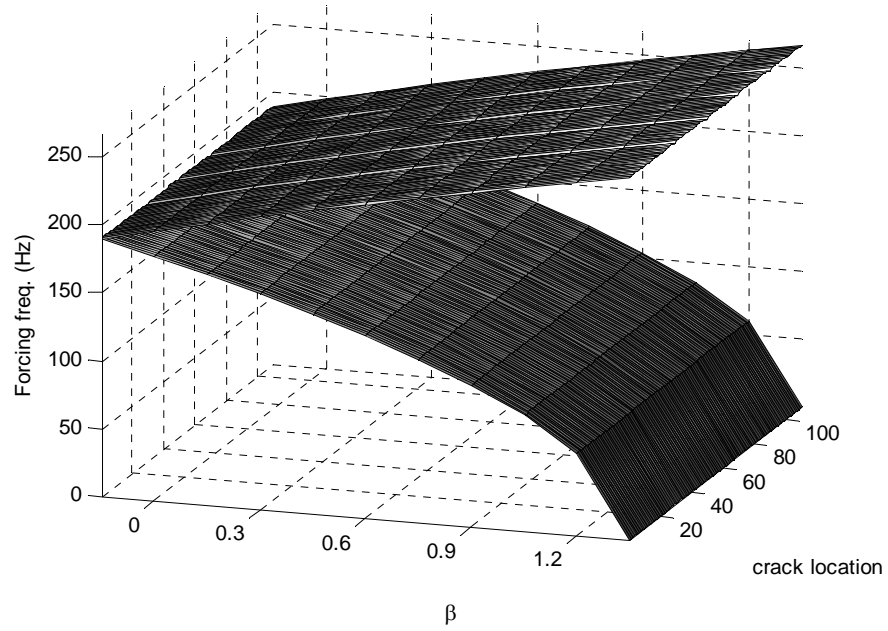
Figure 5.59 Dynamic Stability of five-bay Frame structure (α=0.2)
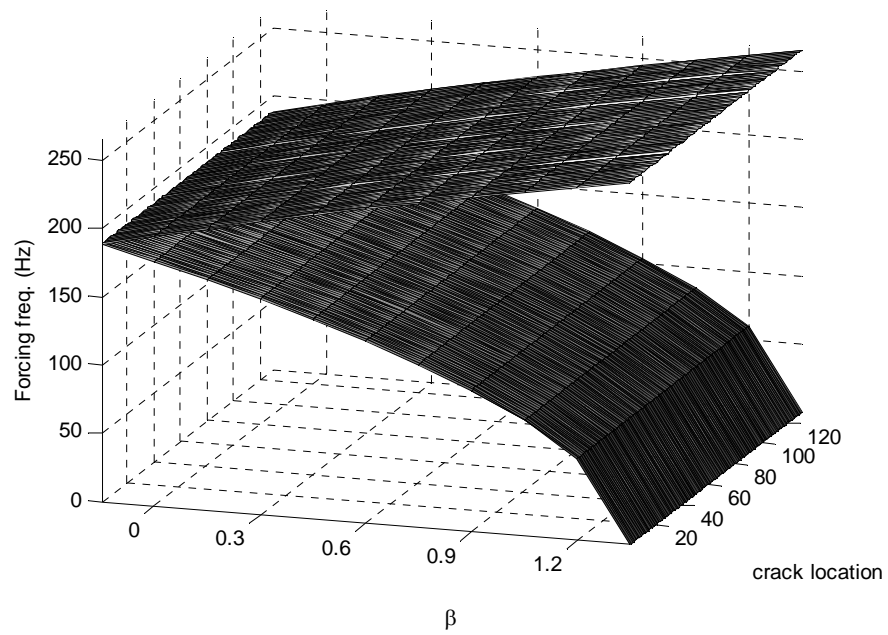
Figure 5.60 Dynamic Stability of six-bay Frame structure (α=0.2)
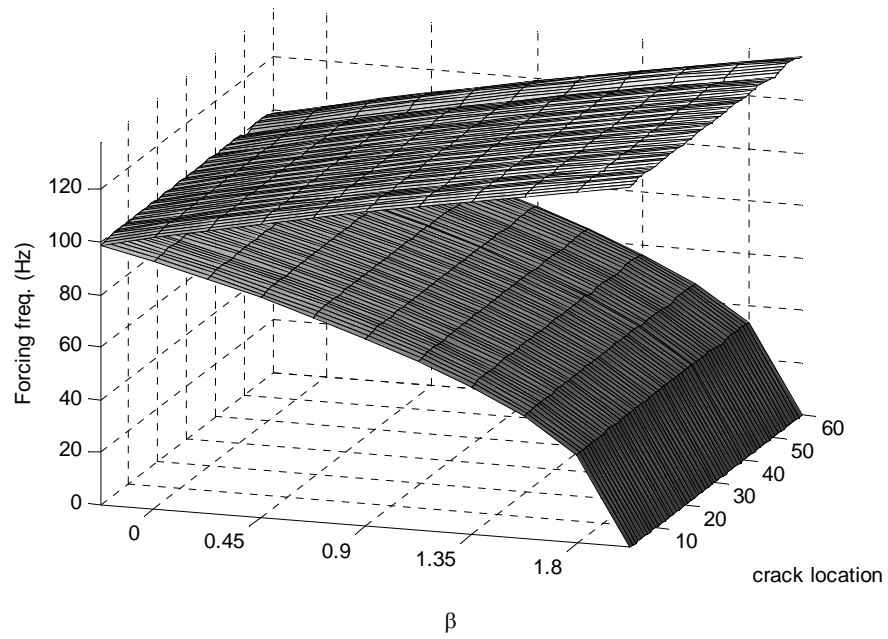
Figure 6.61 Dynamic Stability of two-story Frame structure (α=0.2)
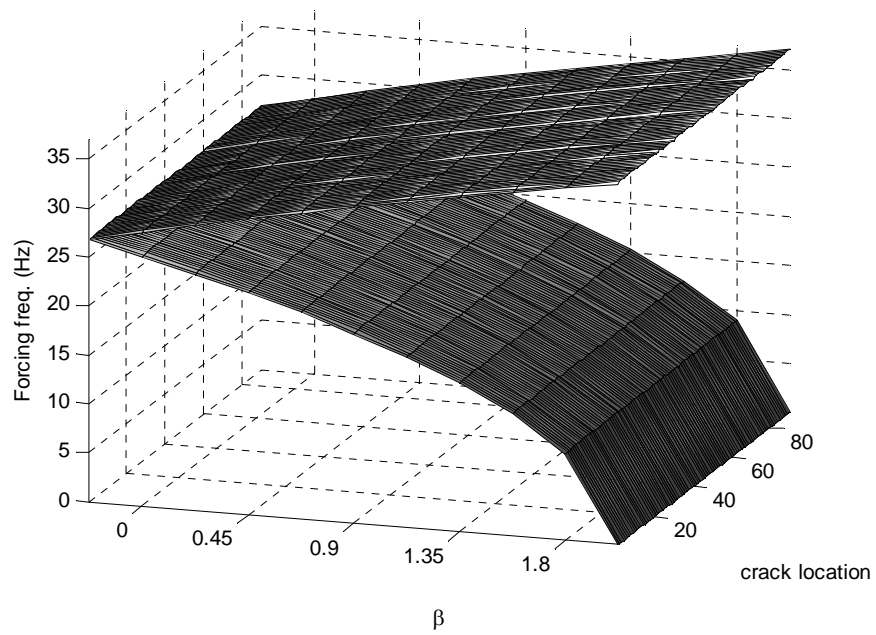
Figure 5.62 Dynamic Stability of three-story Frame structure (α=0.2)
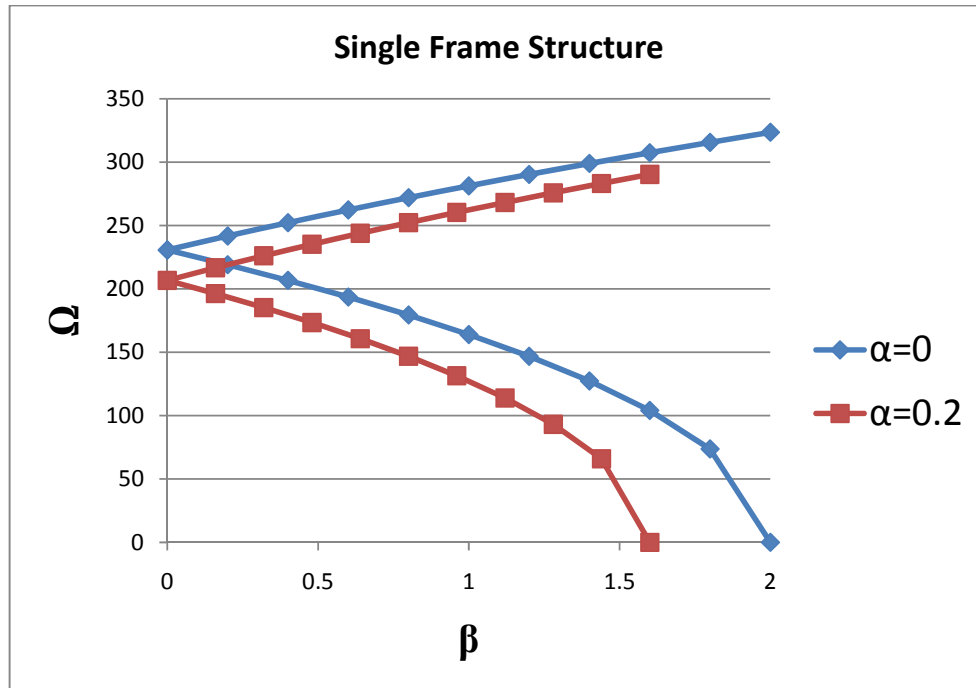
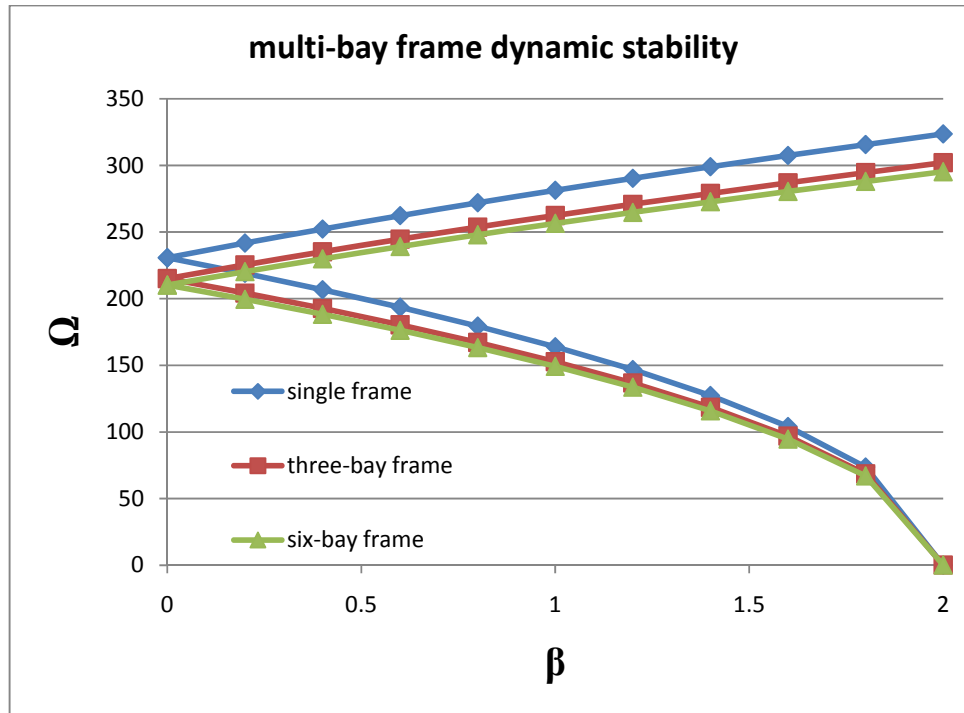Figure 5.63 Dynamic Stability of Single Frame Structure (α= 0, 0.2)
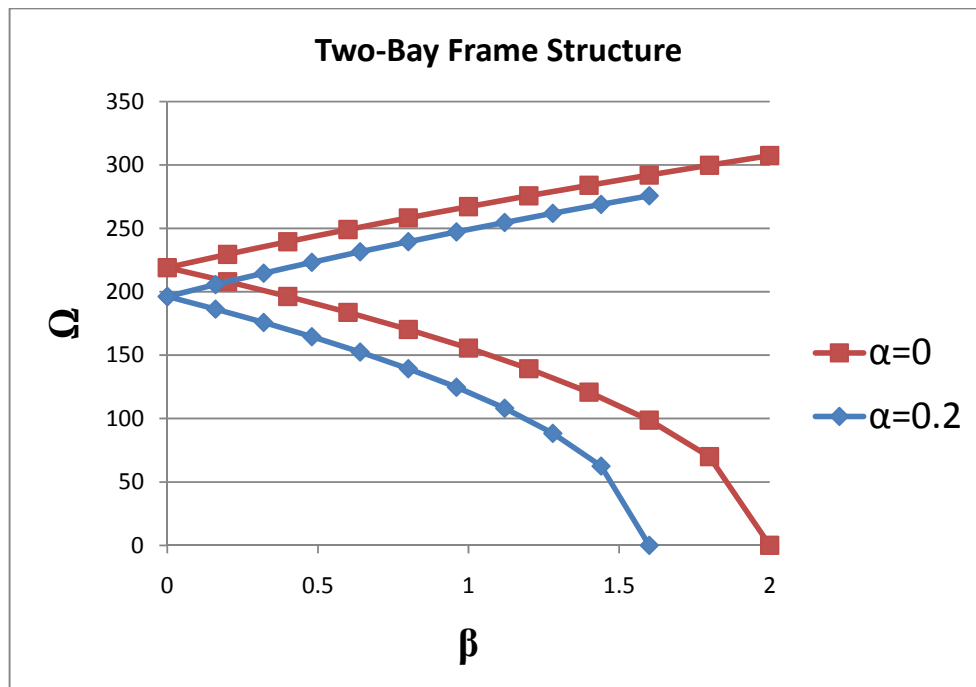
Figure 5.64 Dynamic Stability of Two-Bay Frame Structure (α= 0, 0.2)

Figure 5.65 Dynamic Stability of Three-Bay Frame Structure (α= 0, 0.2)

Figure 5.66 Dynamic Stability of Four-Bay Frame Structure (α= 0, 0.2)

Figure 5.67 Dynamic Stability of Five-Bay Frame Structure (α= 0, 0.2)

Figure 5.68 Dynamic Stability of Six-Bay Frame Structure (α= 0, 0.2)

Figure 5.69 Dynamic Stability of two-story Frame Structure (α= 0, 0.2)

Figure 5.70 Dynamic Stability of three-story Frame Structure (α= 0, 0.2)

Figure 5.71 Dynamic Stability of Multi-Bay Frame Structure

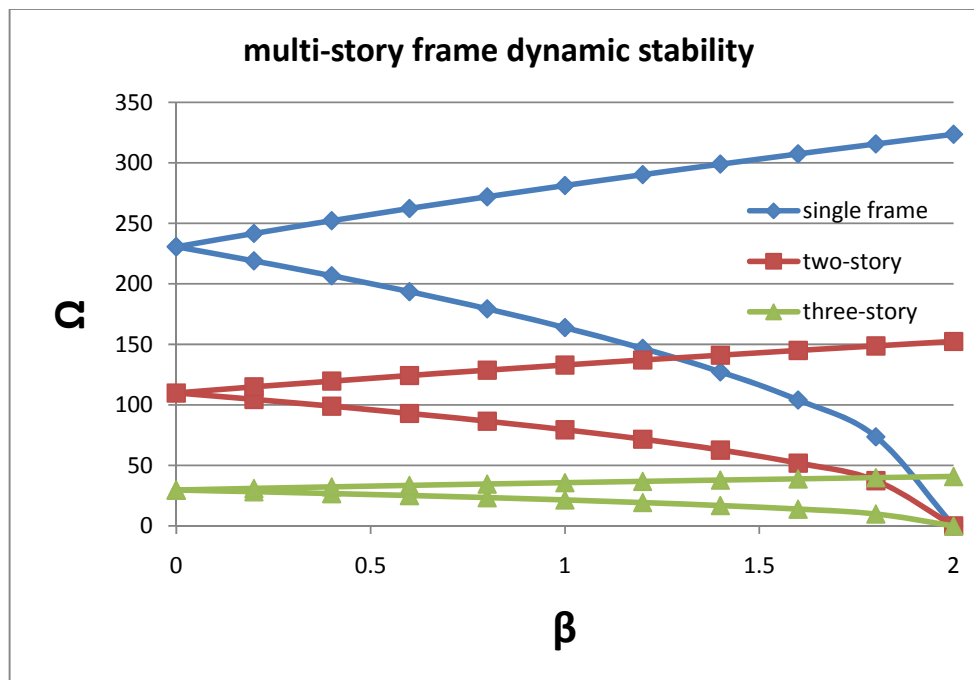

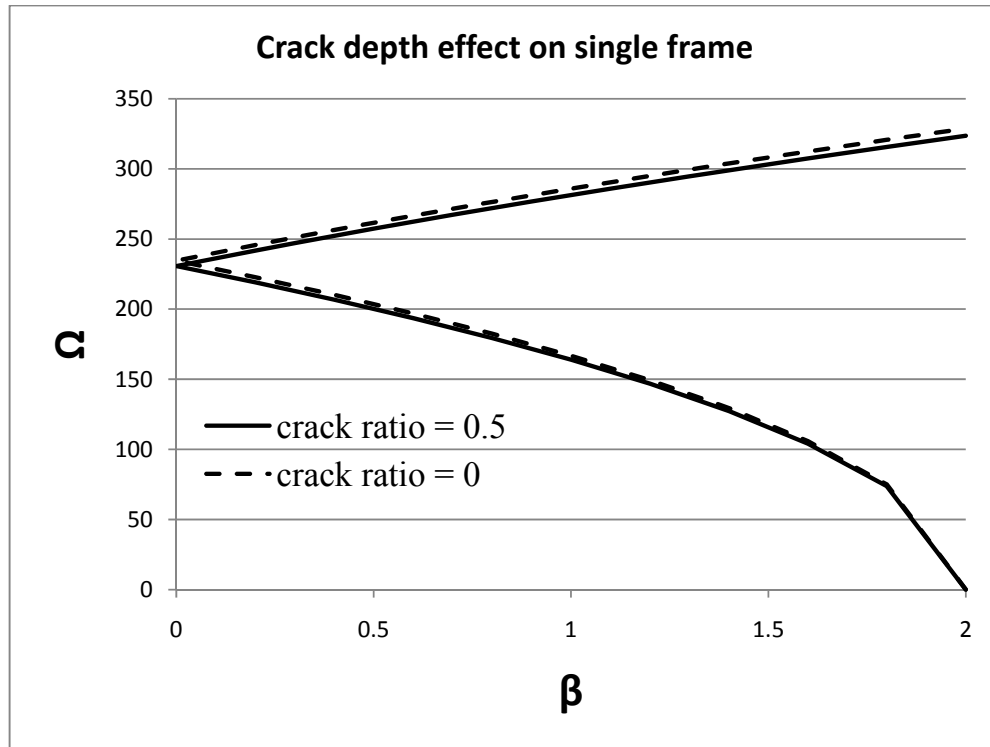Figure 5.72 Dynamic Stability of Multi-Story Frame Structure

Figure 5.73 Dynamic Stability of single Frame Structure with Different Ratio of Crack

CHAPTER SIX
CONCLUSIONS

In this study, the effect of crack depth and crack location on the in-plane free vibration, buckling and dynamic stability of cracked frame structures have been investigated numerically by using The Finite Element Method. The following conclusions are drown.

1. The reduction of both buckling load and natural frequency depends on the crack depth, crack location and crack direction with respect to load direction which changes crack mode (Opening, Sliding and Tearing mode).

2. The higher drops in the buckling load and in-plane natural frequency are observed when the crack is located near the roots or corners of the frames.

3. There is no effect of the crack on the in-plane natural frequency when the crack is located at the nodal points of the mode shape and located at the maximal amplitudes of the mode shape.

4. When the number of blades increases in the multi-bay frame structures, the effect of the crack decreases.

5. Maximum first natural frequency drop occurs when the crack is located at the roots for multi-bay frames and at the corners for the multi-story frames.

6. There is no effect of a crack, if the crack is located at the member which does not vibrate, this phenomena depends on its mode shape.

7. The dynamic unstable region moves towards the origin when the static load (α) increases.

8. When the numbers of blades increase for multi-bay, the unstable region becomes narrower and shifts to the origin. The similar thing can be obtained when the number of story increase in the multi-story frame structure

REFERENCES

A.S. Sekhar, B.S. Prabhu (1992), Crack detection and vibration characteristics of cracked shafts*, Journal of Sound and Vibration 157 (2) 375-381.*

A.S. Sekhar (1999), Vibration characteristics of cracked rotor with two cracks*, Journal of Sound and Vibration 223 (4) 497-512.*

Bamnios, G. & Trochides, A. (1995), Dynamic behaviour of a cracked cantilever beam*, Applied Acoustics, Volume 45, Issue 2, 1995, Pages 97-112.*

Chati, M., Rand, R. & Mukherjee, S. (1997), modal analysis of a cracked beam*, jornal of sound and vibration, 207(2), 240-270.*

Christides, S. & Barr, A.D.S. (1984), One-dimensional theory of cracked Bernoulli-Euler beams*, International Journal of Mechanical Sciences, Volume 26, Issues 11-12, 1984, Pages 639-648.*

Chondros, T.G. & Dimarogonas, A.D. (1989), Dynamic sensitivity of structures to cracks, Journal of vibration*, Acoustics, Stress and Reliability in Design 111, 251}256.*

Chondros, T. G. & Dimarogonas, A. D. (1989), dynamic sensitivity of structures to cracks*, journal of vibration, Acoustics, Stress, and Reliability in design, july 1989, Vol. 111/251.*

Gounaris, G. & Dimarogonas, A. (1988), A Finite element of a cracked prismatic beam for structural analysis*, computer & structurres Vol. 28, No.3, 309-313.*

Karaagac, Celalettin. Öztürk, Hasan & Sabuncu, Mustafa, Free vibration and lateral buckling of a cantilever slender beam with an edge crack: Experimental and numerical studies, *Journal of Sound and Vibration, Volume 326, Issues 1-2, 25 September 2009, Pages 235-250*

Kishen, J. M. Chandra & Kumar, Avinash (2004), Finite element analysis for fracture behavior of cracked beam-columns, Finite Elements in Analysis and Design, *Volume 40, Issues 13-14, August.*

Krawczuk, M. (1994), A new finite element for the static and dynamic analysis of cracked composite beams, *Computers & Structures, Volume 52, Issue 3, 3 August 1994, Pages 551-561.*

Lee, H.P. & Ng, T.Y. (1994), Natural frequencies and modes for the flexural vibration of a cracked beam, *Applied Acoustics, Volume 42, Issue 2, 1994, Pages 151-163.*

Ostachowicz, W. M. & Krawczuk, M. (1990), Vibration analysis of a cracked beam, *Computers & Structures, Volume 36, Issue 2, 1990, Pages 245-250.*

Öztürk, Hasan & Sabuncu, Mustafa (2005), Stability analysis of a cantilever composite beam on elastic supports, *Composites Science and Technology, Volume 65, Issue 13, October 2005, Pages 1982-1995.*

Qian, G.-L. , Gu, S.-N. & Jiang, J.-S. (1989), the dynamic behaviour and crack detection of a beam with a crack, *journal of sound and vibration (1990), 138(2), 233-243.*

Rieger, N.F. and McCallion, H. (1964), The natural frequencies of portal frames—II, international Journal of Mechanical Sciences, *Volume 7, Issue 4, April 1965, Pages 263-268, IN1-IN2, 269-276.*

Saavedra, P.N. & Cuitino, L.A. (2001), crack detection and vibration behavior of cracked beams, *computer and structures 79 (2001) 1451-1459.*

Sakar, Gurkan and Sabuncu, Mustafa (2007), Dynamic stability analysis of pretwisted aerofoil cross-section blade packets under rotating conditions, *International Journal of Mechanical Sciences, Volume 50, Issue 1, January 2008, Pages 1-13.*

Sakar, G., & Sabuncu, M. (2003), dynamic stability of a rotating asymmetric crosssection blade subjected to an axial periodic force. *International jurnal of mechanical sciences, 45, 1467-1482.*

Shen, M.-H.H. & Pierre, C. (1990), Natural modes of Bernoulli-Euler beams with symmetric cracks, *ournal of Sound and Vibration, Volume 138, Issue 1, 8 April 1990, Pages 115-134.*

Shen, M.-H.H. & Taylor, J.E. (1991), An identification problem for vibrating cracked beams, *Journal of Sound and Vibration, Volume 150, Issue 3, 8 November 1991, Pages 457-484.*

Shen, M.-H.H. & Pierre, C. (1994), Free Vibrations of Beams With a Single-Edge Crack, Journal of Sound and Vibration, *Volume 170, Issue 2, 17 February 1994, Pages 237-259.*

Thomas, J., Abbas B.A.H (1976), dynamic stability of timoshenko beam by finite element method. *Jurnal of engineering for industry, transactions of the ASME, 89(1), 1145-1151.*

Thomas, J. & Belek, H.T.(1977), free vibration of blade pakets*, journal mechanical engineering science, Vol 19, 13-21.*

Thomas, J. & Sabuncu, M. (1979), Finite element analysis of rotating pre-twisted asymmetric cross-section blades*, ASME 1 (12).*

Yokoyama T, Chen MC.(1998), Vibration analysis of edge-cracked beams using a line-spring model. Engng Fract Mech; 59(3):403-409.

Zheng, D.Y. & Kessissoglou, N.J. (2003), Free Vibration Analysis of a cracked beam by finite element method. *Journal of sound and vibration 273 (2004), 457-475.*